University of Rhode Island

DigitalCommons@URI

1983

Effect of Horizontal Shear Transfer on Stresses Beneath Steel Bearing Plates

Hasan S. Arouri
University of Rhode Island

EFFECT OF HORIZONTAL SHEAR TRANSFER ON STRESSES

BENEATH STEEL BEARING PLATES

BY

HASAN S. AROURI

A THESIS SUBMITTED IN PARTIAL FULFILLMENT OF THE

REQUIREMENTS FOR THE DEGREE OF

MASTER OF SCIENCE

IN

CIVIL ENGINEERING

UNIVERSITY OF RHODE ISLAND

1983

MASTER OF SCIENCE THESIS

OF

HASAN S. AROURI

APPROVED:

Thesis Committee

Major Professor _____

_____

_____

_____

DEAN OF THE GRADUATE SCHOOL

UNIVERSITY OF RHODE ISLAND

1983

ABSTRACT

In practice, the design of pot bearing steel
plates is usually based on assuming that stresses be-
neath the plate are uniformly distributed. There is
also no consideration given to the effect of shear
stresses transmitted through the interface between the
surfaces of the plates and the supporting concrete
abutment.

However, in this analytical investigation, the
behavior of pot bearing steel plates supported by con-
crete abutment was studied using finite elements
analysis. There were no special assumptions made
concerning stresses beneath the plate. Nevertheless,
the interface between the surfaces of the steel plate
and the concrete abutment was simulated using vertical
and horizontal interface spring elements. Normal and
shear stresses were permitted to be transferred through
the interface with slip occurring beyond some limiting
shear strength value.

Different shear transfer conditions were induced
and stresses resulting in the bearing system were
studied using axisymmetric and plane strain solution
methods. Results indicated that assuming uniform stress

distribution beneath the plate is rather too conservative. However, results from different shear transfer conditions showed that the effect of shear transfer is practically insignificant for design purposes.

ACKNOWLEDGEMENTS

I am greatly indebted to and wish to thank with sincere gratitude:

Dr. Everett E. McEwen, my major professor, for his constructive and valuable guidance in the preparation of this thesis, and for his teaching and advice throughout my graduate studies.

Professor Cheng-Jung Chang, Professor Charles Nash, and Professor Martin Sadd for their assistance in so many ways.

Professor Fadel Al-Kazily for his invaluable help in preparation for my thesis defense.

My parents, Mr. and Mrs. Arouri, for their love, sacrifice, encouragement, and unlimited support.

My sister Rima Arouri, and my friends Georgette and Samia Kiriaki for all the help they gave me in assembling the thesis to its final form.

Mrs. Donna Brightman for her concern and good will.

The University of Rhode Island Computer Laboratory, for the use of their facilities.

Mrs. Frances Harvey for typing the final draft of my thesis.

TABLE OF CONTENTS

LIST OF TABLES

LIST OF FIGURES

CHAPTER 1

INTRODUCTION

Pot bearing steel plates have been successfully used for many years in bridges with varying span and magnitude. Pot bearing steel plates can be physically described as steel plates containing a circular disc of an elastomeric material confined in a pot. A "masonry" steel plate is usually placed beneath the pot to distribute stresses to the supporting concrete abutment as shown in fig. (1.1). The width and length of the masonry plate are sized to keep the stresses in the concrete less than an allowable value to avoid failure of the concrete. Normally, for design purposes, a uniform distribution of concrete stresses beneath the masonry plate is assumed. The thickness of the masonry plate is controlled by bending stresses. It is assumed that the critical section of the masonry plate is near the end of the pot bearing. Allowable concrete stresses as given by AASHTO [1] vary from 0.30 f_c' to a maximum of 0.60 f_c' depending on the ratio of the supporting concrete area to the loaded concrete area, where f_c' is the compressive strength of the concrete. The large allowable values attempt to take account of the effect of confining pressure on the failure strength of the concrete.

Allowable steel stresses are taken as 0.55 of the yield stress. Bearing plates of this type permit the bridge girders to expand due to temperature without developing large lateral forces at the supports. They also distribute vertical reactions through the pot to the masonry plate below.

Although the bearing system designed according to the normal design procedure described above does in fact show great performance in actual situations, it should be expected that allowable bending stresses in the critical section of the masonry plate would be very large because of the uniform stress distribution beneath the masonry plate.

Results from previous analysis indicated that stresses beneath the masonry plate actually have shown little lateral stress distribution. Therefore, from the basic knowledge of structural analysis it is expected that the maximum stress in the critical section of the masonry plate should actually be lower than the design stress. Hence, those findings are examined extensively in this investigation in an attempt to study the effect of shear transfer between the surface of the masonry plate and the concrete abutment, on the stresses of the bearing system.

Elastomer

Uniformly applied load

Pot bearing

Masonry plate

Concrete abutment

Fig. (1.1) Bearing System

CHAPTER 2

PREVIOUS ANALYSIS AND SCOPE OF STUDY

2.1 PREVIOUS ANALYSIS OF THE BEARING SYSTEM

There have not been many publications about the
analysis of the bearing system considered in this investi-
gation. However, during the year 1979, a finite element
analysis of the bearing system was conducted by
Dr. E. E. McEwen at the University of Rhode Island [2].
The structural system was modeled as a two-dimensional
elastic solid, and also as beam on elastic foundation,
fig. (2.1) and (2.2). Results of analysis indicated that
for plates designed according to standard practice, there
is in fact little lateral stress distribution in the con-
crete support beneath the masonry plate as shown in
fig. (2.3). The plate thickness had little effect on con-
crete stresses until it becomes 2 or 3 times the normal
design thickness. Since there is little lateral stress
distribution, the bending stresses in the plate are quite
small. Plates that are one-half the normal thickness have
stresses less than the allowable. Results also indicated
that stresses in the concrete are extremely high approach-
ing the applied pressure on the bearing, and this is due
to the little lateral stress distribution. However, as

between the steel masonry plate and the concrete abutment was represented by vertical and horizontal interface spring elements. The horizontal interface spring elements transfer shear until an ultimate shear strength value is reached, where the bond between the steel and concrete elements breaks and slip takes place. Slip along the interface was described as a nonlinear function, and different shear transfer conditions were assumed. The study was conducted using finite element analysis with the aid of the general-purpose finite element computer program NONSAP [4] (Nonlinear Structural Analysis Program).

Fig. (2.1) Beam on elastic foundation model used in the previous analysis.

all 6591#

Symmetrical about z-axis

3295#

nodal force

3295#

Beam elements

| 15 | 16 | 17 | 18 | 19 | 20 | 21 | 22 | 23 | 24 | 25 | 26 | 27 | 28 |

Thickness

Springs

y

14 x 1.8833 = 26.36"

width=1.0 inch
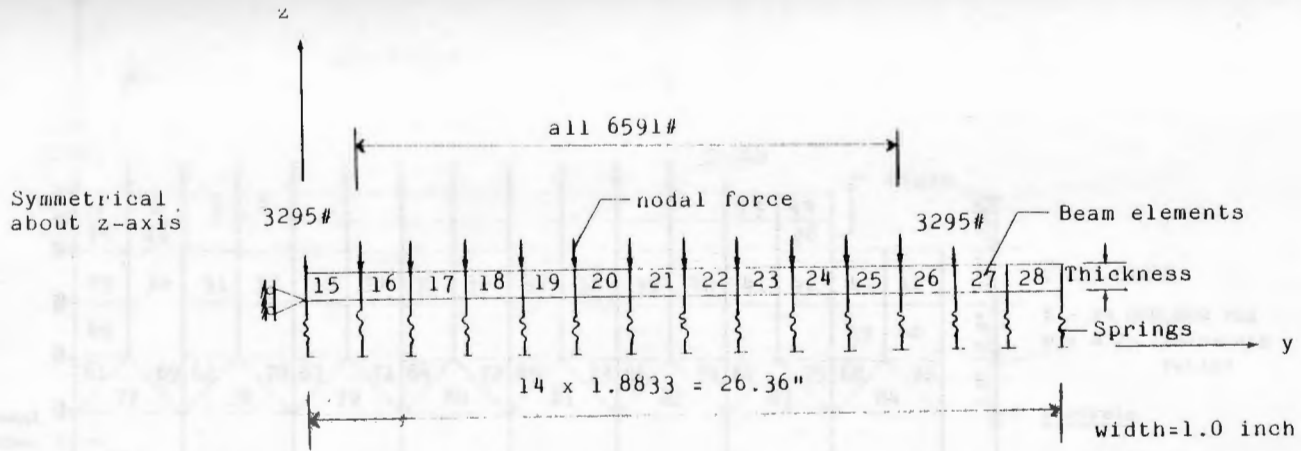
Steel Plate

E = 29,000,000 Psi (modulus of elasticity)
I = varies with thickness (moment of inertia)

Concrete Springs

E = 3,605,000 Psi
$f_c' = 4,000$ Psi

$$K = \frac{AE}{L} = \frac{(1.)(1.8833)(3,605,000)}{18} = 377,000 \text{ #/inch}, \quad K = \text{spring stiffness}$$

A = cross sectional area
E = modulus of elasticity
L = length

Fig. (2.2)   Bearing system finite element two-dimensional model used in the previous analysis.

Pot bearing

Uniformly applied load

Masonry plate

Resulting distribution

Assumed uniform distribution
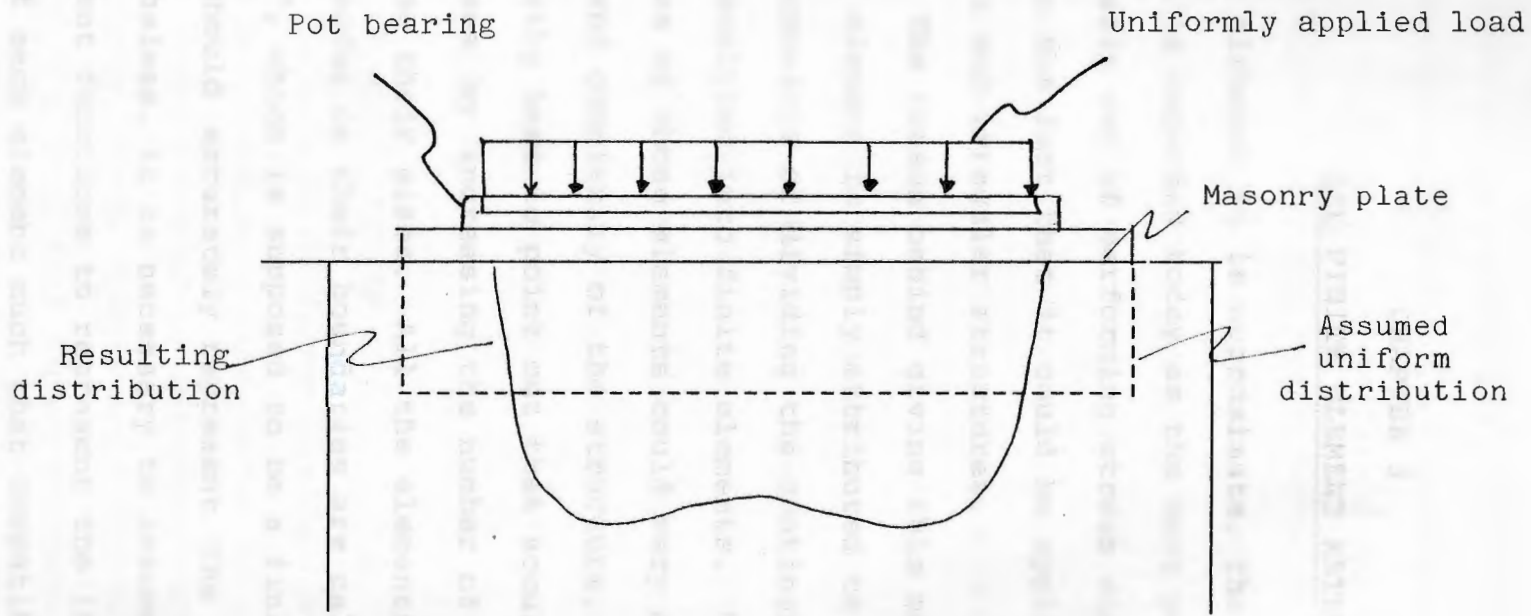
Fig. (2.3) Actual and assumed stress distribution in the concrete beneath the masonry plate.

CHAPTER 3

THE FINITE ELEMENT METHOD

Although it is approximate, the finite element method is regarded today as the most powerful and systematic way of performing stress analysis. Its power lies in the fact that it could be applied on very highly complex and irregular structures.

The reason behind giving this method the name finite element is simply attributed to the procedure, which consists of dividing the continuum of the structure to be analyzed into finite elements. The number, shape, and size of those elements could vary depending on the shape and complexity of the structure. However, it is noteworthy here to point out that accuracy of the results increases by increasing the number of the elements and reducing their sizes. All the elements connected together by nodes on their boundaries are called a "grid system", which is supposed to be a finite element model that should accurately represent the actual structure. Nevertheless, it is necessary to assume adequate displacement functions to represent the internal displacement of each element such that compatibility is satisfied

along common nodes and boundaries.

Generally speaking, the finite element method is composed of two major solution steps. 1) The element solution dealing with the individual elements. Adequate displacement functions are assumed for the different types of elements, such that internal displacements of each element are uniquely described in terms of nodal displacements. Nodal strains are acquired through the derivation of nodal displacements and then related to symbolic nodal stresses through a stress - strain relation. Using energy methods, we could construct a relationship between nodal forces and nodal displacements represented by a stiffness matrix for each individual element. 2) The system solution which is simply combining the stiffness matrices of all the individual elements to construct the structure stiffness matrix. The system solution is independent from the different types of elements used to model the structure.

3.1 HISTORICAL REVIEW

Authors of different finite element textbooks disagreed on selecting a time period as a start of the finite element method of analysis. Moe suggested that the concept of the method was "originally introduced" by Argyris in a series of papers published in 1954-55 [5]. On the other hand, Cook [6] refers to the year 1906 as

the start of the concept which the finite element method was based on. Researchers suggested the "lattice analogy" to solve the continuum problems by approximating the continuum by a regular mesh of elastic bars. Others like Gallagher [7] consider the period from 1850 to 1875 as the "logical starting point" of a review of the history of the finite element method. During this period, the framework analysis developed due to the work of Maxwell, Castigliano, and Mohr, among others. Framework analysis is the base of matrix analysis on which the finite element solution depends to a great extent.

Finite element method is part of a science that depends for its progress on the experiences and accomplishments of past generations. However, progress was extremely slow due to difficulties concerning the solution of algebraic system of equations with many unknowns. Since mid 1950's there has been a concurrent and rapid development of matrix analysis methods and electronic digital computers, and the finite element method was put into practical use. Many important conferences have been devoted exclusively to these subjects, and the first textbooks appeared in 1967 and 1968 [5]. By 1976, about two decades after engineering applications began, there have been more than 7000 publications about the finite element method [6]. General purpose computer programs of finite element analysis are now extensively dispersed

in practice.

3.2 FINITE ELEMENT PROCEDURE

The finite element method is an extension of the stiffness or displacement method. However, unlike skeletal structures, there are now well defined joints where equilibrium of forces can be established. In finite element method, the continuum is divided into elements of different shapes and sizes, and each element is bounded by artificial nodes (internal nodes could exist as well). The system of elements is called the grid system which represents the finite element model that approximates the actual structure. Each node in the grid system has a number of degrees of freedom, which combined, give a number of algebraic equations to be solved numerically so that the analysis would be completed.

It is worthwhile mentioning at this point that there are three types of commonly used elements, [8], 1) Displacement element, using assumed displacement functions, forms the majority of known finite elements; 2) Equilibrium element, based on assumed stress functions; and 3) Hybrid element, which is based on both assumed displacement and stress functions. Elements (2) and (3) are used to a much lesser extent. As described in the next chapter, displacement elements are used in the modeling of the bearing system.

3.2.1 THE GRID SYSTEM

A continuum is divided into two-dimensional finite elements, which are separated by straight or curved lines and bounded by nodal points (internal nodal points could exist), or it could be divided into three-dimensional finite elements, which are separated by flat or curved surfaces. The shapes, sizes, material properties and thicknesses of the elements within the grid system could vary. Therefore, the finite element method could handle problems involving nonhomogeneous properties, complex geometry and support conditions, and various types of loading situations.

A cantilever beam, shown in fig. (3.1.a), is loaded uniformly at its edge. The continuum is approximated by a grid system, shown in fig. (3.1.b), composed of triangular (two-dimensional) elements separated by straight lines, and each element is bounded by three nodal points at its corners. The uniform load on the actual structure is represented by a load system applied at the nodes. Boundary conditions are satisfied through carefully selected characteristics of the boundary nodal points representing the fixed end of the cantilever beam.

In many problems, only one type of element is needed to construct a grid system of a structure. Nevertheless, it is also possible to mix elements of different types, as will be shown in the next chapter, where the steel bearing system is divided into linear elastic

P

a) structure

nodes

finite
element

P_1 P_2 P_3

b) (Model)
Grid
System

boundary
node

finite element

Fig. 3.1 Actual structure and finite element grid system.

isotropic elements, the concrete abutment is divided into nonlinear elasto-plstic isotropic elements, and both are connected by interface spring elements.

3.2.2 ELEMENTS VARIETY

As mentioned in previous sections, the power of the finite element method lies in its ability to represent highly complex structures of homogeneous, as well as nonhomogeneous properties. However, for the results of the analysis to be sufficient, analysts should be very careful in selecting finite element models to represent the structures they wish to analyze.

There is a large element variety of different shapes and properties available for the finite element solution. Hence, it is important to realize that it is totally up to the analyst to select the elements which best represent the structure.

It is not intended here to discuss in depth the available elements, but the intention is to present some of the simple and important ones. Available elements could be separated into three main categories: 1) one-dimensional, 2) two-dimensional, and 3) three-dimensional. Moreover, elements belonging to each of the three mentioned categories also vary in shape, number of degrees of freedom, number of nodes; all could have different material properties depending on the problem.

Some of the elements used in modeling the bearing system will be discussed with more depth in later chapters. Table (3.1) presents some of the simplest types of one-, two-, and three-dimensional elements as examples of available ones [5].

The nodal degrees of freedom normally refer to the displacements and rotations. The order of the element stiffness matrix is usually equal to the number of degrees of freedom in the element, that is because each degree of freedom produces an algebraic equation with one unknown, usually the displacement. The degrees of freedom could also represent relative displacements as shown in Appendix A.

3.2.3 DISPLACEMENT FUNCTIONS

Once the grid system is constructed and the elements are selected, then it is very important to select what is called a "displacement function" which represents internal element displacements expressed in terms of nodal displacements. Displacement functions must be selected such that compatibility along the boundaries of adjacent elements is satisfied.

A displacement function could be defined as an interpolation function which describes the element internal displacement in terms of the nodal displacements. Discussion of displacement functions of three
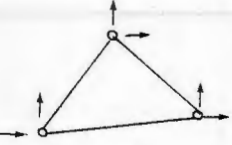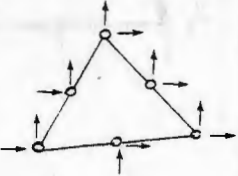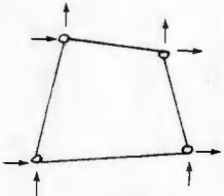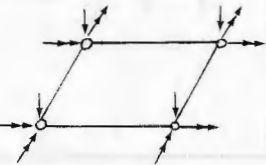
Element		Typical application	No. of nodes	Degrees of freedom at each node
Bar		Trusses	2	1
Beam		Frames	2	3
Triangular; constant strain		Plane stress	3	2
Triangular; linear strain		Plane stress	6	2
Quadri-lateral; plane stress		Plane stress	4	2
Rectan-gular; bending		Plate bending	4	3

Table (3.1) Some typical types of elements (continued on next page)
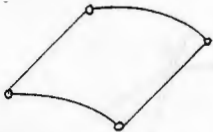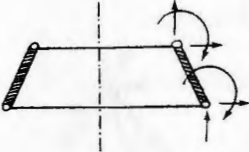
Element	Typical application	No. of nodes	Degrees of freedom at each node
Rect-angular shell element	Cylindrical shells, folded plates	4	5-6
Trun-cated cone	Axi-symmetric shells	2	3
Ring; tri-angular section	Axi-symmetric solids	2	3

Table (3.1) continued

Element	Typical application	No. of nodes	Degrees of freedom at each node
Trian-gular; bending	Plate bending	3	3
Tetra-hedron	Three-dimen-sional stress	4	3
Prism	Three-dimen-sional stress	8	3

Table (3.1) continued

dimensional elements will not be necessary in the scope of this thesis; however, they follow the same pattern considering that they have three coordinates to work with rather than one (one-dimensional elements) or two (two dimensional elements).

There are two ways in which displacement functions could be given, 1) a simple polynomial with undetermined coefficients, or 2) directly in terms of shape functions.

1) If the displacement function is given by a simple polynomial with undetermined coefficients, terms for all nodal displacements could be acquired by substituting the coordinates of the corresponding nodes in the polynomial. A number of equations will result equal to the number of element degrees of freedom. The only unknowns in the resulting system of equations are the undetermined coefficients of the original polynomial equation. By solving for the unknown coefficients and substituting in the original polynomial, we find that the undetermined coefficients were transformed to become the relevant parameters of the nodal displacements, called the shape functions. Let $u(x)$ be the polynomial representing a displacement function, for the one-dimensional beam element shown in fig. (3.2).

$$u(x) = a_1 + a_2x + a_3x^2 + a_4x^3$$

$$\theta(x) = 0 + a_2 + 2a_3x + 3a_4x^2$$

(3.1)

where θ is the first partial derivative of $u(x)$ representing nodal rotations.

Expressing (3.1) in matrix notation,

$$u(x) = [G]\{a\}$$

(3.2)

where $[G] = [1\ x\ x^2x^3]$; $\{a\}^T = \{a_1\ a_2\ a_3\ a_4\}$

As shown, the number of degrees of freedom equals the number of undetermined coefficients in (3.1). Substituting the coordinates of nodes 1 and 2 in (3.1), we acquire terms for the corresponding nodal displacements, $(u_1, \theta_1, u_2, \theta_2)$.

@ x = 0   u = u_1 $\theta = \theta_1$

@ x = L   u = u_2 $\theta = \theta_2$

resulting

$$\begin{Bmatrix} u_1 \\ \theta_1 \\ u_2 \\ \theta_2 \end{Bmatrix} = \begin{bmatrix} 1 & 0 & 0 & 0 \\ 0 & 1 & 0 & 0 \\ 1 & L & L^2 & L^3 \\ 0 & 1 & 2L & 3L^2 \end{bmatrix} \begin{Bmatrix} a_1 \\ a_2 \\ a_3 \\ a_4 \end{Bmatrix}$$

in short form

Fig. (3.2) Beam element.

$$\{\Delta\} = [D] \{a\} \qquad\qquad (3.3)$$

where $\{\Delta\}$ = nodal displacements.

Solving (3.3) for $\{a\}$ will result

$$\{a\} = [D]^{-1} \{\Delta\} \qquad\qquad (3.4)$$

Substituting (3.4) in (3.2) will result

$$u(x) = [G] [D]^{-1} \{\Delta\} \qquad\qquad (3.5)$$

Let $[N] = [G] [D]^{-1}$ \qquad (3.6)

then the displacement function becomes

$$u(x) = [N] \{\Delta\} \qquad\qquad (3.7)$$

where $[N] = [N_1\ N_2\ N_3\ N_4]$
and

N_1, N_2, N_3 and N_4 are the shape functions for the
corresponding element degrees of freedom. It could
be easily verified that N_i is equal unity only at
node (i), and zero at all other nodes. That gives
us the displacement field over an element when node
(i) is given unit displacement while keeping all
other nodes fixed.

For displacement functions of two-dimensional ele-
ments given in terms of simple polynomials, the
analyst could use the Pascal triangle [8] to
determine the combination of terms which should be

used.

2) Displacement functions could also be given directly
   in terms of shape functions as shown in (3.7). There
   are interpolation functions which state the shape
   functions directly, avoiding all the work seen in
   equations (3.2) to (3.7). This is done by replacing
   (a's) in equation (3.1) by (N's) as seen in
   equation (3.7). Many polynomial functions such as
   the Lagrange polynomial and the Hermitian polynomial
   [8] among others, could be used to represent a
   displacement function. Shape functions for most
   available elements can be found tabulated and
   ready for use; in fact many are used in general
   purpose finite element computer programs.

3.2.4 FORMULATION OF STIFFNESS MATRIX AND LOAD MATRIX

The next step which immediately follows the
formulation of the displacement function, is to find
nodal strains and stresses. Those strains and stresses
will be used to construct the stiffness matrix of the
element and its equivalent nodal forces. A general
brief description of the procedure used to formulate
the element stiffness matrix will be presented in this
section. The principle of minimum total potential
energy will be used in the formulation.

As shown in the above section in equation (3.7),
the displacements are expressed in terms of the nodal

displacements by the use of the shape functions which are functions of the coordinates. The strains are calculated by making appropriate differentiation of the displacement function, thus

$$\{\varepsilon\} = [B] \{\Delta\} \tag{3.8}$$

where $\{\varepsilon\}$ = strain matrix

$[B]$ = appropriate derivative of $[N]$

The stresses are related to the strains by the $[C]$ matrix, which is called the elasticity or the property matrix.

$$\{\sigma\} = [C] \{\varepsilon\} \tag{3.9}$$

Substituting (3.8) in (3.9)

$$\{\sigma\} = [C] [B] \{\Delta\} \tag{3.10}$$

Total potential energy (Π) is the sum of the strain energy (U) and the potential energy (V), thus

$$\Pi = U + V \tag{3.11}$$

The strain energy

$$U = \frac{1}{2} \int_{vol} \{\varepsilon\}^T \{\sigma\} \ d_{vol} \tag{3.12}$$

Substituting (3.8) and (3.10) in (3.12)

$$U = \frac{1}{2} \int_{vol} \{\Delta\}^T [B]^T [C] [B] \{\Delta\} \ d_{vol} \tag{3.13}$$

The potential energy is

$$V = -\int_{vol} \{u\}^T \{q\} \ d_{vol} \tag{3.14}$$

where $\{u\}$ is taken from equation (3.7)

and $\{q\}$ is the distributed load matrix

$$V = -\int_{vol} \{\Delta\}^T [N]^T \{q\} \ d_{vol} \tag{3.15}$$

Substituting (3.13) and (3.15) in (3.11)

$$\Pi = \frac{1}{2} \int_{vol} \{\Delta\}^T [B]^T [C] [B] \{\Delta\} \ d_{vol}$$

$$- \int_{vol} \{\Delta\}^T [N]^T \{q\} \ d_{vol} \tag{3.16}$$

The principle of stationary potential energy requires that the first partial differential of the total potential energy with respect to any nodal displacement must be zero. Thus, the equilibrium condition to be satisfied is,

$$\frac{\partial \Pi}{\partial \Delta} = 0 \tag{3.17}$$

Substituting (3.16) in (3.17)

$$\frac{\partial \Pi}{\partial \Delta} = \int_{vol} [B]^T [C] [B] \{\Delta\} \, d_{vol}$$

$$- \int_{vol} [N]^T \{q\} \, d_{vol} = 0 \tag{3.18}$$

or

$$[K] \{\Delta\} - \{P\} = 0 \tag{3.19}$$

where

[K] is the element stiffness matrix and

{P} is the equivalent element nodal force

$$[K] = \int_{vol} [B]^T [C] [B] \, d_{vol} \tag{3.20}$$

$$\{P\} = \int_{vol} [N]^T q \, d_{vol} \tag{3.21}$$

3.3 A GENERAL PURPOSE FINITE ELEMENT PROGRAM (NONSAP)

As described in the sections above, the finite element method of analysis involves rather lengthy and complex computations. In practice, structures might have hundreds or even thousands of nodes resulting in stiffness matrices of very large orders. Hence, it is impossible to perform the analysis without the aid of digital computers. However, many general-purpose finite element programs have been developed to perform the analysis in a matter of minutes of computer time for large problems. The analysis of the bearing system in

this thesis was performed by NONSAP [4], a general-purpose nonlinear finite element structural analysis program. Several element types as well as a selection of material models are available in this program.

3.3.1 ELEMENT TYPES

There are three types of elements available for use in NONSAP: (1) truss elements, (2) two-dimensional elements, and (3) three-dimensional elements. Since elements used in modeling the bearing system were two-dimensional, special attention will be given to this type of element in this section.

(1) Truss Elements

A truss element is one-dimensional, has two nodes, and is only capable of transmitting axial forces, see fig. (3.3). For the truss element, the following formulations have been incorporated into NONSAP:

a) Linear elastic, small displacement analysis.

b) Small displacement analysis with material non-linearities only.

c) Updated Lagrangian, but assuming small strains (with large displacements).

Since the material models considered are only defined for small strains, small strains are assumed in the calculation of stresses, and the changes in the cross sectional areas of the truss

Node 1

Node 2

$u_{\overline{x}}^1$

$u_{\overline{x}}^2$

u_z

u_y

u_x

(x_1, y_1, z_1)

$u_{\overline{x}}^1$ & $u_{\overline{x}}^2$ = nodal displacements in local coordinates.

u_x, u_y, u_z = displacement components in global coordinates.

Fig. (3.3)   Truss element in space.

element is neglected during deformation.

(2) Two-dimensional Elements

The two-dimensional elements available in NONSAP are: 1) Plane stress elements, with the assumption that out of plane shears and stresses are negligible. 2) Plane strain elements where the out of plane strains are negligible. 3) Axisymmetrical elements. Figure (3.4) demonstrates examples of possible finite element analysis involving the different types of two-dimensional elements.

For the two-dimensional elements the following formulations have been incorporated into NONSAP:

a) Linear elastic, small displacement analysis.

b) Small displacement analysis with material non-linearities only.

c) Total Lagrangian formulation.

d) Updated Lagrangian formulation.

All formulations are described in the NONSAP commentary by Bathe, Wilson and Iding [4].

All two-dimensional elements in NONSAP could have from 3 to 8 nodes depending on the nature of the problem and the choice of the analyst. Figure (3.5) represents a general two-dimensional element with the nodal points numbered as shown.
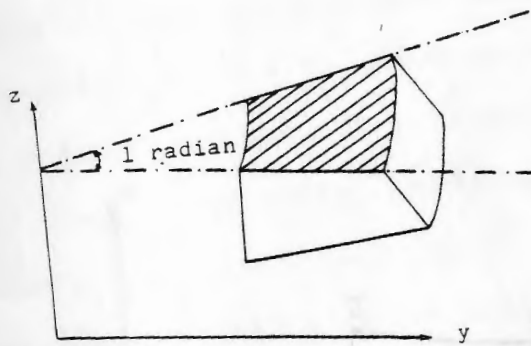
Axi-symmetric finite element model of a ring.
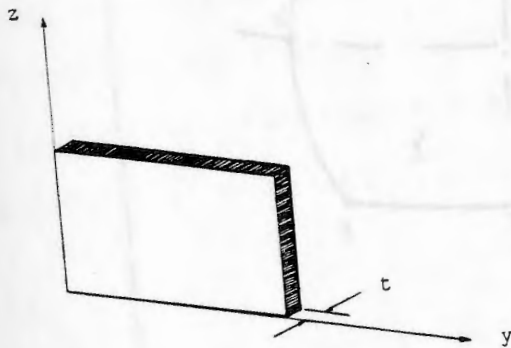
Plane stress finite element model of a cantilever beam
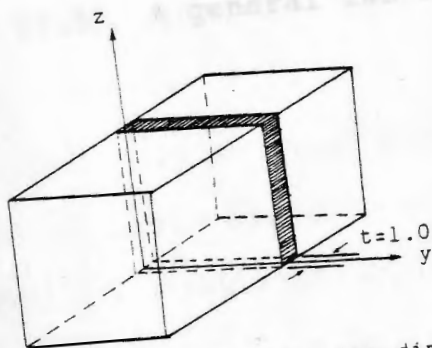
Plane strain finite element model of a concrete abutment.

Fig. (3.4) Possible two-dimensional finite element analysis.

Fig. (3.5)   A general two-dimensional element.

A system of natural coordinates (r,s) were given to the element such that $r = +1$ along edge (1-8-4), and $r = -1$ along edge (2-6-3); while $s = +1$ along edge (2-5-1) and $s = -1$ along edge (3-7-4). The global coordinate is given in cartesian coordinates (y,z); however, polar co-ordinates could also be used. Let (u_y, Δ_y) and (u_z, Δ_z) represent the displacement functions, nodal displacements in the y-direction and the z-direction respectively. The displacement function for the element, expressed in matrix notation, is:

$$\begin{Bmatrix} u_y \\ u_z \end{Bmatrix} = \begin{bmatrix} h_1, \ldots, h_8, 0, \ldots, 0 \\ 0, \ldots, 0, h_1, \ldots, h_8 \end{bmatrix} \begin{Bmatrix} \Delta_{y_1} \\ \vdots \\ \Delta_{y_8} \\ \Delta_{z_1} \\ \vdots \\ \Delta_{z_8} \end{Bmatrix} \qquad (3.22)$$

where h_i is the shape function associated with node i, given directly in terms of the element natural coordinates (r,s).

Rewriting (3.22) in short form

$$\begin{Bmatrix} u_y \\ u_z \end{Bmatrix} = \begin{bmatrix} h & 0 \\ 0 & h \end{bmatrix} \begin{Bmatrix} \Delta_y \\ \Delta_z \end{Bmatrix} \qquad (3.23)$$

Recalling (3.7), we notice that the shape function matrix [N] is expressed in global coordinates, while in (3.23) of NONSAP, shape functions are expressed in terms of the element natural coordinate system as shown in (3.22). However, derivatives of the shape functions are needed to evaluate the [B] matrix in equation (3.8) which evaluates the nodal strains in the global coordinate system.

The derivatives needed are:

$$
\left\{
\begin{array}{c}
\dfrac{\partial u_y}{\partial y} \\[2mm]
\dfrac{\partial u_y}{\partial z} \\[2mm]
\dfrac{\partial u_z}{\partial y} \\[2mm]
\dfrac{\partial u_z}{\partial z}
\end{array}
\right\}
=
\left[
\begin{array}{ccccc}
\dfrac{\partial h}{\partial y} & 0 & 0 & 0 \\[2mm]
\dfrac{\partial h}{\partial z} & 0 & 0 & 0 \\[2mm]
0 & 0 & \dfrac{\partial h}{\partial y} & 0 \\[2mm]
0 & 0 & \dfrac{\partial h}{\partial z} & 0
\end{array}
\right]
\left\{
\begin{array}{c}
\Delta_y \\[2mm]
0 \\[2mm]
\Delta_z \\[2mm]
0
\end{array}
\right\}
\qquad (3.24)
$$

The derivatives in (3.24) are calculated using a Jacobian transformation, where the chain rule relating (y,z) to (r,s) derivatives is:

$$
\left\{
\begin{array}{c}
\dfrac{\partial}{\partial r} \\[2mm]
\dfrac{\partial}{\partial s}
\end{array}
\right\}
= \left[J \right]
\left\{
\begin{array}{c}
\dfrac{\partial}{\partial y} \\[2mm]
\dfrac{\partial}{\partial z}
\end{array}
\right\}
\qquad (3.25)
$$

where J is the Jacobian operator, written as

$$J = \begin{bmatrix} \dfrac{\partial y}{\partial r} & \dfrac{\partial z}{\partial r} \\[2ex] \dfrac{\partial y}{\partial s} & \dfrac{\partial z}{\partial s} \end{bmatrix} \qquad (3.26)$$

Inverting J and multiplying it by both sides of (3.25), we get

$$\begin{Bmatrix} \dfrac{\partial}{\partial y} \\[2ex] \dfrac{\partial}{\partial z} \end{Bmatrix} = \frac{1}{\det J} \begin{bmatrix} \dfrac{\partial z}{\partial s} & -\dfrac{\partial z}{\partial r} \\[2ex] -\dfrac{\partial y}{\partial z} & \dfrac{\partial y}{\partial r} \end{bmatrix} \begin{Bmatrix} \dfrac{\partial}{\partial r} \\[2ex] \dfrac{\partial}{\partial s} \end{Bmatrix} \qquad (3.27)$$

where the Jacobian determinant is

$$\det J = \left(\frac{\partial y}{\partial r} \; \frac{\partial z}{\partial s} \right) - \left(\frac{\partial y}{\partial s} \; \frac{\partial z}{\partial r} \right) \qquad (3.28)$$

Once the derivatives are evaluated, the [B] matrix could be determined. Following the formulation incorporated in NONSAP, the stiffness matrix could be evaluated to complete the analysis.

(3)   Three-dimensional Elements

The general three-dimensional element in NONSAP is an 8 to 21 variable-number-nodes element. For this element, the following formulations have been incorporated in NONSAP:

a)   Linear elastic small displacement analysis.

b)   Small displacement analysis with material nonlinearities only.

The formulation of the three-dimensional element is similar to the formulation of the two-dimensional element, with the consideration of the difference in the element shape function.

3.3.2   MATERIAL MODELS

Several different material models, presented in the NONSAP commentary [4], were incorporated in NONSAP. The material model library of NONSAP [9] is shown in tables (3.2), (3.3), and (3.4) for the truss element, two-dimensional element, and the three-dimensional element respectively.

Nevertheless, NONSAP has been written to accept material models not currently available in the NONSAP material model library, where the overlay subroutines for the new material model must be provided by the user.

FORMULATION	MATERIAL MODEL
Linear analysis	Linear elastic
Materially nonlinear only	Nonlinear elastic
Updated Lagrangian formulation	Linear elastic and nonlinear elastic

Table (3.2)   Truss element material models.

FORMULATION	MATERIAL MODEL
Linear analysis	Linear isotropic and linear orthotropic
Materially nonlinear only	Variable tangent moduli. Curve description model (plane strain or axi-symmetric only.) Curve description model with tension weakening (plane strain only) Elastic-plastic, von Mises yield condition. Elastic-plastic, Drucker Prager yield condition.

Table (3.3)   Two-dimensional material models (continued next page)

FORMULATION	MATERIAL MODEL
Total Lagrangian formulation	Incompressible nonlinear elastic, Mooney-Rivlin material (plane stress only).
	Elastic plastic, von Mises yield condition.
	Variable tangent moduli.
	Linear isotropic.
	Linear orthotropic.
Updated Lagrangian formulation	Linear isotropic.

Table (3.3)   Continued

FORMULATION	MATERIAL MODEL
Linear analysis	Linear isotropic elastic
Material nonlinearity only	Curve description model

Table (3.4)   Three-dimensional material models.

CHAPTER 4

MODELING OF THE BEARING SYSTEM

Consider a concrete abutment loaded in several locations by steel or concrete girders. The load is transferred vertically by pot bearing plates as described in chapter 2. For analysis purposes, a single bearing is considered to act on an isolated block of concrete as shown in fig. (4.1). A three-dimensional solid model will require a great calculation effort and computer time because of its complexity. However, the complexity of the problem could be reduced significantly by the use of the following models as possible approximations.

1) The bearing system could be represented by an axisymmetrical solid which requires that the pot bearing plate and the masonry plate have a circular shape and requires the concrete block to have a cylindrical shape. Then the finite element grid system representing the bearing system could be composed of a number of two-dimensional axisymmetric elements instead of three-dimensional solid elements. 2) Another approximation is to take a 1-inch strip through the bearing system and analyze it as a two-dimensional plane strain or plane

Pot bearing plate

Masonry plate

Concrete block
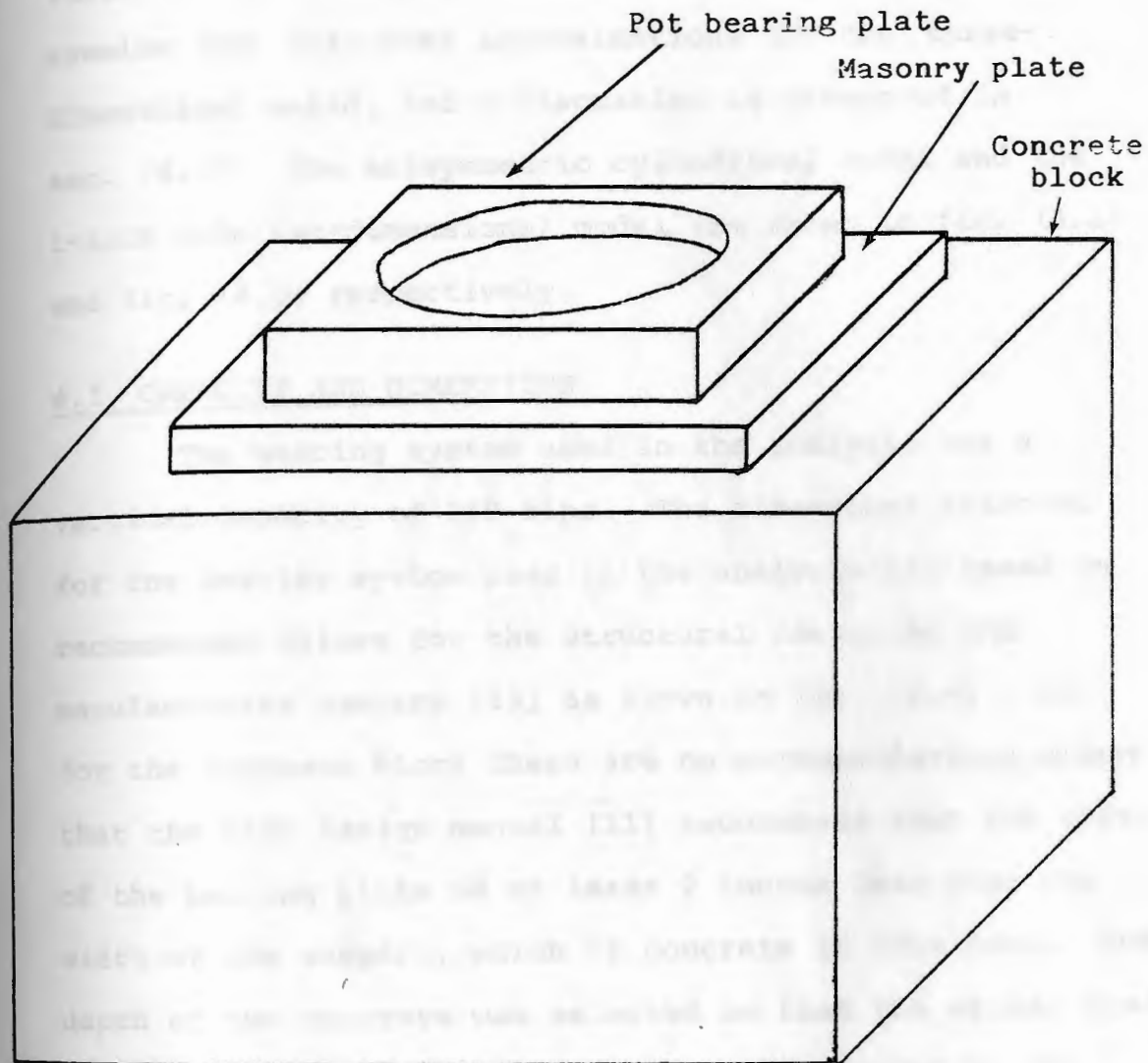
Fig. (4.1)   Three-dimensional solid model

stress model. Example problems have been executed to examine the different approximations of the three-dimensional solid, and a discussion is presented in sec. (4.3). The axisymmetric cylindrical model and the 1-inch wide two-dimensional model are shown in fig. (4.2) and fig. (4.3) respectively.

4.1 CAPACITY AND DIMENSIONS

The bearing system used in the analysis has a vertical capacity of 150 kips. The dimensions selected for the bearing system used in the analysis are based on recommended values for the structural design by the manufacturing company [10] as shown in fig. (4.4). As for the concrete block there are no recommendations except that the AISC design manual [11] recommends that the width of the bearing plate be at least 2 inches less than the width of the support, which is concrete in this case. The depth of the concrete was selected so that the stress distribution on the top of it will not be affected by the boundary conditions applied at the nodal points at the bottom supports. For the axisymmetric model, all square surfaces are changed to circular such that, referring to fig. (4.4), (A) is the radius of the pot bearing plate, (B) is the radius of the masonry plate, and (C) is the radius of the concrete surface.

Uniformly applied load

Circular pot bearing plate

Circular masonry plate

Concrete cylinder

Fig. (4.2) Axisymmetric cylindrical model

Uniformly applied load

Pot bearing plate

Masonry plate

Concrete
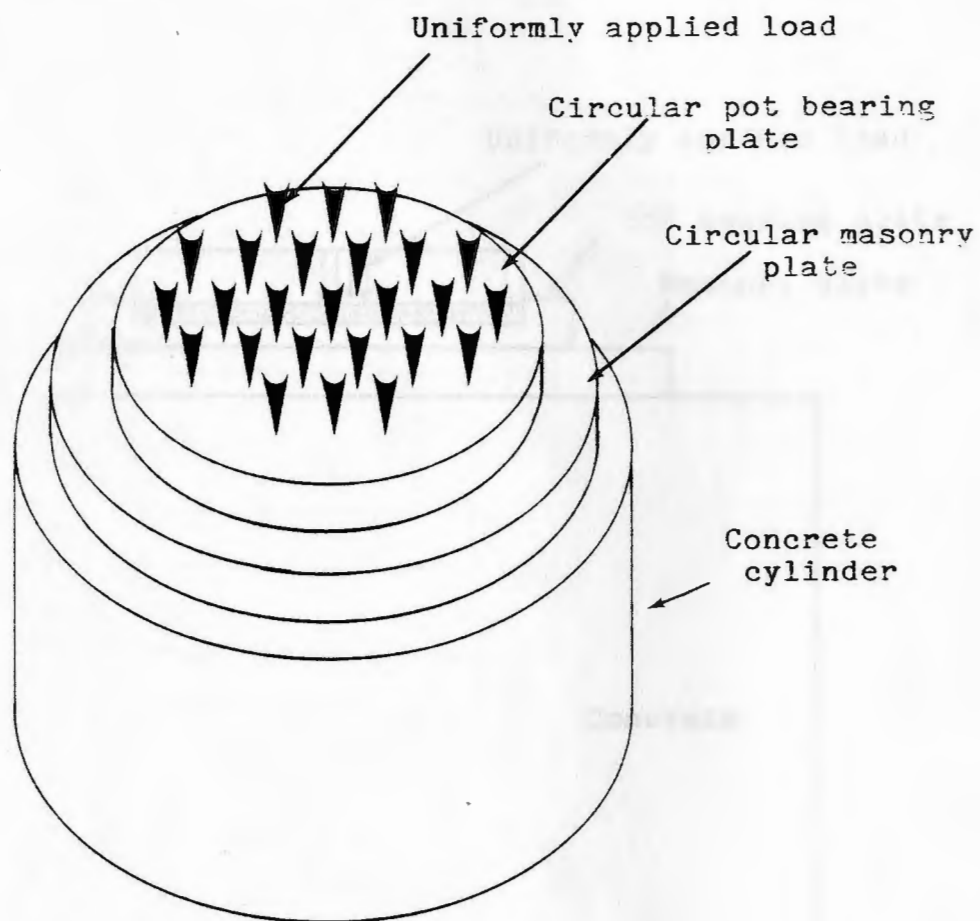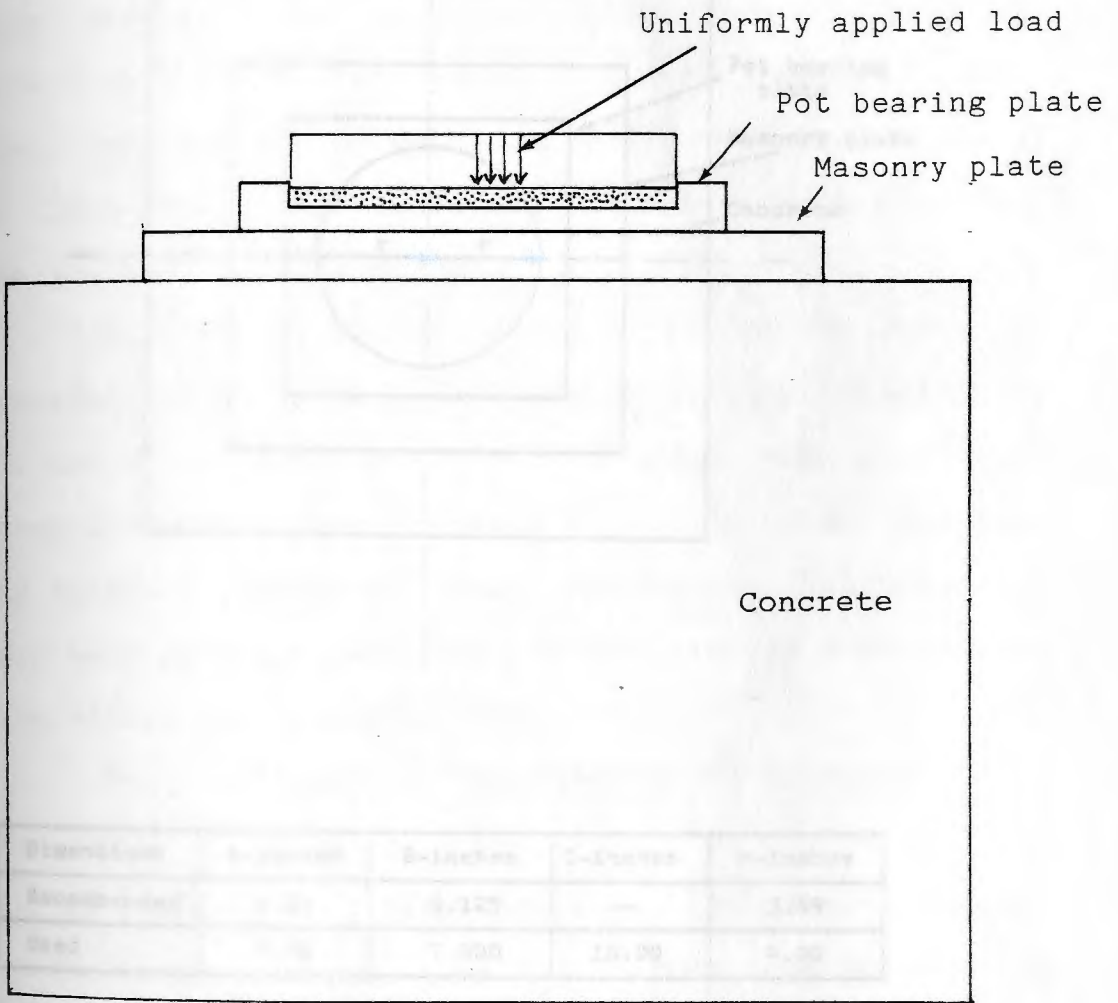
Fig. (4.3)   Two-dimensional 1-inch wide model

Fig. (4.4) Dimensions of 150-Kips bearing system
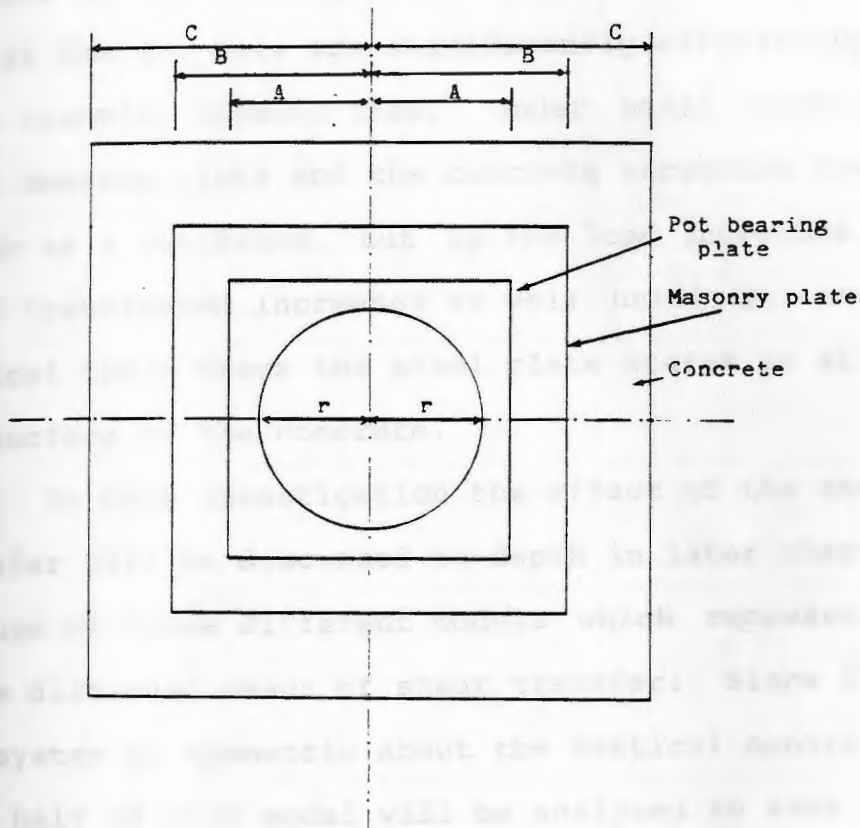
Dimensions	A-inches	B-inches	C-inches	r-inches
Recommended	4.56	6.125	--	3.69
Used	5.00	7.000	10.00	4.00

4.2 THE FINITE ELEMENT GRID SYSTEMS FOR THE DIFFERENT SHEAR TRANSFER CONDITIONS

Preliminary studies have shown that bending stresses in the bearing plates and the stress distribution in the concrete are significantly affected by the shear transfer between them. Under small loads, the steel bearing plate and the concrete structure tend to behave as a continuum, but as the load increases, the shear transferred increases as well until it reaches a critical limit where the steel plate starts to slip over the surface of the concrete.

In this investigation the effect of the shear transfer will be discussed in depth in later chapters by the use of three different models which represent the three different cases of shear transfer. Since the bearing system is symmetric about the vertical central axis, only half of each model will be analyzed to save calculation effort and computer time.

The following are the three cases of shear transfer:

1) The case of zero shear transfer. There is no shear force transferred along the contact zone between the steel masonry plate and the concrete abutment. The finite element grid system shown in fig. (4.5) consists of 165 nodes and 132 elements. The interface zone is represented by stiff springs (one-

Steel
E = 29000 Ksi
ν = 0.25

Concrete
E = 3605 Ksi
ν = 0.180
f'_c = 4 Ksi

132 Elements
165 Nodes

Node 53
Element 49

Node 67
Element 63

inches

inches
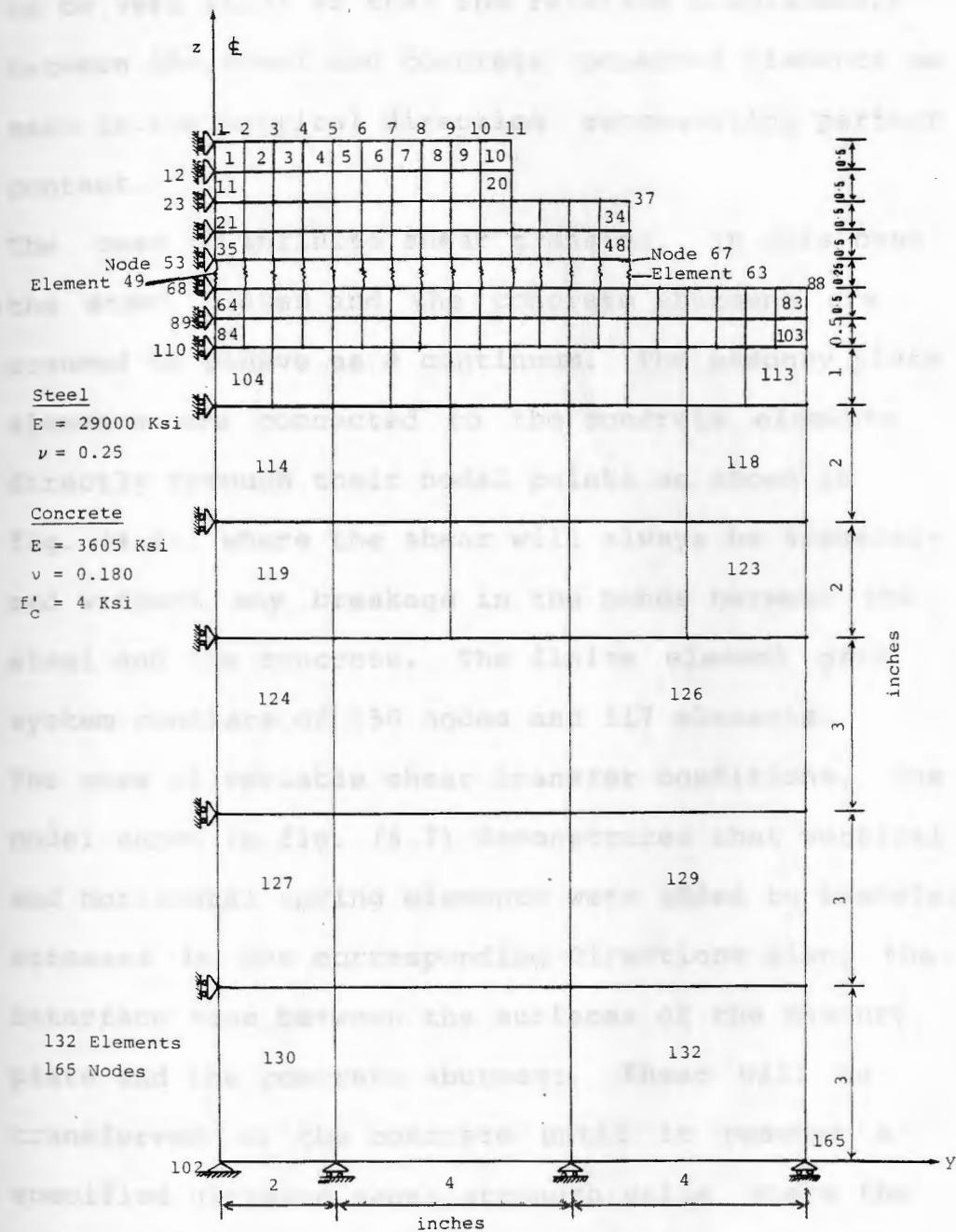
Fig. (4.5) Finite element grid system for the zero shear transfer case.

dimensional truss elements) which only transfer axial stresses. The springs are linear-elastic; they have to be very stiff so that the relative displacement between the steel and concrete connected elements be zero in the vertical direction representing perfect contact.

2) The case of infinite shear transfer. In this case the steel plates and the concrete abutment are assumed to behave as a continuum. The masonry plate elements are connected to the concrete elements directly through their nodal points as shown in fig. (4.6), where the shear will always be transferred without any breakage in the bonds between the steel and the concrete. The finite element grid system consists of 150 nodes and 117 elements.

3) The case of variable shear transfer conditions. The model shown in fig. (4.7) demonstrates that vertical and horizontal spring elements were added to transfer stresses in the corresponding directions along the interface zone between the surfaces of the masonry plate and the concrete abutment. Shear will be transferred to the concrete until it reaches a specified ultimate shear strength value, where the bonds will break and the masonry plate will start to slip over the surface of the concrete abutment. Characteristics of all material elements are presented
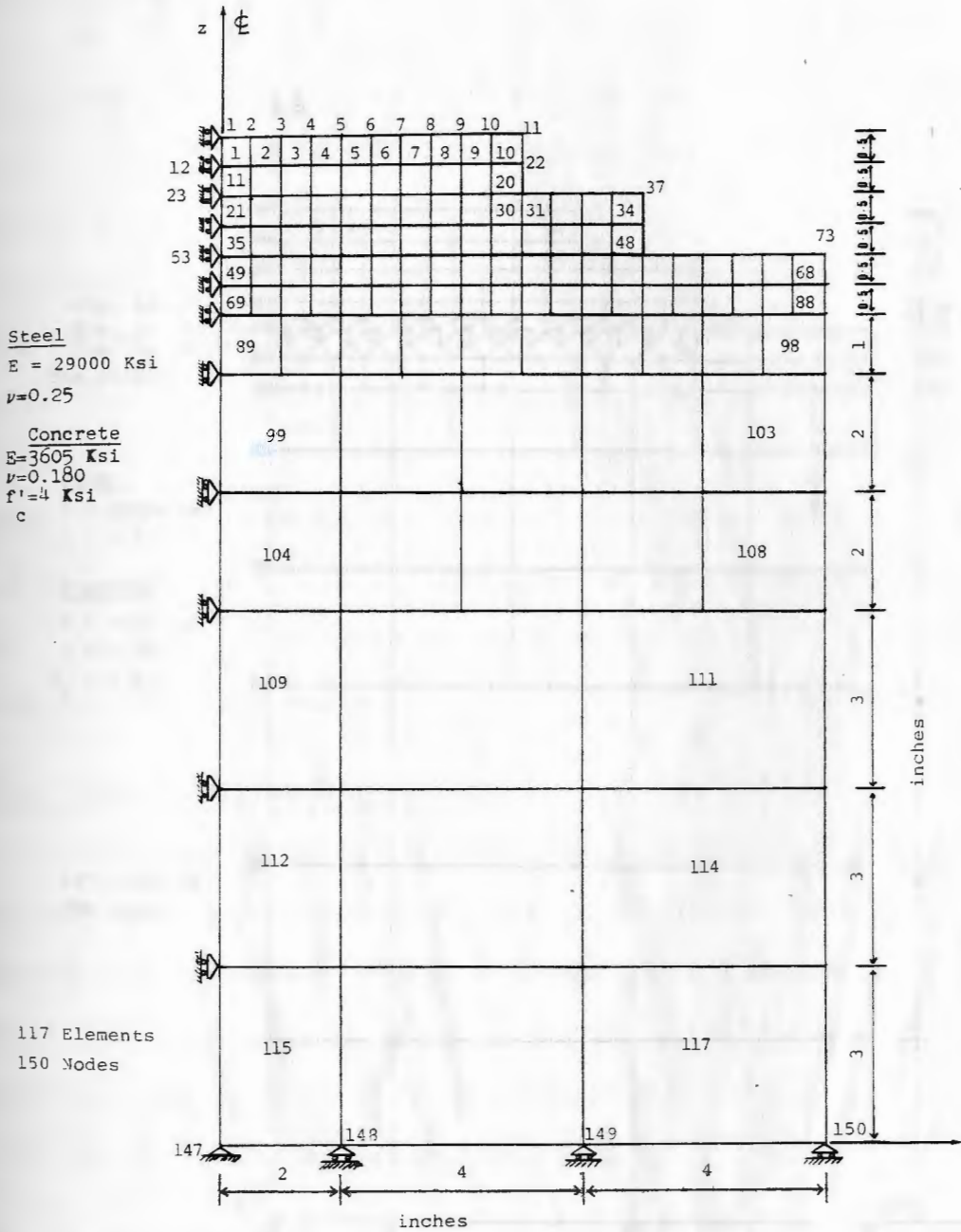
Fig. (4.6)   Finite element grid system for the continuum case.
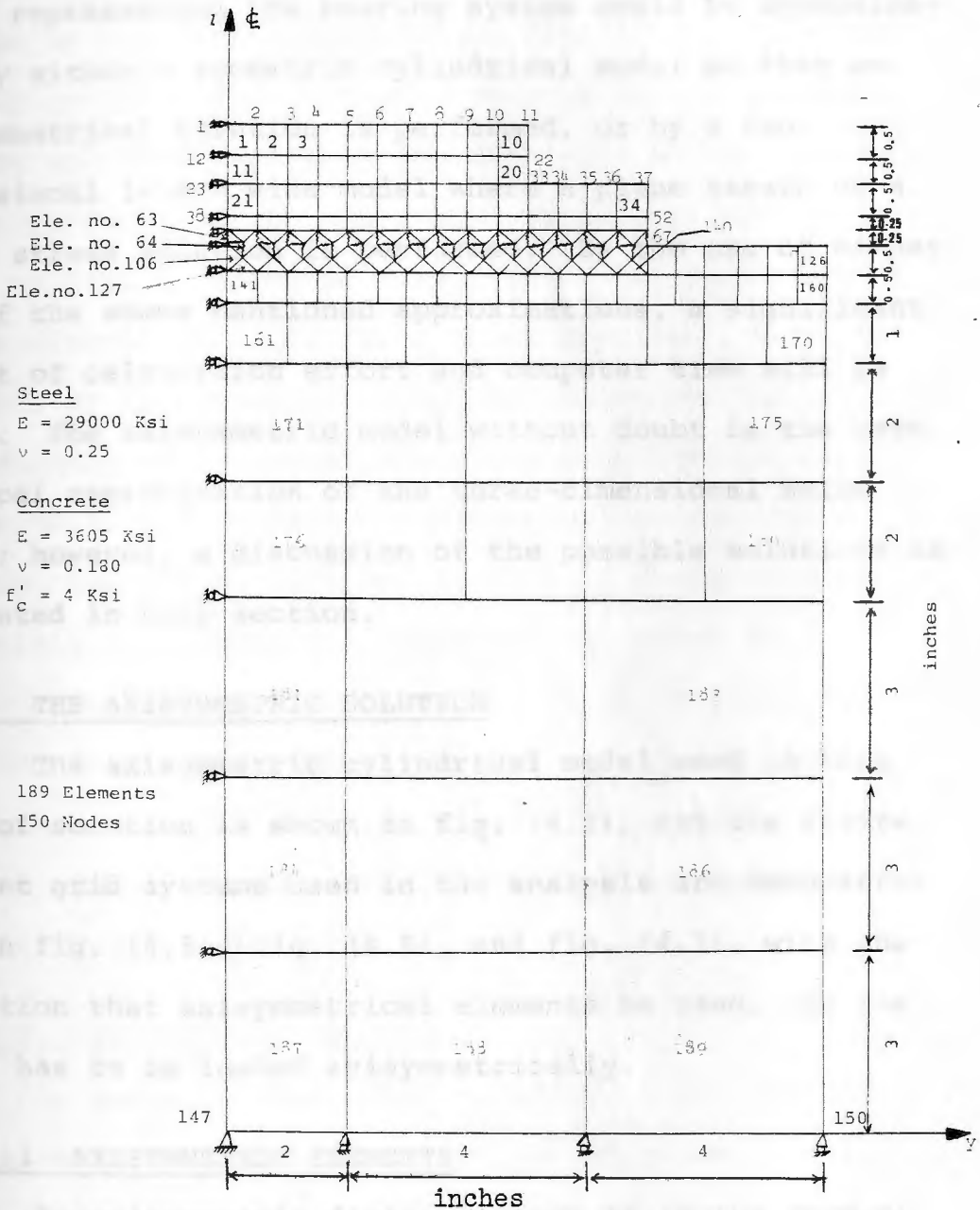
Fig. (4.7) Finite element grid system for the bearing
system including interface spring elements.

presented in chapter 5.

4.3 POSSIBLE SOLUTION METHODS

As mentioned above, the three-dimensional solid model representing the bearing system could be approximated by either a symmetric cylindrical model so that an axisymmetrical solution is performed, or by a two-dimensional 1-inch wide model where a plane strain or a plane stress solution is performed. By the use of either one of the above mentioned approximations, a significant amount of calculation effort and computer time will be saved. The axisymmetric model without doubt is the best physical approximation of the three-dimensional solid model; however, a discussion of the possible solutions is presented in this section.

4.3.1 THE AXISYMMETRIC SOLUTION

The axisymmetric cylindrical model used in this type of solution is shown in fig. (4.2), and the finite element grid systems used in the analysis are demonstrated in fig. (4.5), fig. (4.6), and fig. (4.7), with the condition that axisymmetrical elements be used, and the model has to be loaded axisymmetrically.

4.3.1.1 AXISYMMETRIC ELEMENTS

An axisymmetric finite element is in the form of a ring of constant cross-section as shown in fig. (3.4).

The element is usually described in a cylindrical co-ordinate system whose axis of symmetry is the (z-axis) and for which radial distances are defined by the co-ordinate (r) and the circumferential coordinate is de-scribed by an angle θ as shown in fig. (4.8). However, in this investigation the axisymmetric set of elements will be selected such that (z-axis) will be the axis of symmetry, (y-axis) is the radial direction and $\theta = 1$ radians as shown in fig. (4.9). The nodal points of the element are, in fact, nodal circles. Thus, the analysis of axisymmetric solids for axisymmetric loads is a two-dimensional problem since the displacement field can be described by just two components on the cross-section, the radial (u_y) and axial (u_z) displacements. The strain components are radial (ε_y), axial (ε_z), circumferential (ε_θ), and shearing (γ_{yz}) strains. The corresponding stress components are σ_y, σ_z, σ_θ, and τ_{yz}. Circumferential stresses and strains exist because the uniform radial displacement increases the circumferen-tial (or hoop) length [7].

4.3.1.2 AXISYMMETRIC LOADING

As shown in fig. (4.2) and fig. (4.3), the uni-form load is applied directly to the elastomeric disc which is 8 inches in diameter. Referring to fig. (4.9), (A) is the loaded area where

$$A = \sum_{i=1}^{8}$$ (4.1)

and if (P) is the uniformly applied load, then the resultant load is (R), where

$$R = P \cdot A$$ (4.2)

but since the analysis is done by the finite element method, then nodal forces $(R_n, n=1$ to 9) have to be calculated. The method followed in this study is to calculate the resultant load (R_i) applied to each area (A_i) shown in fig. (4.9), and ...
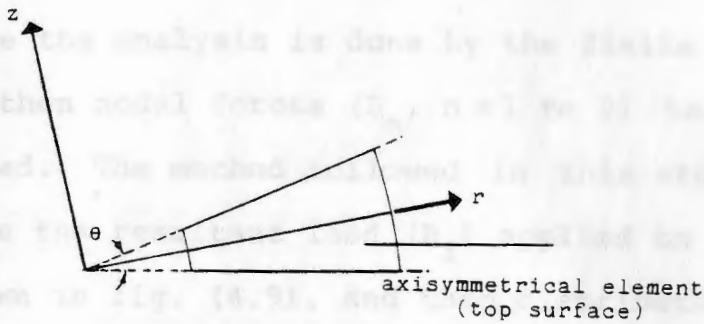
Fig. (4.8) Cylindrical coordinates.

Let r_i be the y-coordinate (radial) of the ith nodal point, such that $r_1 = 0$, r_2 is the y-coordinate of point 2, etc., then
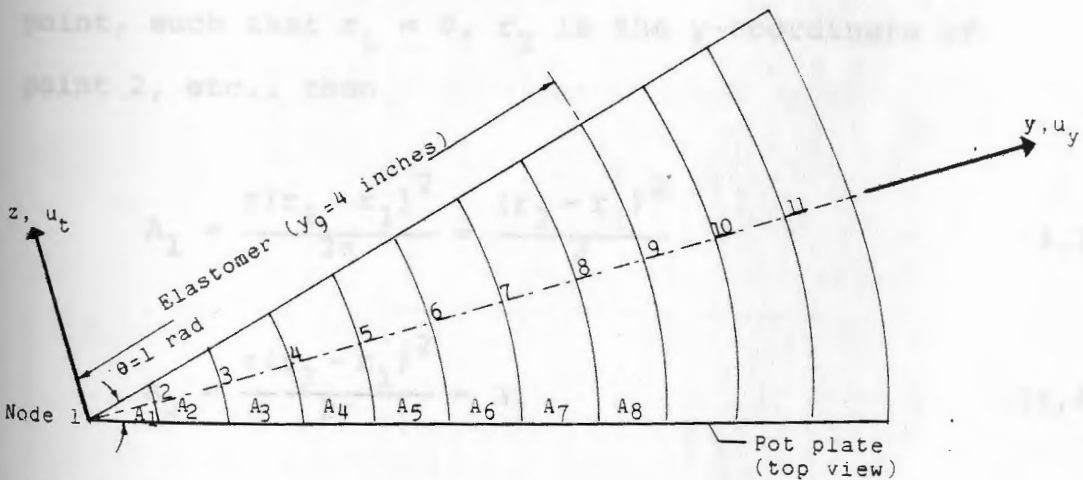
Fig. (4.9)   Top view of the axisymmetric section of the pot plate.

$$A = \sum_{i=1}^{8} A_i \tag{4.1}$$

and if (P) is the uniformly applied, load, then the resultant load is (R), where

$$R = P \cdot A \tag{4.2}$$

but since the analysis is done by the finite element method, then nodal forces (L_n, n = 1 to 9) have to be calculated. The method followed in this study is to calculate the resultant load (R_i) applied on each area (A_i) shown in fig. (4.9), and then distributing them on the nodal points.

Let r_i be the y-coordinate (radial) of the ith nodal point, such that $r_1 = 0$, r_2 is the y-coordinate of point 2, etc., then

$$A_1 = \frac{\pi (r_2 - r_1)^2}{2\pi} = \frac{(r_2 - r_1)^2}{2} \tag{4.3}$$

$$A_2 = \frac{\pi (r_3 - r_1)^2}{2\pi} - A_1 \tag{4.4}$$

substituting (4.3) in (4.4),

$$A_2 = \frac{(r_3 - r_1)^2}{2} \quad \frac{(r_2 - r_1)^2}{2} \tag{4.5}$$

Node number n	Applied nodal Load (L_n)	Magnitude
1	L_1	$\frac{1}{3} R_1$
2	L_2	$\frac{2}{3} R_1 + \frac{1}{2} R_2$
3	L_3	$\frac{1}{2} (R_2 + R_3)$
4	L_4	$\frac{1}{2} (R_3 + R_4)$
5	L_5	$\frac{1}{2} (R_4 + R_5)$
6	L_6	$\frac{1}{2} (R_5 + R_6)$
7	L_7	$\frac{1}{2} (R_6 + R_7)$
8	L_8	$\frac{1}{2} (R_7 + R_8)$
9	L_9	$\frac{1}{2} R_8$

$$\sum_{n=1}^{9} L_n = \sum_{i=1}^{8} R_i = R$$
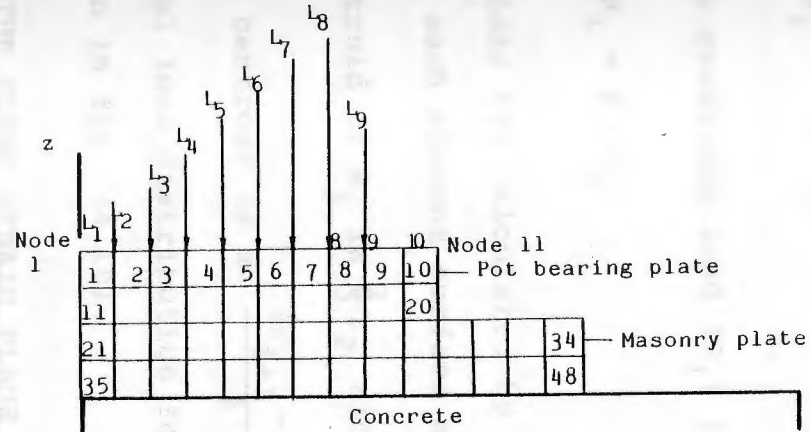
Fig. (4.10) Distribution of the axisymmetrical model nodal loads.

Generalizing (4.5),

$$A_i = \frac{(r_{i+1} - r_1)^2}{2} - \frac{(r_i - r_1)^2}{2} \text{ , } i = 2 \text{ to } 8 \quad (4.6)$$

then the resultant load (R_i) is

$$R_i = P \cdot A_i \quad\quad\quad\quad\quad\quad (4.7)$$

Nodal loads are calculated by proportioning the resultant load of each element surface area. It is assumed that the centroid of A_i is $\frac{2}{3} r_2$ along the y-axis, where for A_i, the centroid is at $\frac{(r_{i+1} - r_i)}{2}$, (i = 2 to 8). The nodal load distribution for the axisymmetrical model is shown in fig. (4.10).

4.3.2 THE PLANE STRAIN PLANE STRESS SOLUTION

The two-dimensional 1-inch wide model used in this type of solution is shown in fig. (4.3). The finite element grid systems for the plane strain or plane stress solution are the same used for the axisymmetrical problem. However, plane strain or plane stress elements are used instead of axisymmetrical elements. The uniform load is distributed evenly among the nodal points of the loaded surface except for the ones which are on its edges as explained in sec. (4.3.2.3).

3.2.1 PLANE STRAIN ELEMENTS

Consider the plane strain element shown in fig. (3.4); the element is fixed against displacement in the x-direction. Under this condition, the longitudinal strain (ε_x) is zero, as well as the shear stresses (τ_{yx}) and (τ_{zx}) [7].

3.2.2 PLANE STRESS ELEMENTS

A plane stress element is shown in fig. (3.4). The element is assumed to be very thin so that the in-plane stresses (σ_y and σ_z) and the shearing stresses (τ_{zy} and τ_{yz}) are constant across the thickness (t). Nevertheless, the out-of-plane stress (σ_x) and the shear stresses (τ_{yx} and τ_{zx}) are assumed to be negligible.

4.3.2.3 PLANE STRAIN PLANE STRESS LOADING

A top view of the loaded pot plate is shown in fig. (4.11), considering that a 1-inch wide strip was cut out from the bearing system so that it could be analyzed as a two-dimensional model representing the structure. All areas shown in fig. (4.11) are 1-inch wide and of equal lengths (b). If the uniformly applied load is (P), then the resultant load (R_i) in equation (4.7) is equal for all areas. The nodal load distribution for the plane strain or plane stress model is shown in fig. (4.12).
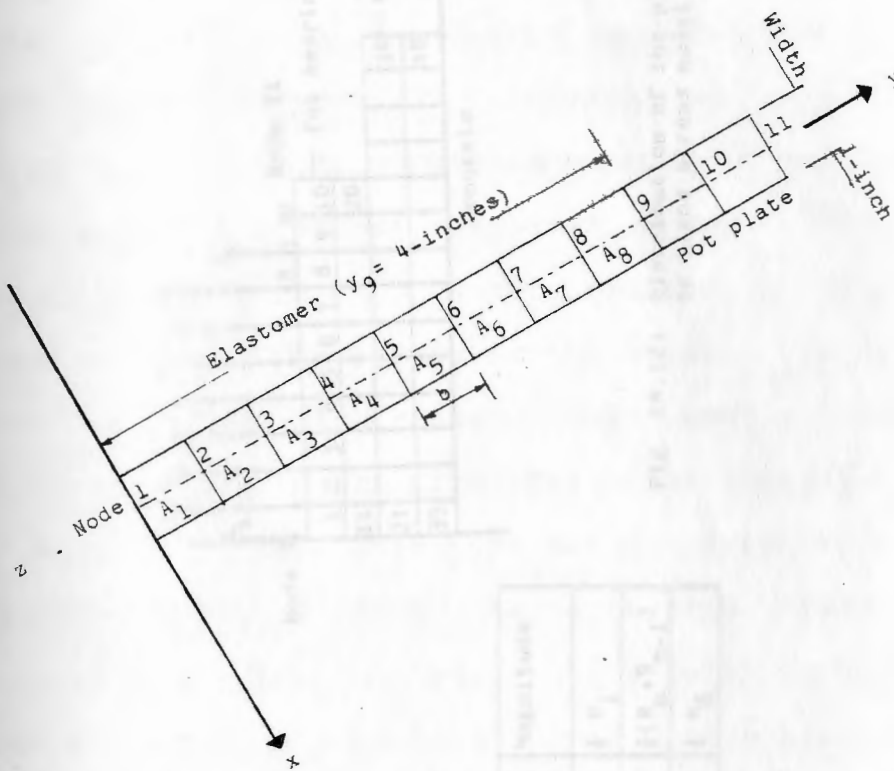
Fig. (4.11)   Top view of the plane-strain or plane-stress
section of the pot plate.

Fig. (4.12) Distribution of the plane strain or plane stress nodal loads.

Node number n	Applied nodal Load (L_n)	Magnitude
1	L_1	$\frac{1}{2} R_1$
n=2 to 8	L_n	$\frac{1}{2}(R_n + R_{n-1})$
9	L_9	$\frac{1}{2} R_8$

4.3.3 A COMPARATIVE LOOK AT THE PROPOSED SOLUTION METHODS

It has been mentioned earlier that an axisymmetrical solution would seem to be the best approximation to analyze the three-dimensional solid system shown in fig. (4.1), from a physical point of view. However, analytically, the characteristics of the elements discussed in section (4.3) indicate that in plane strain or plane stress problems, the internal work is always associated with three strain components in the coordinate plane (y,z). The stress component normal to this plane, (out-of-plane stresses), is not involved due to zero values of either the stress or the strain. In the axisymmetric problem, any radial displacement automatically induces a strain in the circumferential direction. As the stresses in this direction are non-zero, this fourth component of strain and of the associated stress has to be considered. Nevertheless, in any solution method, internal work in a structure should always balance the external work to satisfy the equilibrium condition. Hence, stresses in the bearing system are expected to be larger when using a plane stress or plane strain solution method, [12].

CHAPTER 5

MATERIAL ELEMENT MODELS

The modeling of the bearing system has been discussed in chapter (4), however, the discussion of the material element models which represent the properties and behavior of the different materials used in the construction of such a structure, is left to this chapter.

The different materials used in the construction of the bearing system are divided into three main groups, 1) steel, which is used to manufacture the pot bearings and masonry plates, 2) concrete, which is usually used to build abutments for such structures, and 3) material model to simulate the interface between the steel masonry plate and the concrete abutment. It is noteworthy here to point out that there is no such material that exists in nature; however, it is essential for the completion of this investigation to develop certain material models which best approximate the behavior of the interface zone depending on which case of shear transfer is being investigated, see sec. (4.2). Since it is assumed that the load will be uniformly applied in all loading stages at all times, there were no material elements used to represent the elastomeric material, see chapter (1).

Nevertheless, a complete discussion of the elastomeric material properties and behavior is presented in the National Cooperative Highway Research Program Report 248 [13].

5.1 STEEL ELEMENTS

All bearing plates used in the bearing system under investigation are fabricated from ASTM A-36 steel, the pot being machined from a solid steel plate to provide complete security and eliminate welding and distortion problems. All surfaces internal and external are treated with a 10 mil epoxy coal tar paint system to resist corrosion.

According to the manufacturing company, Spencer Dynamics [10], bending stresses used in the design of the bearings are a maximum of 16 Ksi; due to the rather conservative stressing method and design assumptions, actual stresses are about half this value. Thus, the bearing plates can be supplied proof-loaded to twice the rated capacity specified for the bearing system, under investigation, as 150 Kips. Hence, if the bearing was loaded uniformly by a relatively small load, such as 3500 Psi, the steel plate will not yield, and it will always stay in the elastic range. With respect to the above-mentioned information, a linear elastic isotropic material model was used to represent all the steel ele-

ments of the pot bearing and masonry plates.

1.1 LINEAR ELASTIC ISOTROPIC MODEL

This model assumes that the elements of the constitutive matrix are constant, i.e., independent of magnitude or history of stresses and strains. The material (property) matrix, which relates element strains to element stresses in (3.9), is formed from the two elastic constants E (Young's modulus of elasticity) and ν (Poisson's ratio) [9].

For axisymmetric analysis the material matrix is,

$$[C] = \begin{bmatrix} C_1 & C_2 & 0 & C_2 \\ C_2 & C_1 & 0 & C_2 \\ 0 & 0 & C_3 & 0 \\ C_2 & C_2 & 0 & C_1 \end{bmatrix} \tag{5.1}$$

where

$$C_3 = \frac{E}{2(1 + \nu)}. \tag{5.1.a}$$

$$C_2 = \frac{2\nu C_3}{(1 - 2\nu)} \tag{5.1.b}$$

$$C_1 = C_2 + C_3 \tag{5.1.c}$$

and the corresponding stress σ and strain ε vectors are, for example, in small displacement analysis at time (t)

$$\{{}^t\sigma_{yy} \quad {}^t\sigma_{zz} \quad {}^t\sigma_{yz} \quad {}^t\sigma_{xx}\};$$

$$\{{}^t\varepsilon_{yy} \quad {}^t\varepsilon_{zz} \quad {}^t\varepsilon_{yz} \quad {}^t\varepsilon_{xx}\}$$

respectively.

5.2 CONCRETE ELEMENTS

No one mathematical model can describe the actual behavior and strength of concrete materials because it is very complex, however, the properties that are essential to the problem being considered will be represented by a simple model.

Typical concrete compressive stress - strain curves are shown in in fig. (5.1) obtained by appropriate strain measurements on cylinder tests at moderate testing spees on concrete 28 days old, for various cylinder compressive strength f'_c [14]. All curves shown in the figure have somewhat similar character. They consist of an initial relatively straight elastic portion, then begin to curve to the horizontal, reaching the maximum compressive strength at a strain of approx-
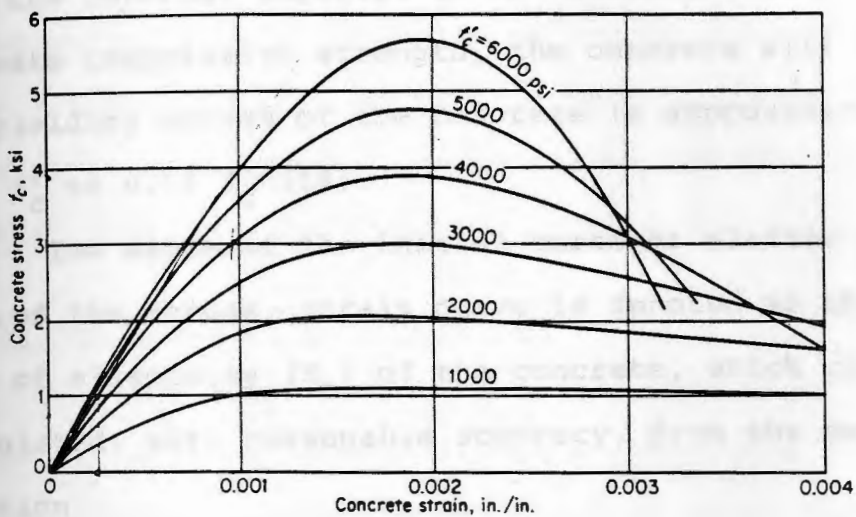
Fig. (5.1) Typical concrete compressive
stress-strain curves

imately 0.002 in/in, and finally show a descending branch. This is described as the elastic - plastic behavior of the concrete, which is attributed to the fact that under uniformly applied load, increasing at a moderate speed, micro cracks within the concrete will take place and become larger as the load increases. When the internal stresses in the concrete reach the ultimate compressive strength, the concrete will crush. The yielding stress of the concrete is approximately 0.45 f'_c to 0.50 f'_c [14].

The slope of the initial straight elastic portion of the stress - strain curve is denoted as the modulus of elasticity (E_c) of the concrete, which could be calculated, with reasonable accuracy, from the empirical equation

$$E_c = 33 \ w^{3/2} \ \sqrt{f'_c} \quad \text{Psi} \tag{5. 2}$$

where w is the unit weight of the hardened concrete in pcf. Equation (5.2) has been obtained by testing structural concretes with values of w from 90 to 155 pcf.

Tensile strength (f_t) is a more variable property than compressive strength, and is about 0.10 f'_c to 0.15 f'_c [14]. It has been found to be proportional to $\sqrt{f'_c}$. The ACI code has indirectly used $f_t = 6.7 \ \sqrt{f'_c}$ psi for normal-weight concrete and

$f_t = 5.7 \sqrt{f_c'}$ for all light-weight concrete (ACI-11.2).

There are two elastic-plastic material models available in the NONSAP library, elastic-plastic von Mises yield condition, and elastic-plastic Drucker Prager yield condition, see table (3.3). However, the latter is formulated for an elastic - perfectly plastic material behavior; hence the concrete element in this investigation will be represented by the elastic-plastic von Mises yield condition element material model, assuming that it is the best approximation of the concrete stress - strain curve discussed above.

5.2.1 von MISES YIELD CONDITION

The von Mises yield criterion considers the octahedral shearing stress as the key variable for causing yield of materials which are pressure independent. It states that yielding begins when the octahedral shearing stress reaches a critical value, K, which is defined as the yield stress in pure shear, such that the octahedral shearing stress is, [3]:

$$\tau_{oct} = \sqrt{\frac{2}{3} J_2} = \sqrt{\frac{2}{3}} \ K \qquad (5.3)$$

where (J_2) is the second invariant of the deviatoric stress vector. The material yielding function is obtained by reducing (5.3) to the simple form

$$f(J_2) = J_2 - K^2 = 0 \qquad (5.4)$$

5.2.2   DEVIATORIC STRESS INVARIANTS

Consider the general stress matrix $[\sigma_{ij}]$ where

$$[\sigma_{ij}] = \begin{bmatrix} \sigma_y & \tau_{yz} & \tau_{yz} \\ \tau_{zy} & \sigma_z & \tau_{xz} \\ \tau_{xy} & \tau_{xz} & \sigma_x \end{bmatrix}, \quad \frac{i}{j} = 1,2,3 \quad (5.5)$$

for the solid shown in fig. (5.2), and let the principal stresses be defined as σ_1, σ_2, and σ_3.

The deviatoric stress vector which represents a state of pure shear is defined by

$$[S_{ij}] = [\sigma_{ij}] - \sigma_m [\delta_{ij}] \qquad (5.6)$$

where

$$\sigma_m = \frac{1}{3}(\sigma_y + \sigma_z + \sigma_x)$$

and δ_{ij} is the Kronecker delta such that

$$\delta_{ij} = \begin{vmatrix} +1 & \text{if } i = j \\ 0 & \text{if } i \neq j \end{vmatrix}$$

The invariants of $[S_{ij}]$ are obtained by setting the determinant of $[S_{ij} - S\delta_{ij}]$ equal to zero, resulting in the cubic equation

$$S^3 - J_1 S^2 - J_2 S - J_3 = 0 \qquad (5.7)$$

where σ_1, σ_2 and σ_3 are the three invariants of the deviatoric stress vector.

Solving ...

$$\sigma_1 = \sigma_x + \sigma_y + \sigma_z = 0 \qquad (5.8.a)$$

$$\sigma_2 = \frac{1}{6}\left[(\sigma_y - \sigma_z)^2 + (\sigma_z - \sigma_x)^2 + (\sigma_x - \sigma_y)^2\right] \qquad (5.8.b)$$

$$+ \tau_{yz}^2 + \tau_{zx}^2 + \tau_{xy}^2$$

Fig. (5.2) General stress components.

If the coordinate axis (y, z, x) coincide with the principal directions where σ_1, σ_2 and σ_3 are the principal deviatoric stresses, then

$$J_1 = S_1 + S_2 + S_3 = 0 \qquad (5.9.a)$$

$$+ (\sigma_x - \sigma)^2] \qquad (5.9.b)$$

$$J_3 = \frac{1}{3}(S^3 = S_2^3 + S_3^3) = S_1 S_2 S_3 \qquad (5.9.c)$$
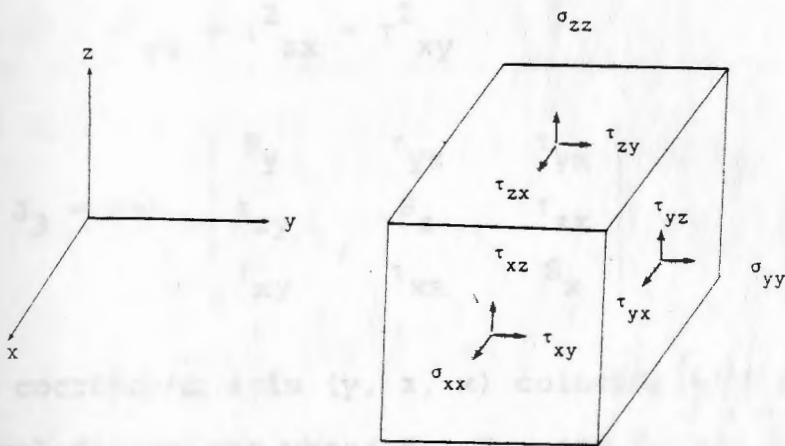
However, in a uniaxial tension test, yielding will occur when $\sigma_1 = \sigma_2$ and $\sigma_2 = \sigma_3 = 0$, where σ_1, σ_2, σ_3 are the

where J_1, J_2, and J_3 are the three invariants of the deviatoric stress vector.

Solving (5.7),

$$J_1 = S_y + S_z + S_x = 0 \qquad\qquad (5.8.a)$$

$$J_2 = \frac{1}{6} [\sigma_y - \sigma_z)^2 + (\sigma_z - \sigma_x)^2 + (\sigma_x - \sigma_y)^2]$$

$$+ \tau^2_{yz} + \tau^2_{zx} + \tau^2_{xy} \qquad\qquad (5.8.b)$$

$$J_3 = \text{det.} \begin{vmatrix} S_y & \tau_{yz} & \tau_{yx} \\ \tau_{zy} & S_z & \tau_{zx} \\ \tau_{xy} & \tau_{xz} & S_x \end{vmatrix} \qquad\qquad (5.8.c)$$

If the coordinate axis (y, z, x) coincide with the principal directions where S_1, S_2, and S_3 are the principal deviatoric stresses, then

$$J_1 = S_1 + S_2 + S_3 = 0 \qquad\qquad (5.9.a)$$

$$J_2 = (S_1^2 + S_2^2 + S_3^2) = \frac{1}{6} [\sigma_1 - \sigma_2)^2$$

$$+ (\sigma_3 - \sigma_1)^2] \qquad\qquad (5.9.b)$$

$$J_3 = \frac{1}{3} (S_1^3 + S_2^3 + S_3^3) = S_1 S_2 S_3 \qquad\qquad (5.9.c)$$

However, in a uniaxial tension test, yielding will occur when $\sigma_1 = \sigma_z$ and $\sigma_2 = \sigma_3 = 0$, where σ_1, σ_2, σ_3 are the

principal stresses.   Substituting in (5.9.b),

$$J_2 = \frac{\sigma_z^2}{3} \qquad (5.10)$$

and substituting (5.10) in (5.4),

$$K^2 = \frac{\sigma_z^2}{3} \qquad (5.11)$$

Then the general von Mises yield function is written, from (5.8.b) and (5.11), as

$$f(J_2) = \frac{1}{6} [(\sigma_y - \sigma_z)^2 + (\sigma_z - \sigma_x)^2 + (\sigma_x - \sigma_y)^2]$$
$$+ \tau_{yz}^2 + \tau_{zx}^2 + \tau_{xy}^2 - K^2 \qquad (5.12)$$

However, equation (5.12) only represents the simplest form of the yield function because it depends fully on the proposed hardening rule for work-hardening materials. A complete description of the NONSAP formulation of the elastic - plastic, von Mises yield criterion is presented in the NONSAP commentary [4] and ref. [9].

3 INTERFACE ELEMENTS

This investigation is primarily concerned with the study of the effect of the shear transfer between the masonry plate and the concrete abutment, on the stress distribution in the concrete, and on the steel bearing plates bending stresses. The analysis is done

by considering the three cases of shear transfer presented in sec. (4.2), however, because of their great importance, the interface material models for each case will be discussed separately in this section.

5.3.1   THE CASE OF ZERO SHEAR TRANSFER

The finite element grid system representing this case is shown in fig. (4.5) where the contact zone between the masonry steel plate and the concrete is modeled by very stiff spring elements.

The springs shown in the grid system are actually one-dimensional truss elements with one degree of freedom on each side, and they are only capable of transferring axial stresses. Hence, only vertical stresses will be transferred from the masonry steel plate elements to the concrete elements. Since the springs are very stiff, their axial displacement will approach zero, so that the vertical displacements of the connected nodes of the steel and concrete elements will be approximately equal, minimizing any portion of the vertical stresses absorbed for the springs axial deformation. However, since there will be no horizontal stresses (shear stresses) transferred, there will be nothing to prevent the bearing plates from slipping over the concrete surface.

There are two material models available in the NONSAP element library for truss elements, linear elastic or nonlinear elastic, see table (3.2).

However, since vertical springs here are only used to transfer vertical stresses, they will be represented by the linear elastic material model.

The stiffness matrix of each spring is

$$[K] = \frac{AE}{L} \begin{bmatrix} 1 & -1 \\ -1 & 1 \end{bmatrix}$$ (5.13)

where

A = the cross sectional area of the spring, calculated to be proportional to the connected areas of concrete and steel elements.

E = Young's modulus of elasticity

L = length of the spring.

It is noteworthy to point out that the stiffness of the springs is increased by selecting a very large (E), so the magnitudes of the area (A) and the length (L) of the springs will have very little significance.

5.3.2 THE CASE OF INFINITE SHEAR TRANSFER

The finite element grid system representing this case is shown in fig. (4.6) where no special consideration has been given to model the interface between the steel and the concrete. As shown in the grid system, the steel elements are directly connected to the concrete elements through their nodal points. In other words, the interface elements in this case are nothing

but the common nodal points of the two different materials. Hence, not only vertical stresses will be transferred, but shear stresses will be transferred infinitely as well, so that the steel bearing plates and the concrete will behave as a continuum.

5.3.3. THE CASE WITH SHEAR TRANSFERRED THROUGH INTERFACE ELEMENTS

The behavior of the interface between material elements is one of great complexity because of the difficulty in finding the most suitable function that describes the slip. Straight interface elements with linear description of slip between rock joints were first introduced by Goodman, Taylor and Brekke (1968) [15]. The bond behavior between steel and concrete was simulated by Ngo and Scordelis (1967) [16], with the help of linear springs placed between element nodes. However, this method leads to incompatibilities between nodes if higher order finite elements were used. Ghaboussi, Wilson and Isenberg (1969) [17,18], have also formulated an interface element covering a wide range of joint properties. Schafer (1975) [19], has developed straight bond elements with linear and parabolic behavior of slip. In 1977, Buragohain and Shah [20,21] proposed curved isoparametric line and axisymmetric interface elements with zero thickness to

simulate curved surfaces and parabolic variation of slip.

None of the interface elements mentioned above was used in this investigation. They were studied in order to help in developing the interface spring elements used to simulate the behavior of the interface zone between the masonry steel plate and the concrete abutment. It has been found that there are two different general approaches in modeling the interface zone. It could be represented by interface spring elements simply transferring horizontal and vertical stresses, or by two-dimensional finite elements. In either approach, the slip could be described by either linear or nonlinear functions as long as compatibility conditions are satisfied. In the following two sections, two different interface elements, each representing a different approach, will be introduced. The discussion of the interface spring elements used to simulate the interface zone in the bearing system will be left to chapter (6).

5.3.3.1 LINKAGE ELEMENT BY NGO AND SCORDELIS

The "linkage element" shown in fig. (5.3) consists of two linear springs parallel to a set of orthogonal local axes H and V. For generality, the linkage element can be oriented at any arbitrary angle θ with the global horizontal y-axis. The linkage element has no physical dimension at all, and only its mechanical properties are

Global
coordinates
z

y
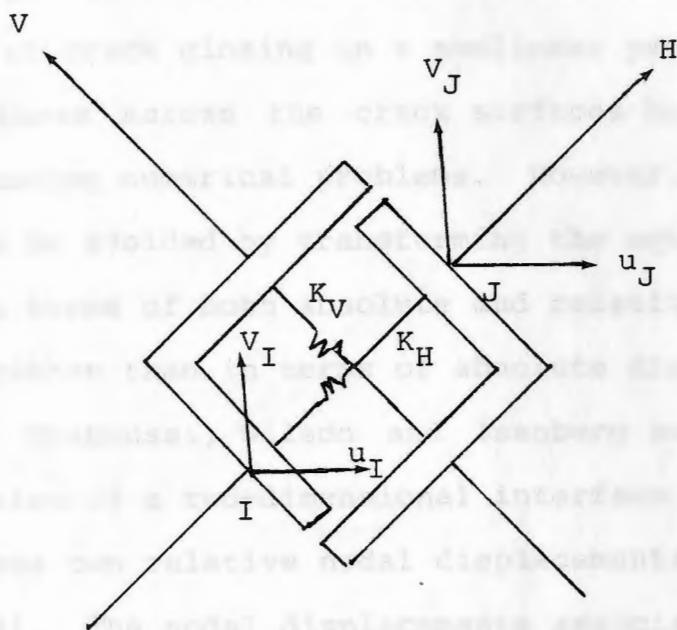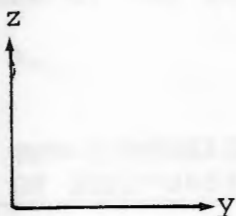
Fig. (5.3)   Linkage element.

of importance. Th erefore, it can be placed anywhere in the structure without disturbing its geometry. The formulation of the stiffness matrix is presented in Appendix A.

5.3.3.2 TWO-DIMENSIONAL INTERFACE ELEMENT BY GHABOUSSI, WILSON AND ISENBERG

At the interface of a structure there can be a significant change in stiffness of the different elements. In the case of crack closing in a nonlinear problem, the normal stiffness across the crack surfaces becomes infinite, causing numerical problems. However, those problems can be avoided by transforming the equilibrium equations in terms of both absolute and relative displacements rather than in terms of absolute displacements only. Ghaboussi, Wilson and Isenberg suggested the formulation of a two-dimensional interface element which involves two relative nodal displacements as shown in fig. (5.4). The nodal displacements associated with the interface element are shown in fig. (5.5), where u's and Δ's represent the absolute and relative displacements respectively. Notice that if the interface thickness h is considered to be very small compared to the size of the upper and lower two standard finite elements, then the assumption that strains do not vary in the thickness direction is valid. The physical behavior of the
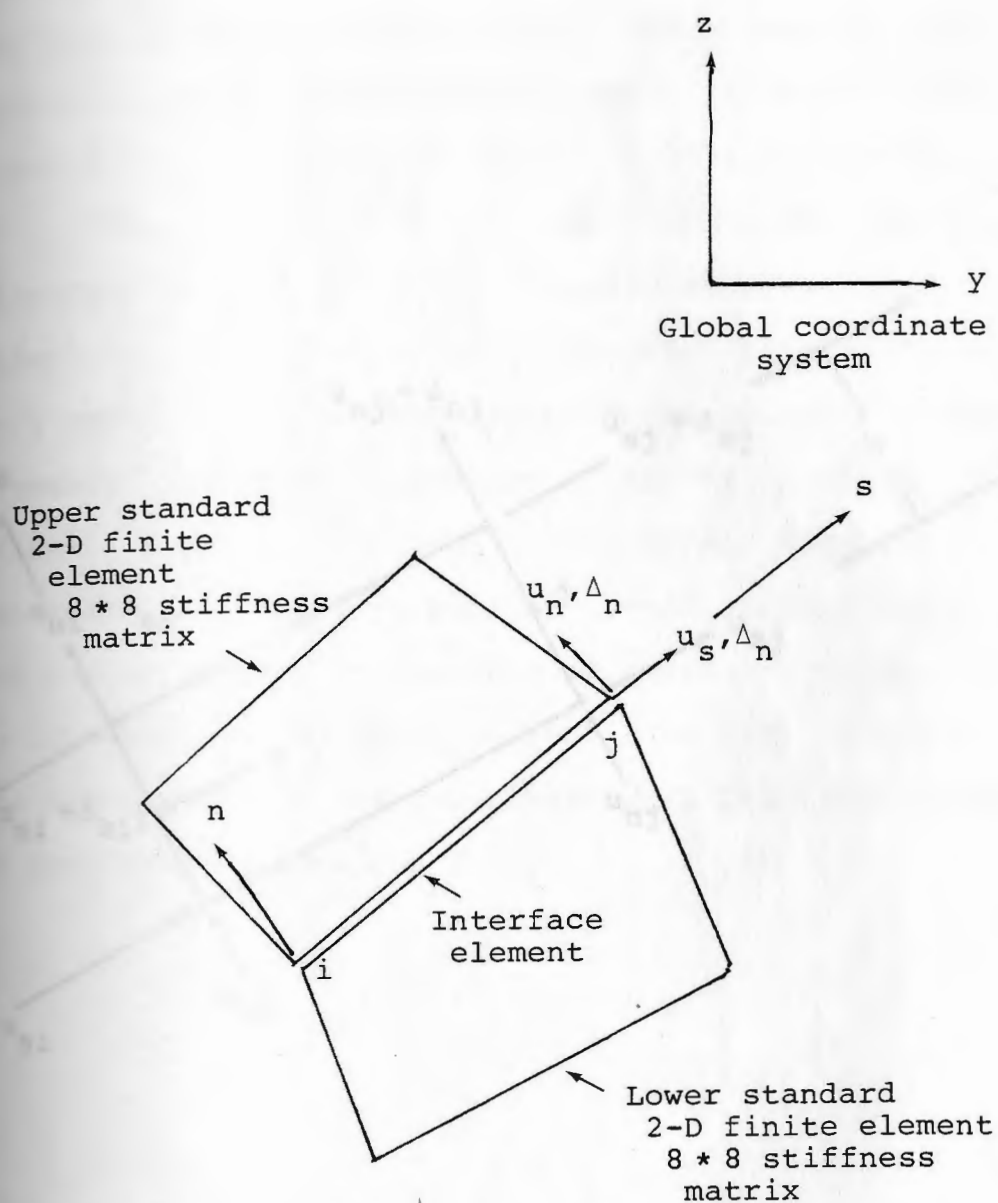
Fig. (5.4)   Two-dimensional interface element.
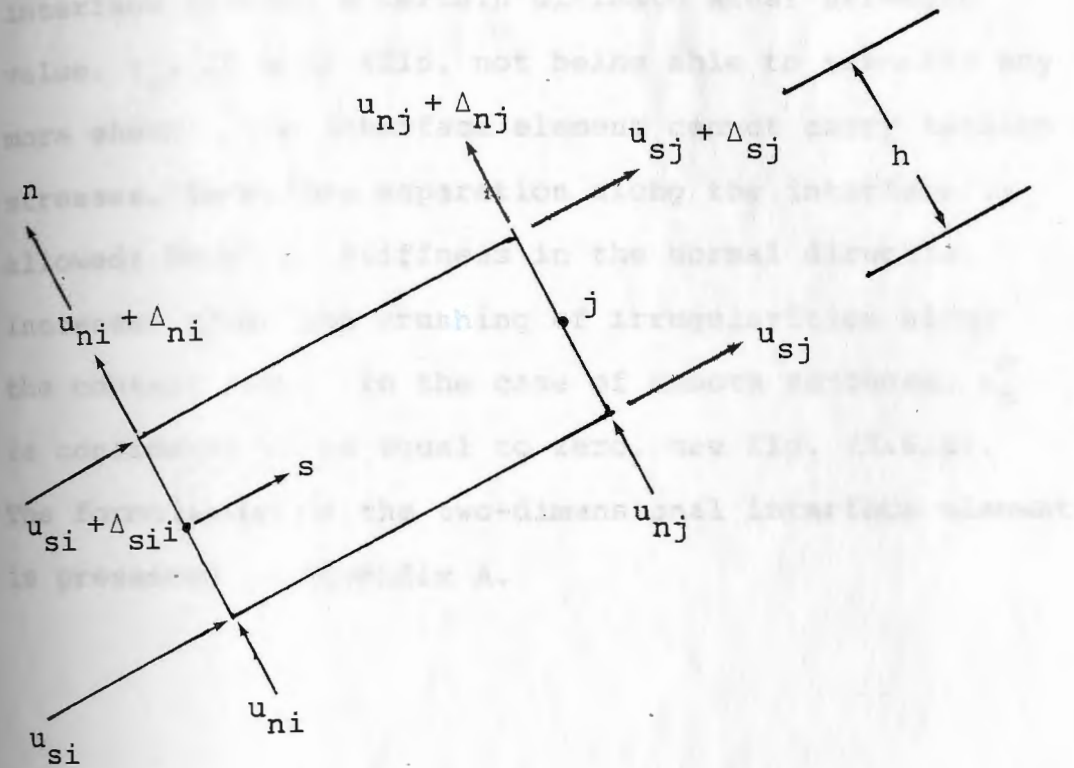
Fig. (5.5)   Interface element displacements.

two-dimensional interface element involves separation and slip along the contact zone. The stress - strain relations in the normal and horizontal direction are shown in fig. (5.6.a) and fig. (5.6.b) respectively.

When the shear stress transferred along the interface reaches a certain ultimate shear strength value, τ_u, it will slip, not being able to transfer any more shear. The interface element cannot carry tension stresses, therefore separation along the interface is allowed; however, stiffness in the normal direction increases after the crushing of irregularities along the contact zone. In the case of smooth surfaces, ε_n^c is considered to be equal to zero, see fig. (5.6.a). The formulation of the two-dimensional interface element is presented in Appendix A.

E_c, E_f = vertical stiffness of the IFE at different stress levels.

ε_n^c = Normal strain at which crushing occurs.
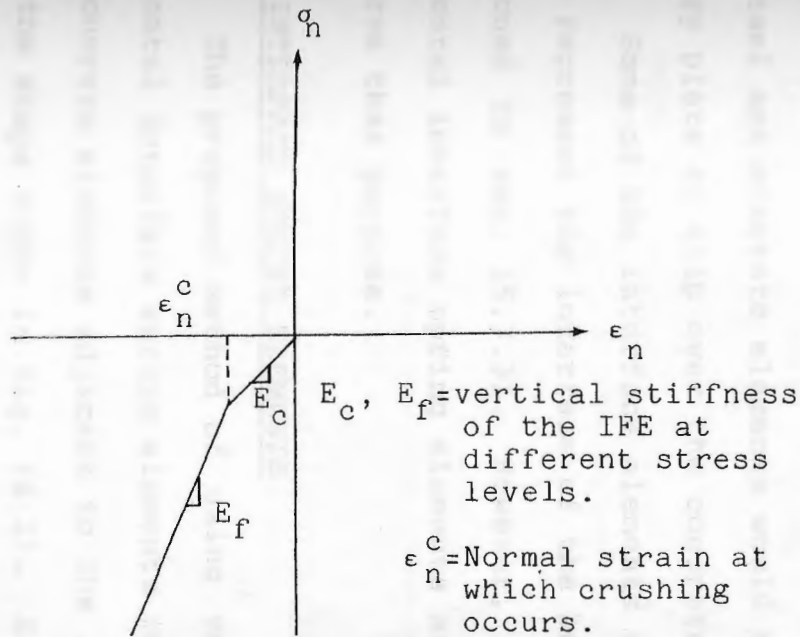
Fig. (5.6.a)   Stress-strain relation in the normal direction.

G = shear stiffness of the IFE.

τ_u = ultimate shear strength
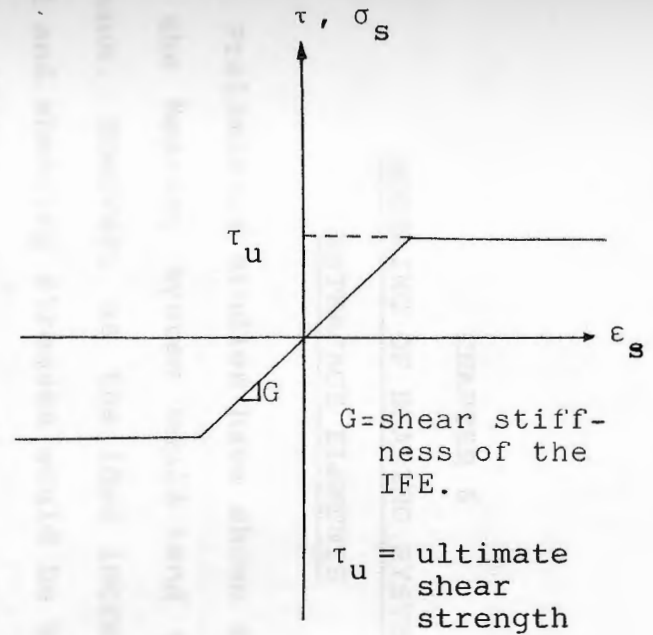
Fig. (5.6.b)   Stress-strain relation in the tangential direction.

CHAPTER 6

MODELING OF BEARING SYSTEM

INTERFACE ELEMENTS

Preliminary studies have shown that under small loads the bearing system would tend to behave as a continuum. However, as the load increases, larger normal and shearing stresses would be transferred along the interface zone between the masonry steel plate and the concrete abutment. When the shear stress reaches a certain ultimate shear strength value, the bond between the steel and concrete elements would break, causing the masonry plate to slip over the concrete surface.

Some of the interface elements which could possibly represent the interface of the bearing system were mentioned in sec. (5.3.3). However, vertical and horizontal interface spring elements are proposed here to serve that purpose.

6.1 INTERFACE SPRING ELEMENTS

The proposed method of using vertical and horizontal interface spring elements requires the steel and concrete elements adjacent to the interface zone to have the shape shown in fig. (6.1). Each vertical
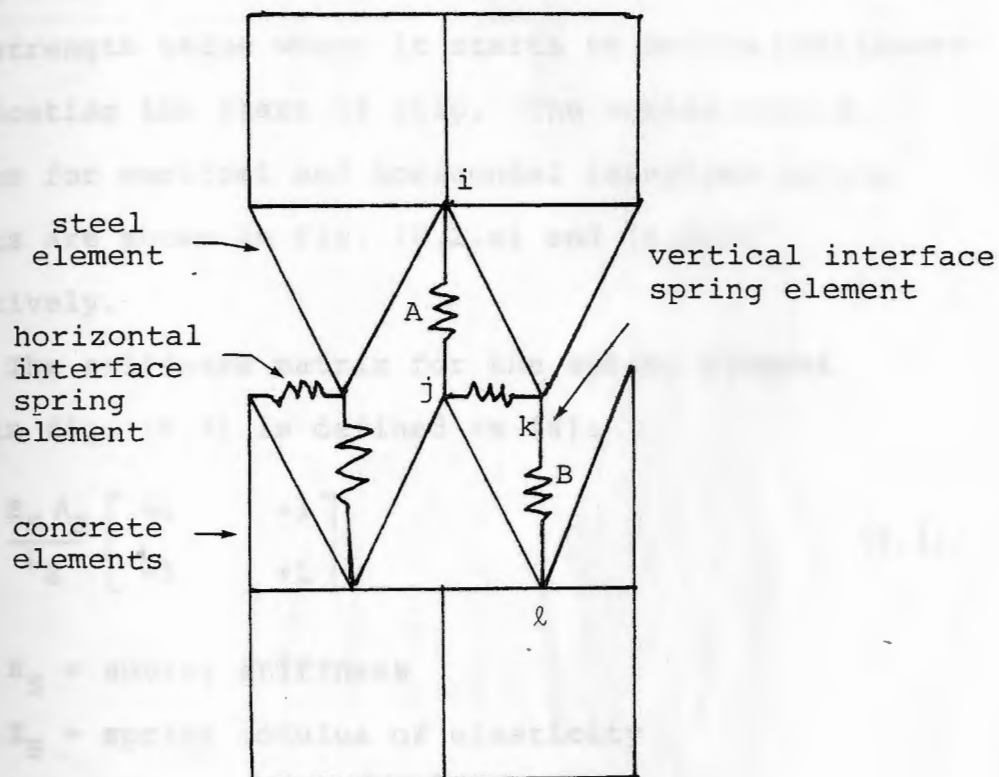
Fig. (6.1)   Vertical and horizontal interface
spring elements.

spring is assumed to be a linear-elastic one-dimensional element transferring normal stresses along its axis. On the other hand, each horizontal spring is assumed to be a nonlinear elastic-plastic one-dimensional element which stays in the elastic range until the shear transferred through it reaches an ultimate shear strength value where it starts to deform nonlinearly indicating the start of slip. The stress-strain diagrams for vertical and horizontal interface spring elements are shown in fig. (6.2.a) and (6.2.b) respectively.

The stiffness matrix for the spring element shown in fig. (6.3) is defined as [8]:

$$[K_S] = \frac{E_S A_S}{L_S} \begin{bmatrix} +1 & -1 \\ -1 & +1 \end{bmatrix} \tag{6.1}$$

where K_S = spring stiffness

E_S = spring modulus of elasticity

A_S = spring cross sectional area

L_S = length of the spring

and the spring stiffness equation is given as

$$\begin{Bmatrix} F_1 \\ F_2 \end{Bmatrix} = \begin{bmatrix} K_S \end{bmatrix} \begin{Bmatrix} u_1 \\ u_2 \end{Bmatrix} \tag{6.2}$$

σ_n

E_{SV}

ε_n

σ_n = normal stress

ε_n = normal strain

E_{SV} = vertical spring modulus of elasticity
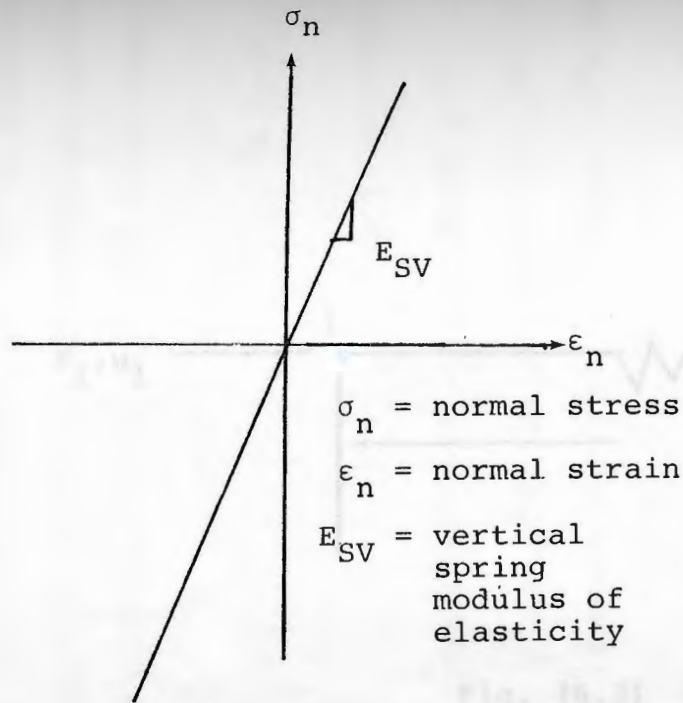
Fig. (6.2.a)   Vertical spring stress - strain diagram.

τ

τ_u

E_P

E_{SH}

ε_s

τ_u = ultimate shear strength

ε_s = horizontal strain

E_P = slip modulus

E_{SH} = initial horizontal spring elastic modulus of elasticity
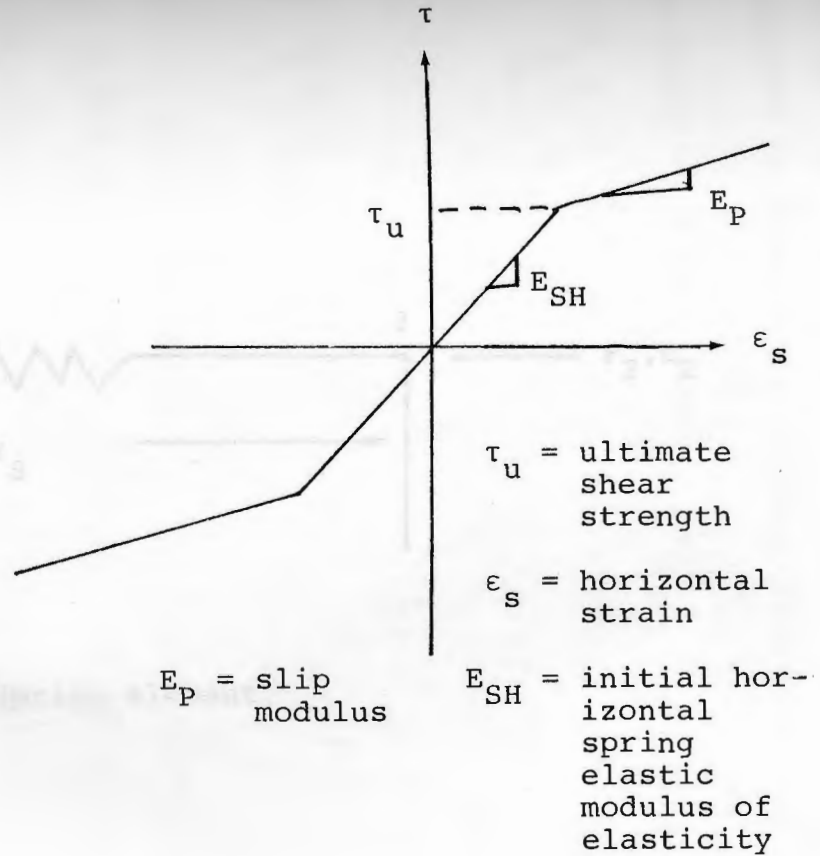
Fig. (6.2.b)   Horizontal spring stress - strain diagram.

where F_1, u_1 and F_2, u_2 represent spring forces and dis-
placements at nodes 1 and 2 respectively.

From equation (6.2) we get:

$$F_1 = \frac{E_S A_S}{L_S}(u_1 - u_2)$$ (6.3.a)

and

$$F_2 = \frac{E_S A_S}{L_S}(-u_1 + u_2)$$ (6.3.b)

Since F_1 and F_2 are equal and opposite, equations
(6.3.a) and (6.3.b) could be rewritten symbolically as

$$F_S = k_S \cdot \Delta_S$$ (6.4)

where F_S = force in the spring element

k_S = spring stiffness constant =

Δ_S = spring relative displacement

Rearranging (6.4),

$$\Delta_S = \frac{1}{k_S} \cdot F_S$$

Equation (6.5) indicates that the spring stiffness
constant controls the relative displacement. If Δ_S
and L_S were assumed to be kept constant, the spring
relative displacement will depend on the value of the
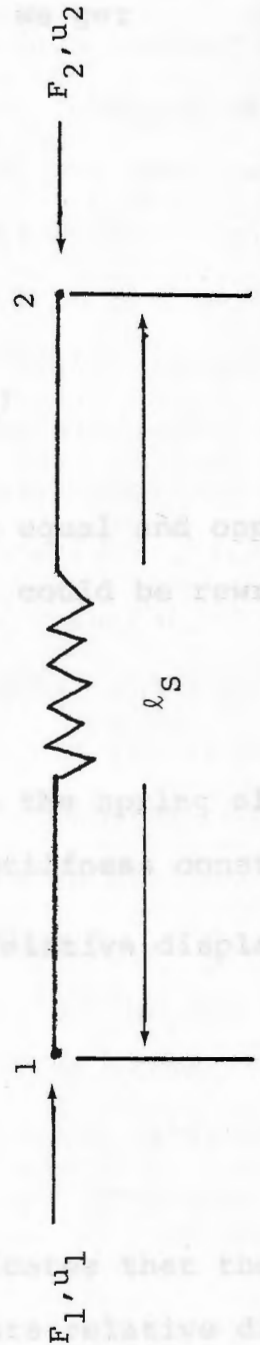
Fig. (6.3) Spring element.

where F_1, u_1 and F_2, u_2 represent spring forces and displacements at nodes 1 and 2 respectively.

From equation (6.2) we get

$$F_1 = \frac{E_S A_S}{L_S} (u_1 - u_2) \qquad (6.3.a)$$

and

$$F_2 = \frac{E_S A_S}{L_S} (-u_1 + u_2) \qquad (6.3.b)$$

Since F_1 and F_2 are equal and opposite, equations (6.3.a) and (6.3.b) could be rewritten symbolically as

$$F_S = k_S \cdot \Delta_S \qquad (6.4)$$

where F_S = force in the spring element

k_S = spring stiffness constant = $\frac{E_S A_S}{L_S}$

Δ_S = spring relative displacement.

Rearranging (6.4),

$$\Delta_S = \frac{1}{k_S} \cdot F_S$$

Equation (6.5) indicates that the spring stiffness constant controls its relative displacements. If A_S and L_S were assumed to be kept constant, the spring relative displacement will depend on the value of the

spring modulus of elasticity E_S.

Referring back to the vertical and horizontal stress—strain diagrams shown in fig. (6.2.a) and fig. (6.2.b), if perfect contact was assumed between the masonry plate and the concrete abutment, the relative displacements of the vertical interface spring elements are expected to be very small approaching zero; therefore, E_{SV} should be assigned a very large value which approaches infinity. Since the masonry plate is not restrained in the horizontal direction and because different displacement functions were assumed for the steel and concrete elements adjacent to the interface zone, when the shear transferred is less than the ultimate shear strength, the relative displacements in the horizontal interface spring elements are not expected to approach zero; however, they are very small. Therefore, E_{SH} should be assigned a large value but significantly less than E_{SV}. However, when shearing stresses transferred through the horizontal springs reach the ultimate shear strength value, those springs will start to slip having large relative displacements indicating that the slip modulus, E_P, should be assigned a very small value.

Nevertheless, there remain two critical unsolved problems. Firstly, what are the values of the moduli of plasticity discussed above? Secondly, what is the shear

strength in the horizontal interface spring elements?

6.2 INTERFACE SPRING ELEMENTS STIFFNESS

The vertical spring element stiffness has to be large enough so that the relative vertical displacements approach zero. However, if the interface zone is too thin, a large normal stiffness might cause an ill-conditioning problem resulting from dividing a very big number by a very small one. The spring stiffness constant was defined in equation (6.4), showing that an ill-conditioning problem will arise if $E_S \gg L_S$. It was recommended that the interface normal stiffness be equal to 10^5 times the stiffness of the adjacent elements [6].

The horizontal interface spring element stiffness could be determined by either a classical theoretical "exact" solution, or experimentally. However, a theoretical solution might involve tedious lengthy calculations, and experimental results might complicate the problem by adding more variable parameters. Therefore, the procedure adopted here for determining the horizontal spring stiffnesses involves trying different values, then comparing the outcoming results against those of known solutions, such as the infinite shear transfer case with E_{SH} equals infinity, and the case of zero shear transfer with E_{SH} equals zero. The interface zone for the infinite and zero shear transfer cases modeled as shown in fig. (6.4) and fig. (6.5) respectively.
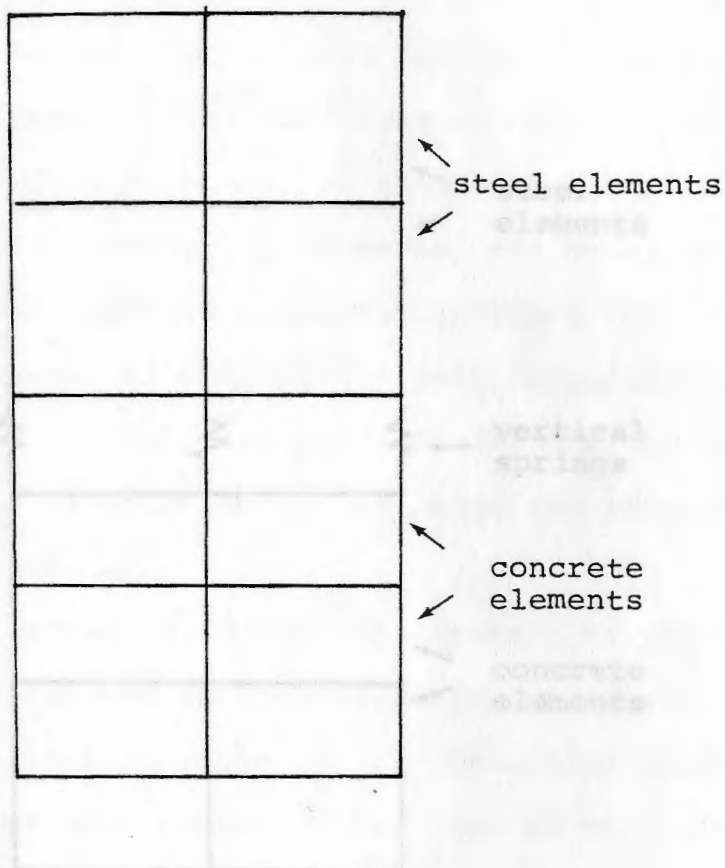
Fig. (6.4)   Case of infinite shear transfer.

steel
elements

vertical
springs

concrete
elements
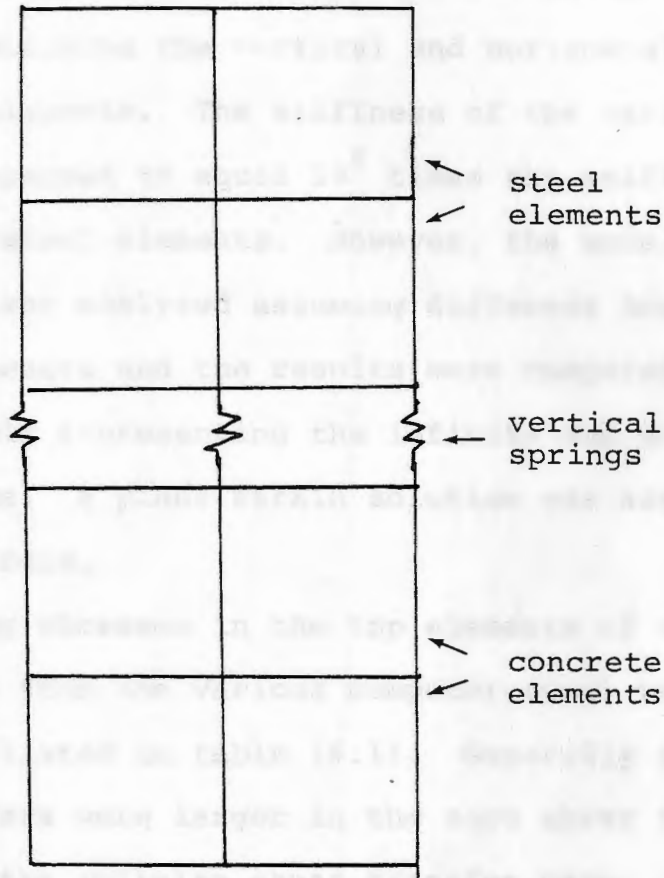
Fig. (6.5)   Case of zero shear transfer.

EXAMPLE PROBLEM

Two steel beams laying on top of each other were analyzed, assuming infinite shear transfer and zero shear transfer conditions modeled as shown in fig. (6.6.a) and fig. (6.6.b) respectively. Then the two beams were modeled by including the vertical and horizontal interface spring elements. The stiffness of the vertical springs was assumed to equal 10^5 times the stiffness of the adjacent steel elements. However, the model in fig. (6.6.c) was analyzed assuming different horizontal spring stiffnesses and the results were compared against those of models representing the infinite and zero shear transfer cases. A plane strain solution was assumed for all computer runs.

Bending stresses in the top elements of the upper beam (results from the various computer runs) were averaged and listed in table (6.1). Generally speaking, bending stresses were larger in the zero shear transfer case than in the infinite shear transfer case. Thus, for the model which includes interface spring elements, results converged toward representing the infinite shear transfer or the zero shear transfer cases, depending on the value of E_{SH}.

When E_{SH} was set to equal 500 Ksi, the averaged negative bending stresses in the center elements (7, 8, and 9) were about 1.1 to 1.7% larger than in the zero
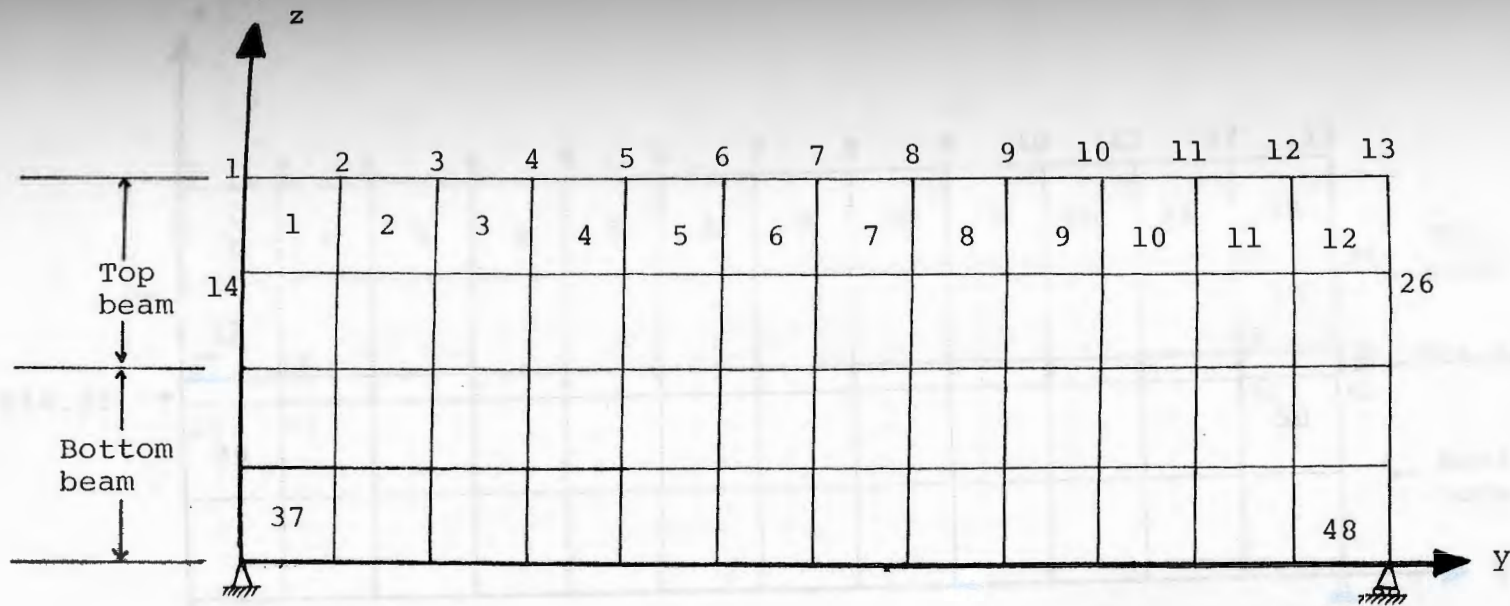
Steel: E = 29000 Ksi

$\nu = 0.25$

Fig. (6.6.a) Two beams with infinite shear transfer condition.
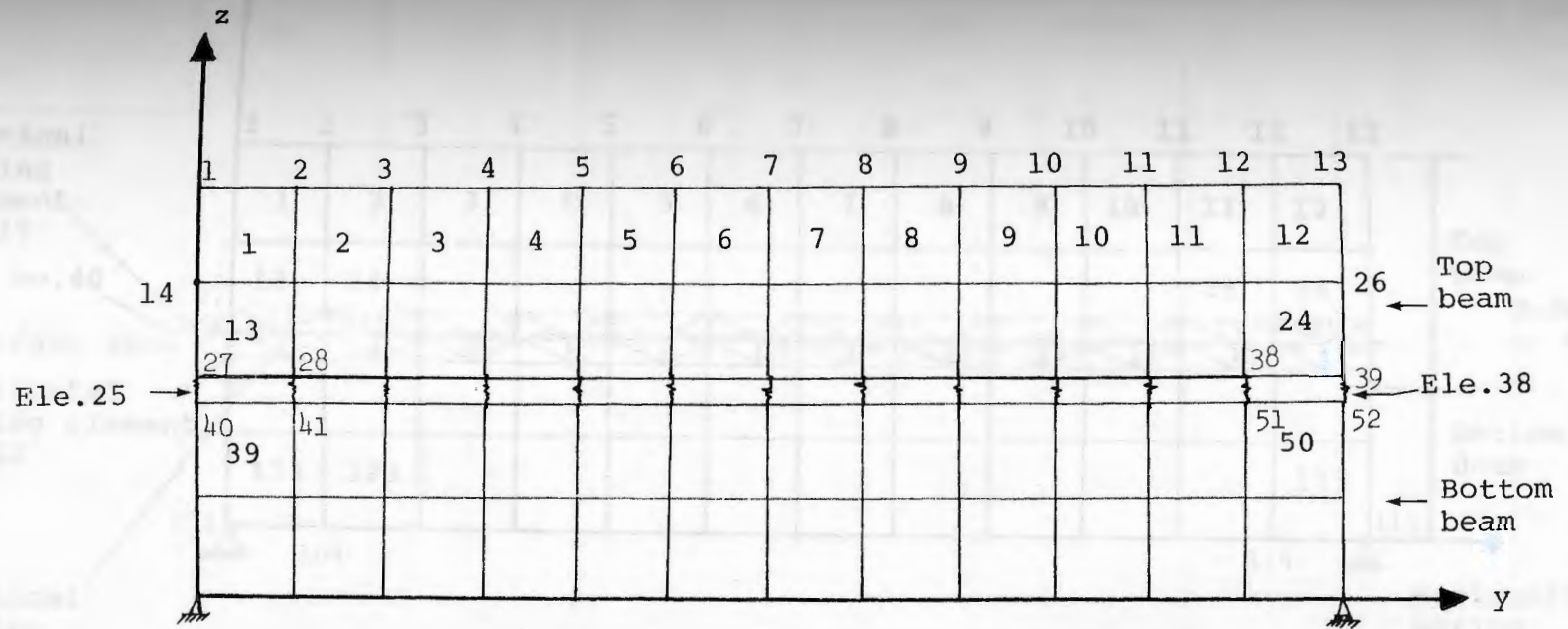
Fig. (6.6.b)   Two beams with zero shear transfer condition.
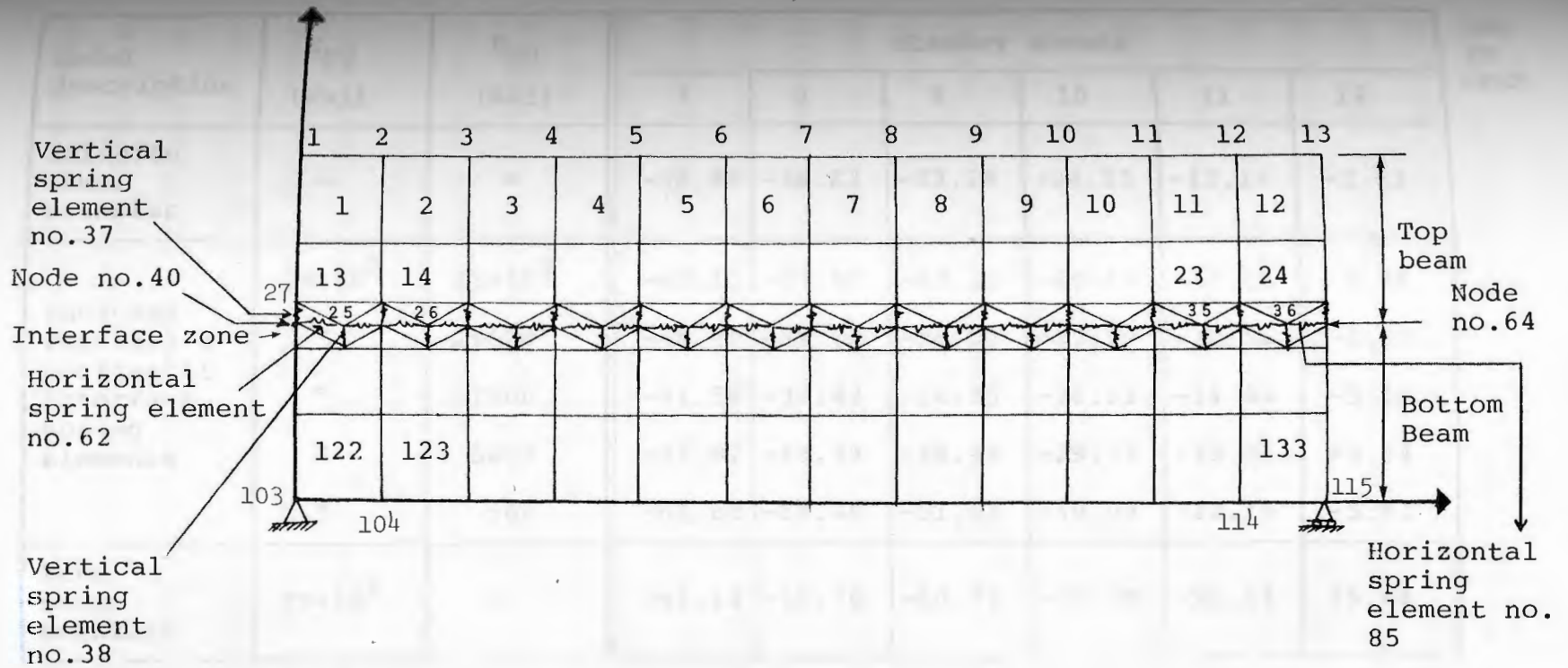
Fig. (6.6.c) Two beams with interface spring elements.

Model description	E_{SV} (Ksi)	E_{SH} (Ksi)	ELEMENT NUMBER					
			7	8	9	10	11	12
Infinite shear transfer	∞	∞	-38.94	-36.82	-32.29	-24.25	-12.16	-2.61
Includes vertical & horizontal interface spring elements	$29*10^8$	$29*10^8$	-40.15	-37.91	-33.32	-25.45	-13.18	-2.96
	"	29000	-40.81	-38.68	-34.25	-26.34	-13.70	-3.09
	"	17500	-41.56	-39.42	-34.95	-26.92	-14.05	-3.19
	"	5000	-45.67	-43.35	-38.49	-29.77	-15.81	-3.74
	"	500	-61.80	-58.48	-51.62	-39.99	-22.15	-5.81
Zero shear transfer	$29*10^8$	0	-61.14	-57.76	-50.71	-38.78	-21.14	15.48

Table (6.1) Plane strain solution. Averaged bending stresses (Ksi) in the top elements of the upper beam. Gauss integration points 2 and 4.

shear transfer case, but that difference increased in
the end elements (10, 11, and 12) to about 3.0 to 5.6%.
When E_{SH} was set to equal 29000 Ksi, the averaged
negative bending stresses in the center elements
(7, 8 and 9) were about 4.6 to 5.7% larger than in the
infinite shear transfer case, but that difference
increased in the end elements (10, 11, and 12) to about
8.0 to 15.5%, and those results would not vary by much
if E_{SH} was increased beyond 29000 Ksi; see results ob-
tained when E_{SH} was set to equal $29 * 10^8$ Ksi in
table (6.1). Results indicated that bending stresses
tend to be more uniformly distributed along the beam if
interface spring elements were used. They also tend to
be slightly larger as a result of the reduction in the
average thickness of the beams enforced by using tri-
angular elements adjacent to the interface zone as shown
in fig. (6.6.c). Relative vertical and horizontal dis-
placements for some of the adjacent nodes along the
interface zone are listed in table (6.2).

Based on the results presented above, the inter-
face spring elements material properties could be approx-
imated. For the vertical springs the modulus of elasti-
city, E_{SV}, equals $29 * 10^8$ Ksi. However, for the horizon-
tal springs, if shear transferred is less than the ulti-
mate shear strength, and E_{SH} equal to 29000 Ksi will be
adequate so that no slip will occur. If shear stresses

| Nodes in models | | | with interface spring elements | 27 – 40 | 38 – 41 | 32 – 45 | 33 – 46 | 34 – 47 | 38 – 51 | 39 – 52 |
| | | | without interface spring elements | 27 – 40 | 28 – 42 | 32 – 50 | 33 – 52 | 34 – 54 | 38 – 62 | 39 – 64 |
Model description	E_{SV} (Ksi)	E_{SH} (Ksi)	Relative displacement (inches)							
Infinite shear transfer	∞	∞	ΔH	0.0	0.0	0.0	0.0	0.0	0.0	0.0
			ΔV	0.0	0.0	0.0	0.0	0.0	0.0	0.0
Includes interface spring elements	$29 * 10^8$	29000	ΔH	-0.0011	-0.0013	-0.00011	0.0	-0.00011	+0.0013	+0.0011
			ΔV	0.0	0.0	0.0	0.0	0.0	0.0	0.0
	$29 * 10^8$	500	ΔH	-0.064	-0.062	-0.016	0.0	+0.016	+0.062	+0.064
			ΔV	0.0	0.0	0.0	0.0	0.0	0.0	0.0
Zero shear transfer	$29 * 10^8$	0.0	ΔH	-0.059	-0.056	-0.0016	+0.018	+0.037	+0.092	+0.094
			ΔV	0.0	0.0	0.0	0.0	0.0	0.0	0.0

Table (6.2) Plane strain solution.
List of relative vertical and horizontal displacements between various nodes adjacent to the interface zone (inches).

transferred in the horizontal springs reach the ultimate shear strength value, then an E_{SH} equal to 500 Ksi will be adequate to represent a slip condition. The cross-sectional areas and lengths of the springs were calculated to be geometrically proportional to the elements adjacent to the interface zone.

6.3 THE BEARING SYSTEM MODELED WITH INTERFACE SPRING ELEMENTS

A finite element grid system of the bearing system modeled with vertical and horizontal interface spring elements was shown in fig. (4.7). The bearing system was analyzed assuming different interface spring elements stiffness values; results were compared against those of bearing system models representing zero and infinite shear transfer conditions, shown in fig. (4.5) and fig. (4.6) respectively. The analysis was carried out using axisymmetric and plane strain solution methods.

Interface spring elements were assumed to be 0.25 inches long, and their cross-sectional areas were calculated to be geometrically proportional to the steel and concrete elements adjacent to the interface zone. Vertical and horizontal springs calculated cross-sectional areas for both solution methods were listed in tables (6.3.a) and (6.3.b) respectively. The vertical springs modulus of elasticity assumed to be 10^5 times the adjacent steel elements modulus of elasticity, equals

Vertical spring element no.	Axisymmetric solution A_S—in^2	Plane strain solution A_S—in^2
63	0.01	0.125
64	0.04	0.25
65	0.09	0.25
66	0.14	0.25
67	0.18	0.25
68	0.22	0.25
69	0.27	0.25
70	0.32	0.25
71	0.36	0.25
72	0.40	0.25
73	0.45	0.25
74	0.50	0.25
75	0.54	0.25
76	0.58	0.25
77	0.63	0.25
78	0.68	0.25
79	0.72	0.25
80	0.76	0.25
81	0.81	0.25
82	0.86	0.25
83	0.90	0.25
84	0.94	0.25
85	0.99	0.25
86	1.04	0.25
87	1.08	0.25
88	1.12	0.25
89	1.17	0.25
90	1.22	0.25
91	0.31	0.125

Table (6.3.a)   Vertical interface spring elements cross-sectional areas.

Horizontal spring element no.	Axisymmetric solution $A_S - in^2$	Plane strain solution $A_S - in^2$
92	1.00	1.25
93	0.12	0.25
94	0.20	0.25
95	0.30	0.25
96	0.38	0.25
97	0.48	0.25
98	0.56	0.25
99	0.66	0.25
100	0.74	0.25
101	0.84	0.25
102	0.92	0.25
103	1.02	0.25
104	1.10	0.25
105	1.20	0.25

Table (6.3.b)   Horizontal interface spring elements cross-sectional areas.

$29 * 10^8$ Ksi. The horizontal springs modulus of elasti-
city was assumed to equal 29000 Ksi representing the
infinite shear transfer condition (initial no slip
modulus, E_{SH}), and 29 Ksi representing the zero shear
transfer condition (slip modulus, E_p), see fig. (6.2.a)
and fig. (6.2.b).

Results from the analyzed models representing the
infinite and zero shear transfer conditions with and
without using the interface spring elements for both
solution methods, were compared and tabulated. Averaged
bending stresses in top of the pot bearing were listed
in tables (6.4.a) and (6.4.b); averaged bending stresses
in top of the masonry plate were listed in tables (6.5.a)
and (6.5.b); averaged concrete vertical stresses were
listed in tables (6.6.a) and (6.6.b); averaged concrete
shearing stresses were listed in tables (6.7.a) and
(6.7.b); refer to fig. (6.7). Generally speaking, results
indicated that negative bending stresses in the pot bear-
ing and the masonry steel plates were slightly lower in
models which included the interface spring elements.
That could be attributed to the fact that horizontal
interface spring elements actually connect nodes adjacent
to the interface zone rather than connecting adjacent
surfaces, hence the shear transferred along the interface
would be concentrated in those springs instead of being
uniformly distributed. Therefore the restraint against
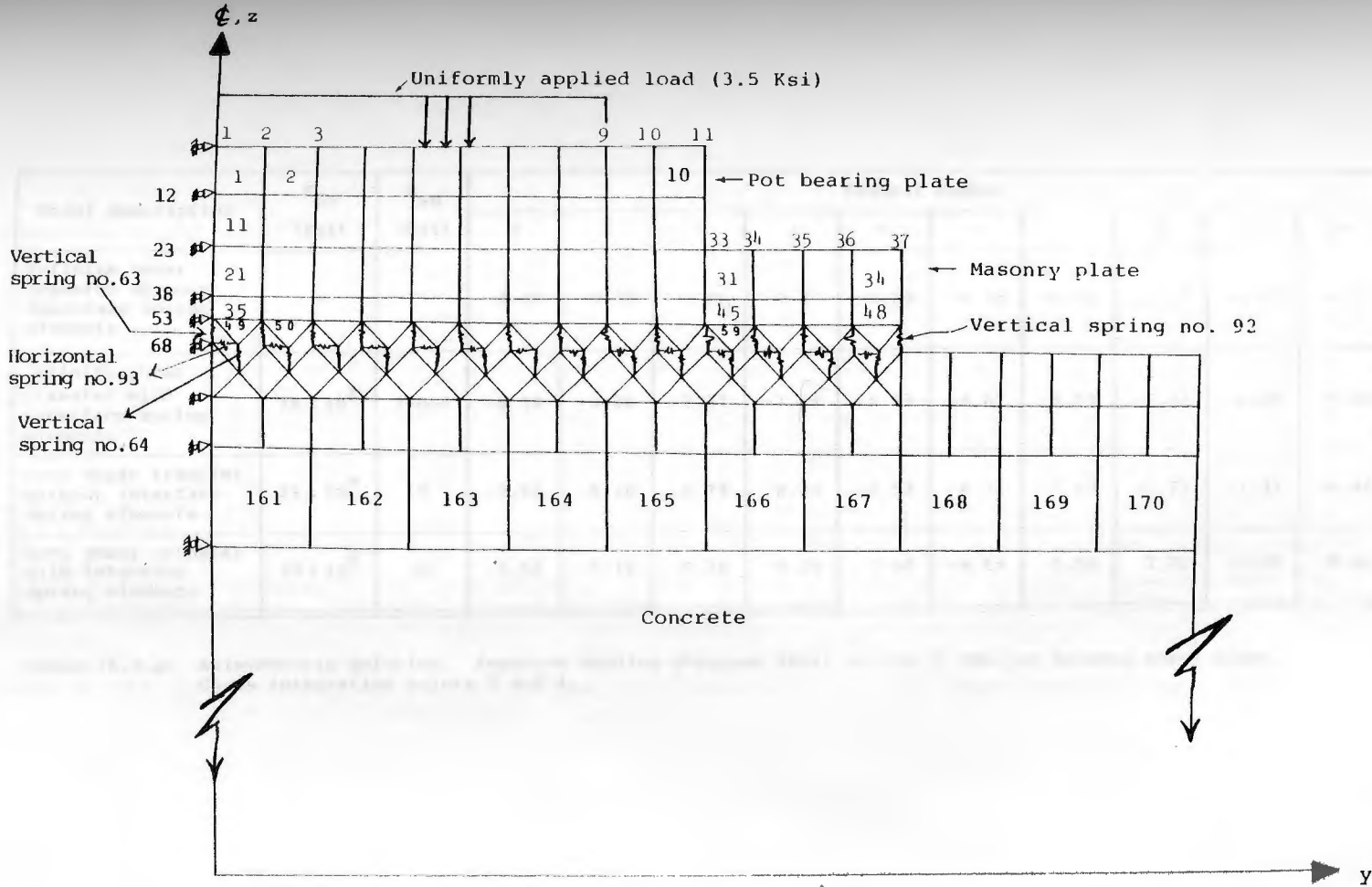
Fig. (6.7)   Top part of the bearing system including interface spring elements.

Model description	E_{SV} (Ksi)	E_{SH} (Ksi)	Element number									
			1	2	3	4	5	6	7	8	9	10
Infinite shear transfer without interface spring elements	∞	∞	-8.65	-8.30	-7.88	-7.43	-6.84	-6.10	-5.13	-3.37	-1.07	-0.08
Infinite shear transfer with interface spring elements	$29 \star 10^8$	29000	-8.59	-8.26	-7.87	-7.43	-6.83	-6.07	-5.09	-3.32	-1.06	-0.08
Zero shear transfer without interface spring elements	$29 \star 10^8$	0	-9.63	-9.20	-8.73	-8.20	-7.53	-6.71	-5.65	-3.78	-1.31	-0.16
Zero shear transfer with interface spring elements	$29 \star 10^8$	29	-9.53	-9.12	-8.70	-8.19	-7.52	-6.68	-5.59	-3.71	-1.29	-0.16

Table (6.4.a)   Axisymmetric solution.   Averaged bending stresses (Ksi) in top of the pot bearing steel plate. Gauss integration points 2 and 4.

Model description	E_{SV} (Ksi)	E_{SH} (Ksi)	Element number									
			1	2	3	4	5	6	7	8	9	10
Infinite shear transfer without interface spring elements	∞	∞	-9.74	-9.60	-9.33	-8.90	-8.30	-7.50	-6.42	-4.47	-1.77	-0.25
Infinite shear transfer with interface spring elements	$29 * 10^8$	29000	-9.38	-9.33	-9.15	-8.78	-8.20	-7.40	-6.31	-4.37	-1.72	-0.24
Zero shear transfer without interface spring elements	$29 * 10^8$	0	-10.35	-10.21	-9.92	-9.47	-8.84	-8.00	-6.87	-4.84	-2.02	-0.33
Zero shear transfer with interface spring elements	$29 * 10^8$	29	-10.02	-9.89	-9.63	-9.20	-8.58	-7.75	-6.62	-4.64	-1.92	-0.31

Table (6.4.b)   Plane strain solution.   Averaged bending stresses (Ksi) in top of the pot bearing steel plate.
Gauss integration points 2 and 4.

Model description	E_{SV} (Ksi)	E_{SH} (Ksi)	Element number													
			21	22	23	24	25	26	27	28	29	30	31	32	33	34
Infinite shear transfer without interface spring elements	∞	∞	-0.84	-0.85	-0.84	-0.81	-0.75	-0.68	-0.71	-0.97	-1.43	-2.02	-2.97	-0.78	+0.05	+0.03
Infinite shear transfer with interface spring element	$29 * 10^8$	29000	-0.36	-0.36	-0.36	-0.36	-0.36	-0.36	-0.46	-0.77	-1.26	-1.82	-2.56	-0.47	+0.13	+0.08
Zero shear transfer without interface spring elements	$29 * 10^8$	0	+0.36	+0.32	+0.28	+0.25	+0.22	+0.19	+0.05	-0.33	-0.98	-1.78	-2.91	-0.85	-0.22	+0.06
Zero shear transfer with interface spring elements	$29 * 10^8$	29	+0.85	+0.81	+0.77	+0.71	+0.63	+0.54	+0.33	-0.11	-0.78	-1.52	-2.37	-0.36	+0.14	+0.07

Table (6.5.a)   Axisymmetric solution.   Averaged bending stresses (Ksi) in top of the masonry steel plate. Gauss integration points 2 and 4.

| Model description | E_{SV} (Ksi) | E_{SH} (Ksi) | Element number |
			21	22	23	24	25	26	27	28	29	30	31	32	33	34
Infinite shear transfer without interface spring elements	∞	∞	-0.77	-0.76	-0.73	-0.68	-0.61	-0.52	-0.52	-0.76	-1.31	-2.06	-3.26	-0.81	+0.0	+0.09
Infinite shear transfer with interface spring elements	$29*10^8$	29000	-0.34	-0.34	-0.26	-0.21	-0.18	-0.16	-0.23	-0.53	-1.10	-1.82	-2.73	-0.39	+0.29	+0.18
Zero shear transfer without interface spring elements	$29*10^8$	0	+1.01	+0.99	+0.97	+0.94	+0.90	+0.86	+0.71	+0.30	-0.46	-1.44	-2.69	-0.64	-0.08	+0.01
Zero shear transfer with interface spring elements	$29*10^8$	29	+1.43	+1.41	+1.38	+1.32	+1.24	+1.15	+0.94	+0.48	-0.25	-1.09	-1.82	+0.15	+0.53	+0.24

Table (6.5.b)   Plane strain solution.   Averaged bending stresses (Ksi) in top of the masonry steel plate. Gauss integration points 2 and 4.

Model description	E_{SV} (Ksi)	E_{SH} (Ksi)	Element number									
			161	162	163	164	165	166	167	168	169	170
Infinite shear transfer without interface spring elements	∞	∞	-1.648	-1.757	-1.576	-1.390	-1.094	-0.825	-0.504	-0.294	-0.130	-0.034
Infinite shear transfer with interface spring elements	$29 * 10^8$	29000	-1.739	-1.854	-1.654	-1.440	-1.114	-0.833	-0.509	-0.272	-0.104	-0.012
Zero shear transfer without interface spring elements	$29 * 10^8$	0	-2.050	-2.169	-1.917	-1.651	-1.243	-0.850	-0.392	-0.169	-0.051	+0.029
Zero shear transfer with interface spring elements	$29 * 10^8$	29	-2.129	-2.254	-1.985	-1.693	-1.254	-0.883	-0.356	-0.141	-0.045	+0.028

Table (6.6.a) Axisymmetric solution. Averaged vertical stresses (Ksi) in concrete elements.
             Gauss integration points 2 and 4.

Model description	E_{SV} (Ksi)	E_{SH} (Ksi)	Element number									
			161	162	163	164	165	166	167	168	169	170
Infinite shear transfer without interface spring elements	∞	∞	-2.675	-2.583	-2.357	-2.095	-1.690	-1.290	-0.787	-0.448	-0.198	-0.020
Infinite shear transfer with interface spring elements	$29 * 10^8$	29000	-2.718	-2.634	-2.398	-2.112	-1.680	-1.271	-0.776	-0.418	-0.164	+0.013
Zero shear transfer without interface spring elements	$29 * 10^8$	0	-2.999	-2.879	-2.587	-2.235	-1.700	-1.150	-0.519	-0.223	-0.049	+0.097
Zero shear transfer with interface spring elements	$29 * 10^8$	29	-3.028	-2.904	-2.600	-2.229	-1.677	-1.129	-0.496	-0.201	-0.054	+0.085

Table (6.6.b) Plane strain solution. Averaged vertical stresses (Ksi) in concrete elements.
Gauss integration points 2 and 4.

Model description	E_{SV} (Ksi)	E_{SH} (Ksi)	Element number									
			161	162	163	164	165	166	167	168	169	170
Infinite shear transfer without interface spring elements	ω	ω	+0.2718	+0.2101	+0.3894	+0.4005	+0.4861	+0.4300	+0.3835	+0.2313	+0.1118	+0.0246
Infinite shear transfer with interface spring elements	$29 * 10^8$	29000	+0.2873	+0.2216	+0.4155	+0.4271	+0.5028	+0.4262	+0.3719	+0.2200	+0.0878	+0.0145
Zero shear transfer without interface spring elements	$29 * 10^8$	0	+0.2940	+0.1570	+0.3194	+0.3034	+0.4010	+0.3657	+0.3081	+0.1195	-0.0193	-0.0114
Zero shear transfer with interface spring elements	$29 * 10^8$	29	+0.3056	+0.1668	+0.3454	+0.3337	+0.4276	+0.3864	+0.3207	+0.1075	+0.0139	-0.0116

Table (6.7.a)   Axisymmetric solution.   Averaged shearing stresses (Ksi) in concrete elements.
Gauss integration points 2 and 4.

Model description	E_{SV} (Ksi)	E_{SH} (Ksi)	Element number									
			161	162	163	164	165	166	167	168	169	170
Infinite shear transfer without interface spring elements	∞	∞	+0.1700	+0.2449	+0.5261	+0.5469	+0.6971	+0.6271	+0.5861	+0.3392	+0.1580	+0.0301
Infinite shear transfer with interface spring elements	$29 * 10^8$	29000	+0.1637	+0.2549	+0.5494	+0.5724	+0.7110	+0.6179	+0.5631	+0.3224	+0.1295	+0.0139
Zero shear transfer without interface spring elements	$29 * 10^8$	0	+0.1363	+0.1502	+0.3945	+0.3829	+0.5325	+0.4834	+0.3985	+0.1251	-0.0118	-0.0387
Zero shear transfer with interface spring elements	$29 * 10^8$	29	+0.1463	+0.1737	+0.4351	+0.4324	+0.5750	+0.5119	+0.4319	+0.1317	-0.0041	-0.0337

Table (6.7.b)   Plane strain.   Averaged shearing stresses (Ksi) in concrete elements. Gauss integration points 2 and 4.

plates bending would be higher. Add to that in the case of zero shear transfer the fact that a horizontal spring modulus of elasticity equalling 29 Ksi is small but not zero makes the plates bending restraint even higher. Notice that the effect of using interface spring elements on bending stresses was different in the two-beams example problem presented in sec. (6.3.1). However, here a different structure is considered, and the interface spring elements connect steel to concrete rather than steel to steel. The concrete negative vertical and positive shearing stresses were lower in models which included interface spring elements due to the lower bending stresses resulting in those models as discussed above. Reduction of steel plate bending against the concrete surface would cause less compression in the vertical spring elements. Furthermore, in the model representing the case of infinite shear transfer, a vertical spring modulus of elasticity equal to $29 * 10^8$ is very large but not really infinite. Add to that for the case of infinite shear transfer, the fact that a horizontal spring modulus of elasticity equal to 29000 Ksi is considerably less than infinity. Therefore, shear stresses transferred to the concrete would be lower. Effect of using interface spring elements on the maximum averaged stresses in the bearing system modeled to represent the cases of infinite and zero shear transfer conditions for the axisymmetric and plane

strain solution methods, is summarized in table (6.8).
In general, the use of interface spring elements induces
a larger effect on the bearing stresses in the plane
strain solution than in the axisymmetric solution, be-
cause the horizontal springs have no effect on the
circumferential stresses which are induced by circumfer-
ential displacements in the axisymmetrical solution and
neglected in the plane strain solution. Furthermore,
the averaged maximum bending stress in top of the
masonry plate, was the most to be affected by the use of
the interface spring elements. That portion of the
masonry plate being relatively thin and close to the
interface zone, it has been the part of the bearing sys-
tem most affected by the geometrical change of the ele-
ments adjacent to the interface zone. Notice that the
pot plate is modeled with the part of the masonry plate
beneath it as a continuum acting as a thick plate.

Based on the discussion presented above, it has
been found that for those specified interface spring
element lengths and cross-sectional areas, the vertical
springs modulus of elasticity equalling $29 * 10^8$ Ksi
provides a satisfactory interface normal stiffness. For
the horizontal interface spring elements, a modulus of
plasticity equalling 29000 Ksi provides a satisfactory
no slip interface horizontal stiffness, and a value

Solution method	Shear transfer condition %	Maximum averaged bending stress in top of pot bearing %	Maximum averaged bending stress in top of masonry plate %	Maximum averaged vertical stress in concrete elements %	Maximum averaged shearing stress in concrete elements %
Axisymmetric	Infinite shear transfer	-0.7	-13.8	+5.2	+3.3
Axisymmetric	Zero shear transfer	-1.0	-18.6	+3.8	+6.2
Plane strain	Infinite shear transfer	-3.7	-16.3	+1.9	+2.0
Plane strain	Zero shear transfer	-3.2	-32.3	+0.9	+7.4

Table (6.8)   Effect of using interface spring elements on maximum bearing system stresses modeled to represent the cases of infinite and zero shear transfer conditions for axisymmetric and plane strain solution methods.

equalling 29 Ksi could satisfactorily be considered as the full slip modulus.

A NONLINEAR DESCRIPTION OF SLIP

The masonry steel plate will start to slip when shear stresses transferred through the horizontal inter- face spring elements reach an ultimate shear strength, where slip will actually occur in the individual spring elements. The ultimate shear strength in the horizontal spring interface elements used in the bearing system will be defined as the point on the spring's stress - strain diagram where the modulus of elasticity starts to decrease nonlinearly from the no slip modulus equalling 29000 Ksi, indicating start of slip, until it reaches the full slip modulus equalling 29 Ksi, indicating complete slip of the spring element, see fig. (6.8). The exact ultimate shear strength in the horizontal springs is not known; however, it will be assumed that it equals X% of the maximum shear stress value transferred in any horizontal interface spring element in the model repre- senting the case of infinite shear transfer condition, where slip is not allowed. Shear stresses transferred through the horizontal springs in the model representing infinite shear transfer condition in both axisymmetric and plane strain solution methods are listed in table (6.9), refer to fig. (6.7). In both solution

methods the maximum shear stress transferred appeared to be in spring element no. 102, where in the axisymmetric solution it equals 1.39189 Ksi, and in the plane strain solution it equals 1.29987 Ksi. The value of X was selected randomly to equal (30, 50, and 70). Data for the stress - strain relation of the different induced slip conditions for both solution methods is presented in Appendix B.

6.5 REMARKS

It should be noted that the moethod of representing the interface by the use of the interface spring elements proposed here involves a physical change in the geometry of the structure. Note also that the thickness of the interface cannot be let very small approaching zero as in reality, because if it is, an ill-conditioning problem will occur, resulting from dividing the large normal modulus of elasticity by the small length of the spring when the normal stiffness of the interface becomes very large in the case of joint closing or perfect contact.

There has been no tension cut-off consideration for the vertical interface spring elements to account for the separation of the masonry plate and the concrete abutment. Results from analyzing a model representing the case of zero shear transfer condition, (horizontal inter-

Spring element number	Axisymmetric solution Transferred shearing stress	Plane strain solution Transferred shearing stress
92	+0.633897D − 01	+0.440319D + 00
93	+0.336047D + 00	+0.317365D + 00
94	+0.603019D + 00	+0.494136D + 00
95	+0.785314D + 00	+0.663890D + 00
96	+0.100999D + 01	+0.838462D + 00
97	+0.114836D + 01	+0.999273D + 00
98	+0.130028D + 01	+0.113609D + 01
99	+0.133951D + 01	+0.121588D + 01
100	+0.136297D + 01	+0.124478D + 01
101	+0.134815D + 01	+0.126545D + 01
102	+0.139189D + 01	+0.129987D + 01
103	+0.133600D + 01	+0.126031D + 01
104	+0.126027D + 01	+0.116754D + 01
105	+0.125103D + 01	+0.114125D + 01

Table (6.9) Shear stresses transferred through the
horizontal interface spring elements
in the case of infinite shear transfer.

face spring elements not included, see fig. (4.5)), have
shown that all vertical springs along the interface were
in compression except for the end spring. That end spring
in tension was taken out of the model and the analysis
was repeated. Resulting normal stresses in the vertical
spring elements are listed in table (B.4) of Appendix B.
The elimination of that end vertical spring does not have
a significant effect on the resulting stresses in the
bearing system, because in the early loading stages,
(initial load increments), before the spring goes in
tension, it is only expected to transfer a very little
portion of the normal stresses to the concrete elements.
Normal stresses transferred through vertical interface
spring elements (model including horizontal and vertical
interface spring elements, see fig. (4.7)), for different
shear strength value along the interface, were listed in
tables (B.5.a) and (B.5.b) for an axisymmetric and a
plane strain solution method, respectively, see
Appendix B sec. (B.3). Results indicated that when the
slip along the interface was described as a nonlinear
function, separation of the masonry plate from the
concrete became more obvious due to the nonlinear varia-
tion of the bending stresses along the steel plate ele-
ments; the explanation of that behavior will be left for
chapter 7. Notice that because the masonry plate is

assumed to be rigidly connected with the concrete abut-
ment (no tension cut-off), very large tension could
appear in some of the vertical interface spring elements
due to the multiplication of positive relative displace-
ments by the large normal stiffness values, refer to
equation (6.4). However, there appeared to be some in-
consistencies in the results where vertical springs along
the interface alternated from negative to positive
unrealistically.

Referring to fig. (6.1), notice that vertical
spring elements located in the interface similar to
spring B tend to become in tension (separation) before
springs similar to spring A. Moreover, in the interface
zone where separation is not likely to happen, springs
similar to spring B in fig. (6.1) will have larger com-
pression stresses than springs similar to spring A.
Those inconsistencies are due to the geometry of the
interface where it was modeled such that elements
adjacent to the interface were altered to have a tri-
angular shape so that nodes such as j and k in fig. (6.1)
could be connected by a horizontal interface spring
element as shown in fig. (6.1). Problems resulting from
the geometry of the interface could be resolved by using
interface spring elements having a geometry similar to
the linkage element shown in fig. (5.3), where there

will be no need to change the geometry of the steel and concrete elements adjacent to the interface. The interface behavior described above could also be improved by considering tension cut-off for the vertical interface elements, so that the separation of the masonry plate and the concrete abutment would be allowed along the interface. Nevertheless, for an axisymmetric model, a special interface element could be used to account for displacements in the circumferential direction, see element formulation in Appendix A, sec. (A.2).

CHAPTER 7

EFFECT OF SHEAR TRANSFER

It is customary to analyze the bearing system assuming either infinite or zero shear transfer conditions without paying much attention to the effect of the shear transfer. However, simulating the behavior of the interface between the masonry steel plate and the concrete abutment by the method proposed in the previous chapter, the bearing system was analyzed with different shear transfer conditions.

7.1 ASSUMED DIFFERENT SHEAR TRANSFER CONDITIONS

Shear stresses transferred through the horizontal spring elements will keep increasing as the load increments applied on the bearing system increase until slip starts in those spring elements whose ultimate shear strength value is reached. Since the slip is described by a nonlinear relation, spring elements which started to slip will transfer nonlinearly decreasing shear stress increments. Hence, the shear stress transferred through a horizontal spring element depends on its ultimate shear strength value, such that larger shear stresses will be

transferred through horizontal interface spring elements with higher shear strength values.

The horizontal spring elements ultimate shear strength value is not known. However, three different shear transfer conditions were induced by assuming the horizontal interface spring elements ultimate shear strength value to equal 70%, 50%, and 30% of the maximum shear stress value transferred in the infinite shear transfer condition, see Appendix B, sec. (B.1) for complete information about the formulation of the horizontal spring elements stress - strain relations for the three ultimate shear strength values. The bearing system was analyzed under those different shear transfer conditions and results were compared against those of infinite and zero shear transfer conditions. Both axi-symmetric and plane strain solution methods were considered, and the bearing system was loaded by 3.5 Ksi uniformly applied load in all computer runs. For all shear transfer conditions, horizontal spring elements shear stresses, slip status, and the slip modulus were listed in tables (7.1.a), (7.1.b), (7.1.c), (7.1.d) and (7.1.e), see fig. (6.7). The average percentage change in the shear stresses transferred through the interface for the different shear transfer conditions with respect to the shear stresses transferred through the interface in the infinite shear transfer condition, are listed in

table (7.2).

Shear stresses transferred in the horizontal interface spring elements near the end of the interface are higher because as the plates bend under the uniformly applied load, the end steel elements of the relatively thin masonry plate would tend to slip over the concrete. Therefore, slip will occur first in those horizontal spring elements transferring larger shear stresses. As the ultimate shear strength of the springs is decreased, more of them would slip and shear stresses transferred through the interface zone would decrease nonlinearly because of the nonlinear slip function, see stress - strain curve in Appendix B, fig. (B.1). Shear stress distributions for the different shear transfer conditions were approximated by the continuous curves shown in fig. (7.1), where τ_u represents the ultimate shear strength for the horizontal springs and τ_{max} represents the maximum shear stress transferred in the infinite shear transfer condition. Notice that shear stresses become more uniformly distributed as the ultimate shear strength of the horizontal spring elements decreases.

Shear stresses transferred through the horizontal interface spring elements are higher in the axisymmetric solution than in the plane strain solution because of shear stresses resulting from the circumferential

displacements, which are not restrained by the horizontal spring elements in the axisymmetric elements. Therefore, the horizontal spring elements in the axisymmetric solution will slip earlier, causing more reduction in the shear stresses transferred in the interface zone than in the plane strain solution for the same reduction in the spring elements ultimate shear strength, see table (7.2). Hence, in the shear transfer condition where τ_u was reduced to equal 30% of τ_{max}, and in the zero shear transfer condition, shear stresses transferred through the horizontal interface spring elements became larger in the plane strain solution than in the axisymmetric solution.

From a physical point of view, it is expected that slip should occur only in those horizontal spring elements which are near the end of the interface zone; however, results from both solution methods indicated that when the horizontal spring elements ultimate shear strength was as high as 70% of τ_{max}, slip still occurred in spring elements closer to the center, see table (7.1.b). Therefore, the horizontal interface spring elements shear strength value is expected to be higher than 70% of τ_{max}. Nevertheless, the assumed shear strength values sufficiently represent various shear transfer conditions.

Table (7.1.a)   Infinite shear transfer condition

Spring element number	Axisymmetric solution			Plane strain solution		
	Shear stress (Ksi)	Slip status	Slip modulus (Ksi)	Shear stress (Ksi)	Slip status	Slip modulus (Ksi)
92	+0.0633897	No slip	29000	+0.440319	No slip	29000
93	+0.336047	"	"	+0.317365	"	"
94	+0.603019	"	"	+0.494136	"	"
95	+0.785314	"	"	+0.663890	"	"
96	+1.00999	"	"	+0.838462	"	"
97	1.14836	"	"	+0.999273	"	"
98	1.30028	"	"	+1.13609	"	"
99	1.33951	"	"	+1.21588	"	"
100	1.36297	"	"	+1.24478	"	"
101	1.34815	"	"	+1.26545	"	"
102	1.39189	"	"	+1.29987	"	"
103	1.33600	"	"	+1.26031	"	"
104	1.26027	"	"	+1.16754	"	"
105	1.25103	"	"	+1.14125	"	"

Table (7.1.b) Shear transfer condition resulting from assuming the horizontal spring elements equal 70% of the maximum shear stress transferred in the infinite shear transfer condition.

Spring element number	Axisymmetric solution			Plane strain solution		
	Shear stress (Ksi)	Slip status	Slip modulus (Ksi)	Shear stress (Ksi)	Slip status	Slip modulus (Ksi)
92	+0.0639190	No slip	29000	+0.441935	No slip	29000
93	+0.355382	"	"	+0.330101	"	"
94	+0.649642	"	"	+0.520400	"	"
95	+0.861154	"	"	+0.707766	"	"
96	+1.01219	Slipped	2900	+0.907023	"	"
97	+1.10441	"	290	+1.00361	Slipped	290
98	+1.13225	"	290	+1.00921	"	290
99	+1.17219	"	29	+1.09659	"	29
100	+1.17417	"	"	+1.10061	"	"
101	+1.17449	"	"	+1.10356	"	"
102	+1.17560	"	"	+1.10626	"	"
103	+1.17308	"	"	+1.10512	"	"
104	+1.13836	"	290	+1.10111	"	"
105	+1.13021	"	290	+1.09927	"	"

Table (7.1.c) Shear transfer condition resulting from assuming the horizontal spring elements equal 50% of the maximum shear stress transferred in the infinite shear transfer condition.

Spring element number	Axisymmetric solution			Plane strain solution		
	Shear stress (Ksi)	Slip status	Slip modulus (Ksi)	Shear stress (Ksi)	Slip status	Slip modulus (Ksi)
92	+0.0664691	No slip	29000	+0.464894	No Slip	29000
93	+0.483019	"	"	+0.456233	"	"
94	+0.785027	Slipped	290	+0.674586	Slipped	2900
95	+0.835160	"	29	+0.772402	"	290
96	+0.855361	"	"	+0.801996	"	29
97	+0.866509	"	"	+0.817552	"	"
98	+0.875867	"	"	+0.833375	"	"
99	+0.882820	"	"	+0.844934	"	"
100	+0.887012	"	"	+0.853055	"	"
101	+0.889261	"	"	+0.859819	"	"
102	+0.891770	"	"	+0.865047	"	"
103	+0.889983	"	"	+0.864591	"	"
104	+0.886308	"	"	+0.861204	"	"
105	+0.883179	"	"	+0.858193	"	"

Table (7.1.d) Shear transfer condition resulting from assuming the horizontal spring elements equal 30% of the maximum shear stress transferred in the infinite shear transfer condition.

Spring element number	Axisymmetric solution			Plane strain solution		
	Shear stress (Ksi)	Slip status	Slip modulus (Ksi)	Shear stress (Ksi)	Slip status	Slip modulus (Ksi)
92	+0.0694736	No slip	29000	+0.437055	Slipped	290
93	+0.502030	Slipped	29	+0.474454	"	29
94	+0.522173	"	"	+0.496576	"	"
95	+0.539746	"	"	+0.519480	"	"
96	+0.557222	"	"	+0.542826	"	"
97	+0.571878	"	"	+0.565416	"	"
98	+0.584116	"	"	+0.585614	"	"
99	+0.593045	"	"	+0.601413	"	"
100	+0.598572	"	"	+0.613039	"	"
101	+0.601955	"	"	+0.621925	"	"
102	+0.604980	"	"	+0.628754	"	"
103	+0.603457	"	"	+0.629735	"	"
104	+0.598822	"	"	+0.626008	"	"
105	+0.593708	"	"	+0.621533	"	"

Table (7.1.e)   Zero shear stress condition

Spring element number	Axisymmetric solution			Plane strain solution		
	Shear stress (Ksi)	Slip status	Slip modulus (Ksi)	Shear stress (Ksi)	Slip status	Slip modulus (Ksi)
92	+0.00262226	slipped	29	+0.0120080	slipped	29
93	+0.0293357	"	"	+0.0510859	"	"
94	+0.0612690	"	"	+0.0899531	"	"
95	+0.0883243	"	"	+0.127343	"	"
96	+0.112601	"	"	+0.162675	"	"
97	+0.132979	"	"	+0.194923	"	"
98	+0.149670	"	"	+0.223000	"	"
99	+0.161191	"	"	+0.245191	"	"
100	+0.168472	"	"	+0.261605	"	"
101	+0.173255	"	"	+0.273976	"	"
102	+0.176532	"	"	+0.282719	"	"
103	+0.174406	"	"	+0.284153	"	"
104	+0.167586	"	"	+0.279378	"	"
105	+0.158688	"	"	+0.271861	"	"

Table (7.2)

Horizontal spring elements shear strength values with respect to the maximum shear transferred in the infinite shear transfer condition (%)	Change in the shear stresses transferred through the interface spring elements	
	Axisymmetric solution (%)	Plane strain solution (%)
70%	-5.75	-4.07
50%	-15.63	-11.21
30%	-37.10	-31.81
0	-88.75	-80.74
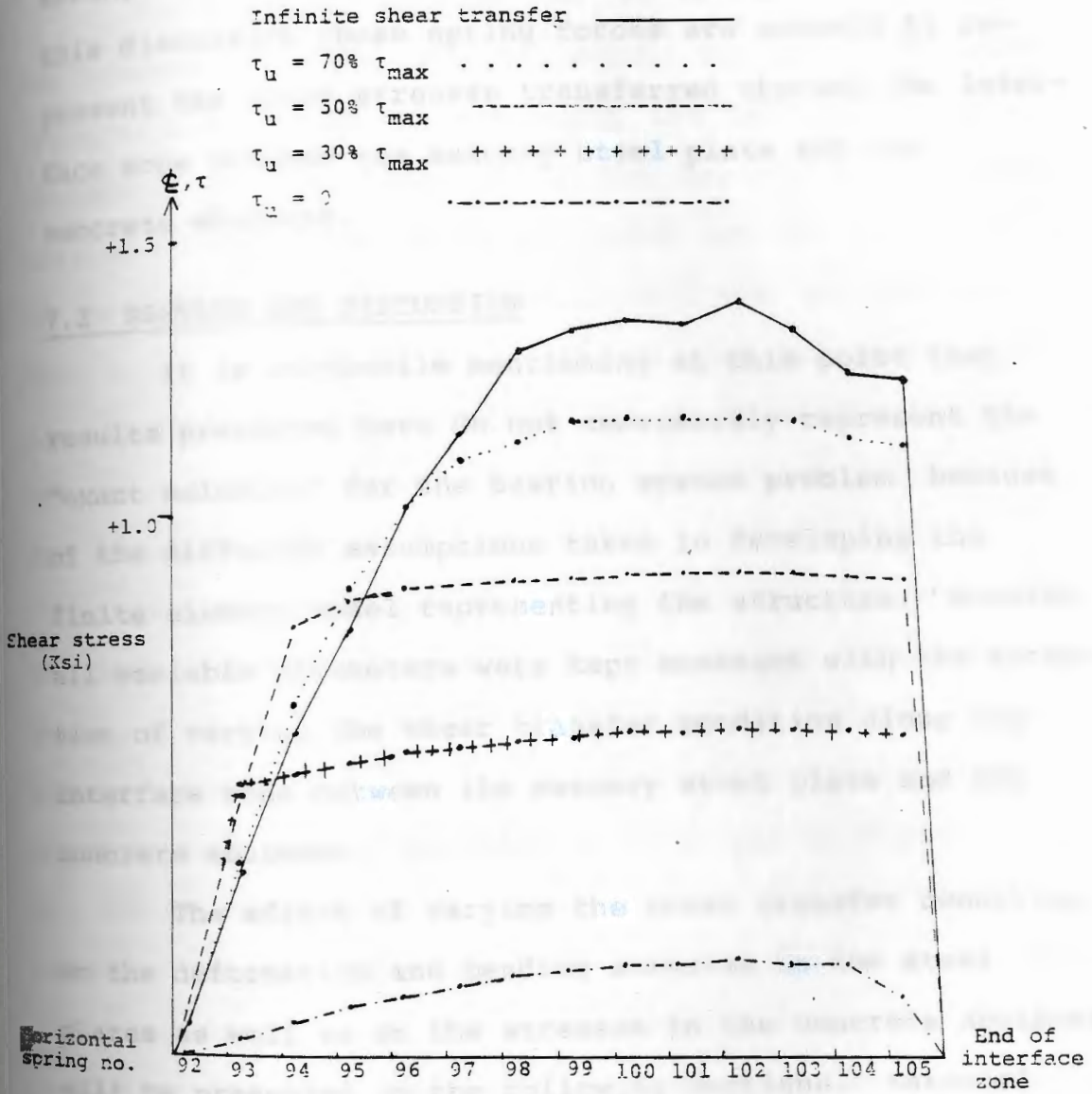
Fig. (7.1) Axisymmetric solution. Shear stress distribution along the horizontal interface spring elements.

Notice that the shear stresses transferred through the horizontal interface spring elements are actually the springs forces defined in equation (6.4). However, in this discussion those spring forces are assumed to represent the shear stresses transferred through the interface zone between the masonry steel plate and the concrete abutment.

7.2 RESULTS AND DISCUSSION

It is worthwhile mentioning at this point that results presented here do not necessarily represent the "exact solution" for the bearing system problem because of the different assumptions taken in developing the finite element model representing the structure. However, all variable parameters were kept constant with the exception of varying the shear transfer condition along the interface zone between the masonry steel plate and the concrete abutment.

The effect of varying the shear transfer condition on the deformation and bending stresses in the steel plates as well as on the stresses in the concrete abutment will be presented in the following sections. Material properties used in analyzing the bearing system are presented in Appendix C.

7.2.1 EFFECT OF SHEAR TRANSFER ON THE POT BEARING AND MASONRY STEEL PLATES DEFORMATION

Since the pot bearing and the masonry steel plates are assumed to behave as a continuum, the effect of shear transfer was studied by examining the deformation of a horizontal section taken along the masonry steel plate passing through nodes 53 to 67, which are the top nodes of the triangular steel elements adjacent to the interface zone, see fig. (6.7). Vertical and horizontal displacements of the nodes along the horizontal section resulting from axisymmetric and plane strain solutions are listed in tables (7.3.a) and (7.3.b) respectively.

Results from sec. (7.1) have shown that shear stresses transferred through the horizontal interface spring elements have higher values beneath the end of the masonry steel plate for all shear transfer conditions. Maximum shear stress appeared to be in spring element no. 102 which is under the section where the pot bearing ends and the masonry steel plate extends freely on top of the concrete surface. The non-uniform shear stress distribution could be physically attributed to the fact that the pot bearing and the masonry plates tend to bend over the concrete surface such that the end steel elements ould slip over the concrete surface and separate away from it. Horizontal displacement curves for the different shear transfer conditions in the axisymmetric solution are

shown in fig. (7.2). Notice that the horizontal dis-
placements along the masonry plate are actually con-
trolled by the nonlinear function which describes the
slip along the interface zone, see Appendix B (sec. (B.1)).
Consider the approximated shear stress distribution
curves along the interface zone, shown in fig. (7.1),
for the axisymmetric solution. In general, it was found
that the shear stress increases along the interface zone
until it reaches a maximum value, which was in all shear
transfer conditions in the horizontal interface spring
element no. 102 located under the portion of the bearing
system where the pot bearing ends and the masonry steel
plate extends freely on top of the concrete surface, see
fig. (6.7). Referring back to fig. (7.2), it was found
that horizontal displacements near the center of the
masonry plate elements above the portion of the interface
where low shear stresses are transferred, were small.
As the shear stress increased along the interface, the
horizontal displacements of the masonry plate increased
as well. Notice also that the maximum horizontal dis-
placement in the masonry plate was near the part where
the pot bearing ends and above the portion of the inter-
face where maximum shear stresses were transferred.
However, the horizontal displacements increased non-
linearly along the masonry plate depending on the non-
linear stress - strain relation that describes the slip
along the interface zone, see fig. (B.1). If the

ultimate shear strength value of the horizontal interface spring elements was lowered, slip along the interface would increase depending on the slip modulus. Nevertheless, at a low ultimate shear strength, (τ_u = 30% τ_{max}, or τ_u = 0), most of the horizontal interface spring elements were in the full slip range (slip modulus equals 29 Ksi) and the horizontal displacements tend to increase "linearly" along the masonry plate, see fig. (7.2); refer to tables (7.1.d) and (7.1.e). Hence, the end of the horizontal displacement curve, representing the displacements of the end part of the masonry plate, became more uniform. At the case representing infinite shear transfer condition, the maximum horizontal displacement appeared at node no. 62 and was about 18.72% higher than the horizontal displacement at node no. 67 located at the end of the masonry plate. However, in the case representing the zero shear transfer condition, the horizontal displacement at node no. 62 was only about 8.04% higher than at node no. 67.

It appeared that if high shear stresses are transferred along the interface zone, they act as a restraint against the deformation of the pot bearing and the masonry steel plates. As the ultimate shear strength of the horizontal interface spring elements was lowered, the masonry plate slipped over the concrete surface as discussed above, where the horizontal displacements increased nonlinearly along the plate. Since the plates

steel elements were assumed to be linear isotropic, the nonlinear increase of the horizontal displacements along the plate must be attributed to the bending of the plate. The vertical displacement distribution curves of the masonry steel plate for the different shear transfer conditions in the axisymmetric solution are shown in fig. (7.3).

The masonry plate was assumed to be rigidly connected to the concrete abutment, therefore, separation of the masonry plate steel elements from the concrete elements is not allowed. Therefore, general deformation curves of the masonry steel plate shown in fig. (7.4) for different shear transfer conditions did not look as one would expect. Horizontal and vertical displacement distribution curves for the plane strain solution are shown in figs. (7.5.a) and (7.5.b) respectively. Notice the difference in results due to absence of circumferential stresses and strains; however, the effect of shear transfer on the deformation of the pot bearing and the masonry steel plates is the same for both the axisymmetric and the plane strain solution methods.

7.2.2 EFFECT OF SHEAR TRANSFER ON THE POT BEARING AND MASONRY STEEL PLATES BENDING STRESSES

It was shown in the previous section how shear stresses transferred through the interface zone control the behavior of the steel plates represented by a

section taken along the masonry steel plate. Results indicated that as the ultimate shear strength of the horizontal spring elements decreases, slip along the interface increases and so does the horizontal and vertical displacement of the steel plate elements. Therefore, it could be stated at this point that shear stresses transferred through the interface actually act as a restraint against plates bending. Hence, it is expected that bending stresses in the pot bearing and the masonry steel plates would increase if the shear stresses transferred along the interface zone are decreased.

Averaged bending stresses in the top of the pot bearing were listed in tables (7.4.a) and (7.4.b) for the axisymmetric and the plane strain solution methods, respectively. Results showed that the averaged negative bending stresses increased nonlinearly in the pot bearing steel elements above the portion of the interface zone which slipped. For example, results from the plane strain solution showed that bending stresses in elements nos. 1,2, and 3, in the case $\tau_u = 70\% \ \tau_{max}$, have actually, even though insignificantly, decreased with respect to resulting bending stresses from the infinite shear transfer condition. In element no. 4, the bending stress has only increased by 0.11%, and in element no. 5 the bending stress has only increased by 1.00%. Referring to

Table (7.3.a) Axisymmetric solution. Vertical and horizontal displacements in top of the triangular steel elements adjacent to the interface zone.

Node number		53	54	55	56	57	58	59	60
Shear transfer condition	Displacement (inch)								
Infinite shear transfer	V	-0.00638	-0.00637	-0.00629	-0.00615	-0.00596	-0.00572	-0.00544	-0.00513
	H	0.0	+0.000076	+0.000148	+0.000216	+0.000279	+0.000334	+0.000378	+0.000407
Shear stress transferred reduced by 5.75%	V	-0.09642	-0.00641	-0.00633	-0.00619	-0.00600	-0.00576	-0.00548	-0.00516
	H	0.0	+0.000077	+0.000150	+0.000220	+0.000285	+0.000342	+0.000389	+0.000421
Shear stress transferred reduced by 15.63%	V	-0.00659	-0.00659	-0.00650	-0.00636	-0.00616	-0.00590	-0.00561	-0.00527
	H	0.0	+0.000084	+0.000164	+0.000242	+0.000316	+0.000384	+0.000438	+0.000476
Shear stress transferred reduced by 37%	V	-0.00678	-0.00678	-0.00669	-0.00653	-0.00631	-0.00604	-0.00573	-0.00537
	H	0.0	+0.000095	+0.000185	+0.000273	+0.000355	+0.000428	+0.000488	+0.000530
Shear stress transferred reduced by 88.75%	V	-0.00708	-0.00706	-0.00696	-0.00678	-0.00655	-0.00625	-0.00591	-0.00553
	H	0.0	+0.000112	+0.000217	+0.000318	+0.000411	+0.000494	+0.000562	+0.000611

V = vertical displacements

H = horizontal displacements

Continuation of Table (7.3.a)

61	62	63	64	65	66	67
-0.00481	-0.00447	-0.00413	-0.00378	-0.00344	-0.00313	-0.00286
+0.000420	+0.000422	+0.000418	+0.000405	+0.000381	+0.000357	+0.000343
-0.00483	-0.00449	-0.00414	-0.00377	-0.00343	-0.00312	-0.00284
+0.000437	+0.000441	+0.000438	+0.000424	+0.000398	+0.000372	+0.000358
-0.00492	-0.00455	-0.00418	-0.00379	-0.00341	-0.00307	-0.00276
+0.000497	+0.000505	+0.000506	+0.000496	+0.000473	+0.000449	+0.000434
-0.00499	-0.00461	-0.00421	-0.00380	-0.00339	-0.00302	-0.00268
+0.000555	+0.000566	+0.000570	+0.000562	+0.000541	+0.000518	+0.000502
-0.00512	-0.00470	-0.00426	-0.00381	-0.00336	-0.00294	-0.00255
+0.000642	+0.000659	+0.000667	+0.000663	+0.000645	+0.000623	+0.000606

Table (7.3.b)   Plane strain solution.   Vertical and horizontal displacements in top of the triangular steel elements adjacent to the interface zone.

Node number		53	54	55	56	57	58	59	60
Shear transfer condition	Displace-ments (inches)								
Infinite shear transfer	V	-0.0113	-0.0113	-0.0112	-0.0110	-0.0107	-0.0104	-0.0100	-0.0095
	H	0.0	+0.000096	+0.000209	+0.000315	+0.000416	+0.000509	+0.000591	+0.000657
Shear stress transferred reduced by 4.07%	V	-0.0113	-0.0113	-0.0112	-0.0110	-0.0108	-0.0104	-0.0100	-0.0096
	H	0.0	+0.000097	+0.000210	+0.000317	+0.000419	+0.000515	+0.000600	+0.000670
Shear stress transferred reduced by 11.21%	V	-0.0115	-0.0115	-0.0114	-0.0112	-0.0109	-0.0105	-0.0101	-0.0096
	H	0.0	+0.000103	+0.000224	+0.000341	+0.000458	+0.000569	+0.000668	+0.000750
Shear stress transferred reduced by 31.81%	V	-0.0117	-0.0117	-0.0115	-0.0113	-0.0110	-0.0106	-0.0102	-0.0097
	H	0.0	+0.000120	+0.000259	+0.000393	+0.000523	+0.000645	+0.000753	+0.000843
Shear stress transferred reduced by 80.74%	V	-0.0120	-0.0119	-0.0118	-0.0116	-0.0112	-0.0108	-0.0103	-0.0098
	H	0.0	+0.000162	+0.000321	+0.000476	+0.000625	+0.000762	+0.000885	+0.000986

Continuation of Table (7.3.b)

61	62	63	64	65	66	67
-0.0090 +0.000703	-0.0085 +0.000733	-0.0079 +0.000752	-0.0074 +0.000756	-0.0068 +0.000743	-0.0062 +0.000726	-0.0057 +0.000717
-0.0090 +0.000720	-0.0085 +0.000753	-0.0079 +0.000773	-0.0073 +0.000777	-0.0068 +0.00076	-0.0062 +0.000741	-0.0057 +0.000731
-0.0091 +0.000810	-0.0085 +0.000852	-0.0079 +0.000881	-0.0073 +0.000891	-0.0067 +0.000881	-0.0061 +0.000866	-0.0055 +0.000858
-0.0091 +0.000910	-0.0085 +0.000957	-0.0079 +0.000990	-0.0072 +0.00100	-0.0065 +0.00100	-0.0059 +0.00098	-0.0053 +0.00098
-0.0091 +0.00106	-0.0085 +0.00112	-0.0078 +0.00116	-0.0071 +0.00118	-0.0064 +0.00118	-0.0057 +0.00117	-0.0050 +0.00116
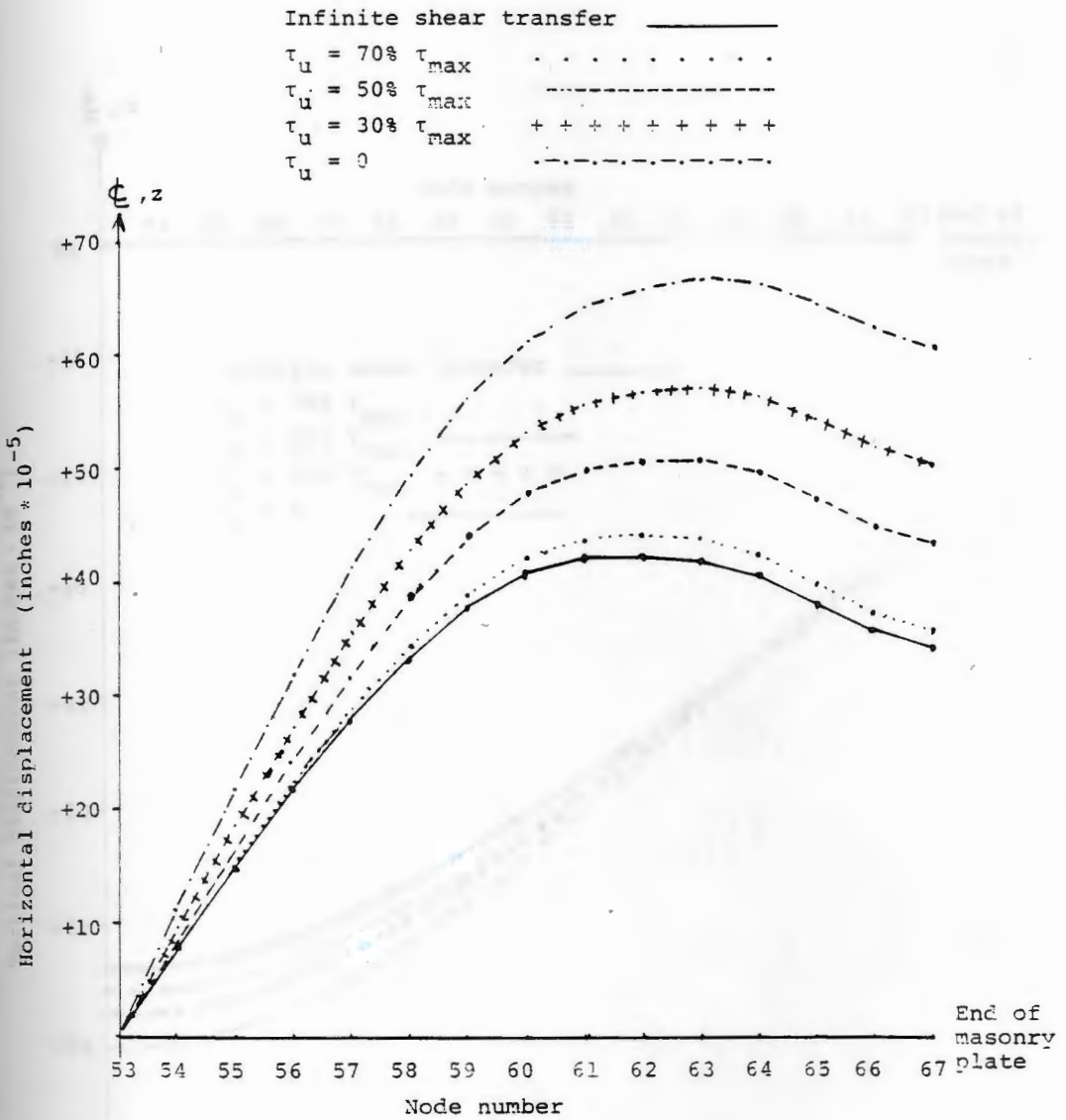
Fig. (7.2) Axisymmetric solution. Horizontal displacement surves
for the different shear transfer conditions.
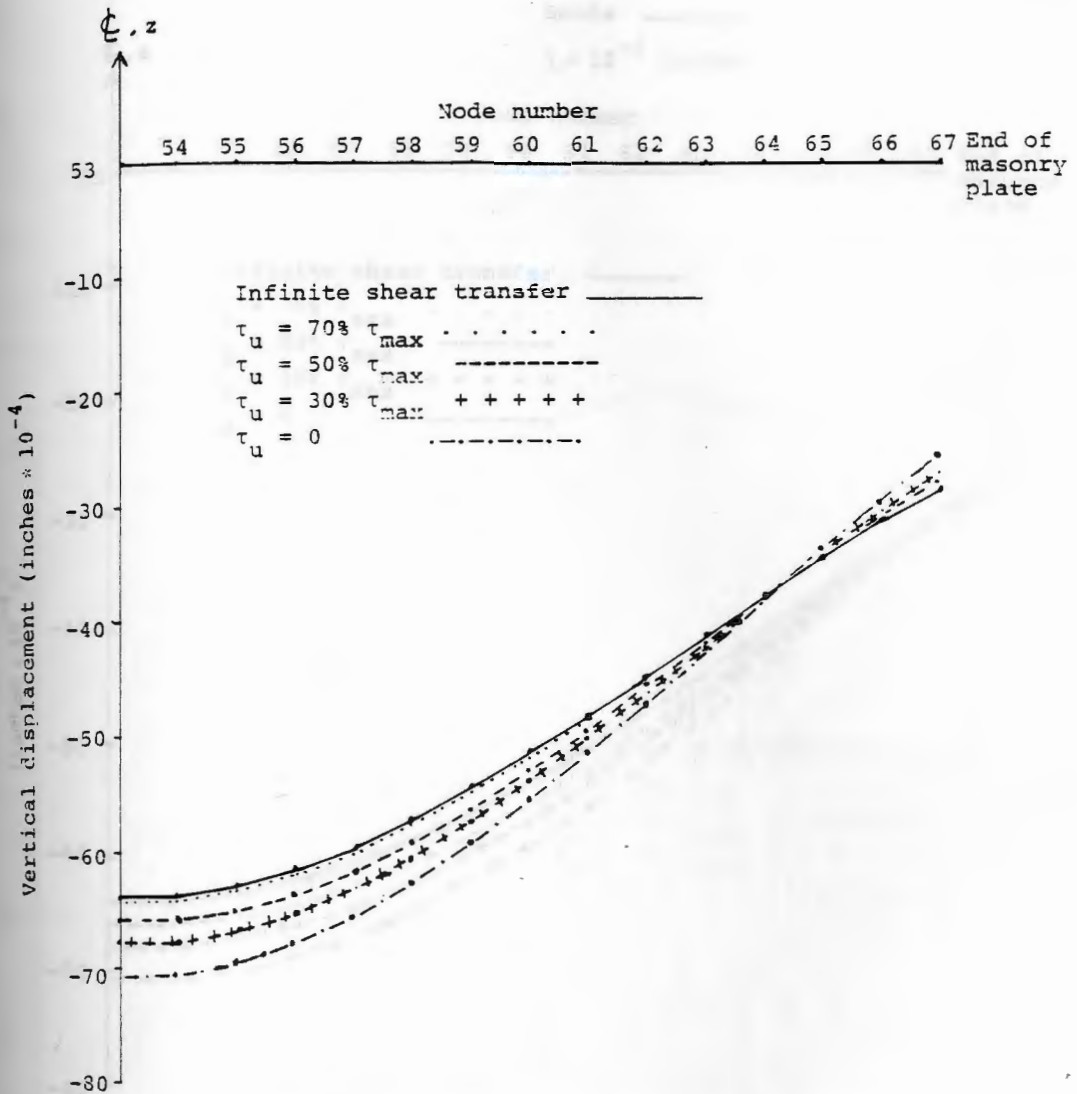
Fig. (7.3) Axisymmetric solution. Vertical displacement
curves for the different shear transfer
conditions.
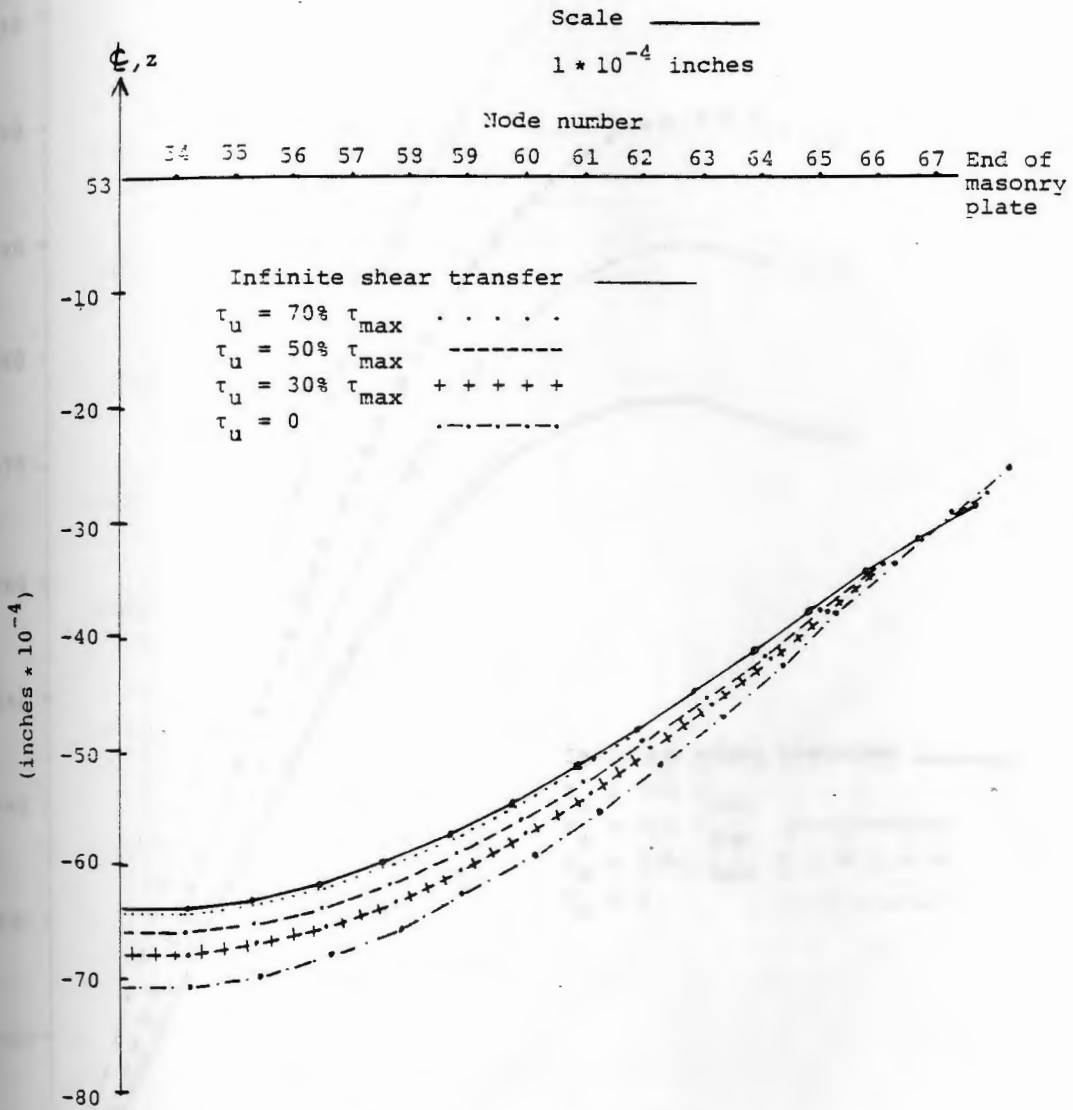
Fig. (7.4) Axisymmetric solution. Deformation of the top nodes of the triangular steel elements adjacent to the interface zone.
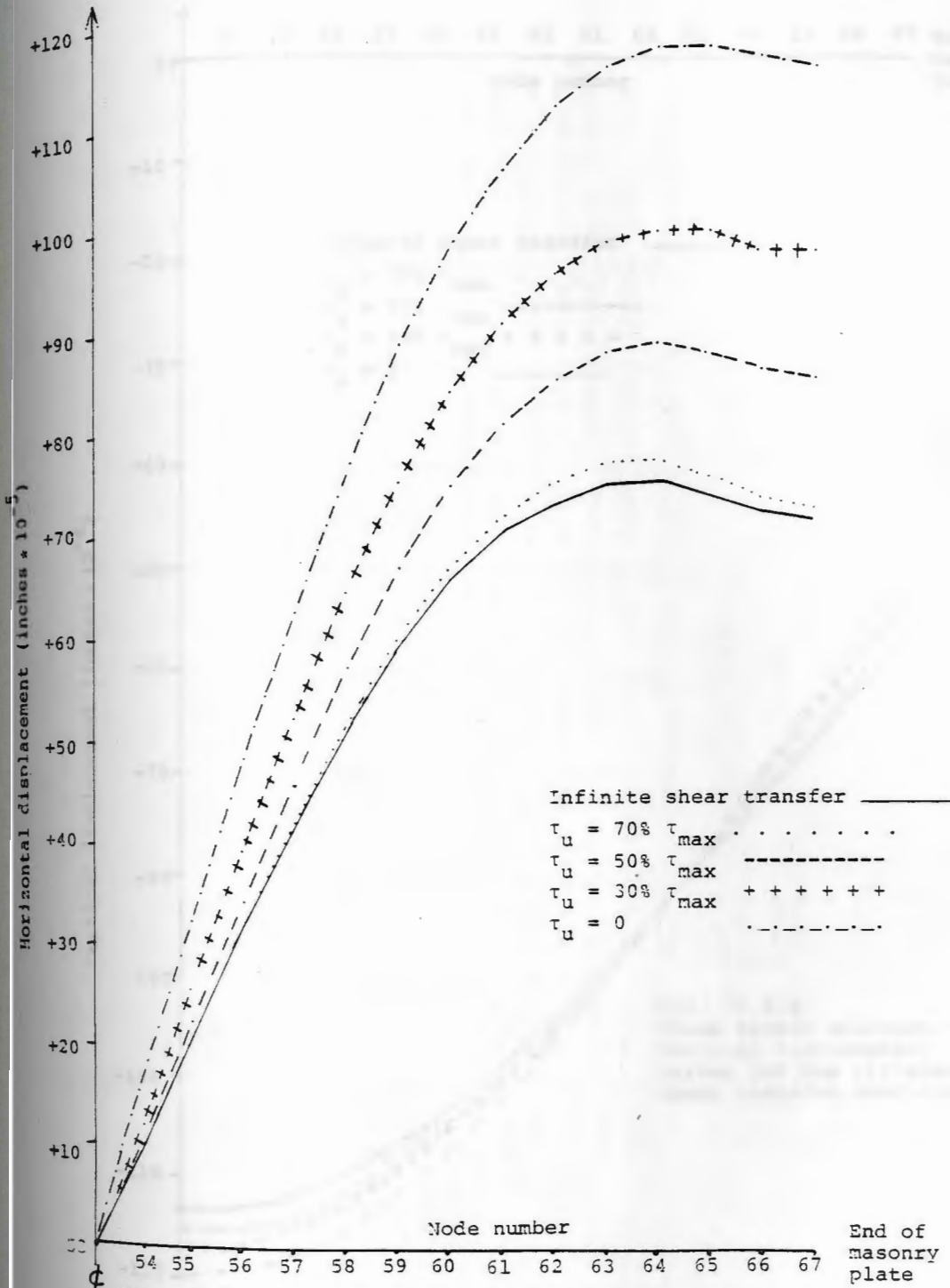
Fig. (7.5.a) Plane strain solution. Horizontal displacement curves for the different shear transfer conditions.

Fig. (7.5.b)
Plane strain solution.
Vertical displacement
curves for the different
shear transfer conditions.
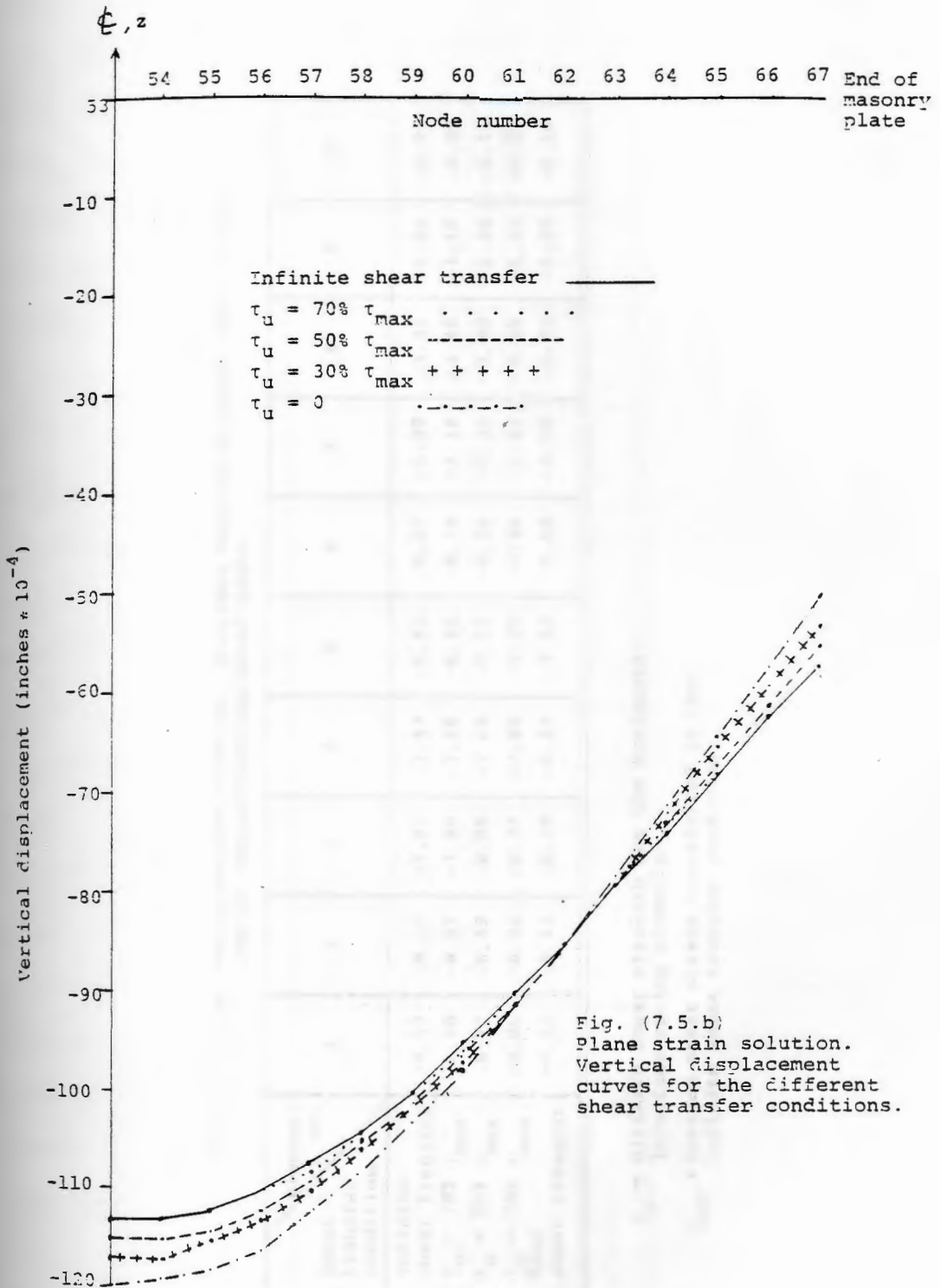
Table (7.4.a) Axisymmetric solution. Averaged bending stresses (Ksi) in the top of the pot bearing steel plate.

Shear transfer condition \ Element no.	1	2	3	4	5	6	7	8	9	10
Infinite shear transfer	-8.59	-8.26	-7.87	-7.43	-6.83	-6.07	-5.09	-3.32	-1.06	-0.08
$\tau_u = 70\% \ \tau_{max}$	-8.60	-8.27	-7.90	-7.48	-6.91	-6.16	-5.18	-3.40	-1.10	-0.09
$\tau_u = 50\% \ \tau_{max}$	-8.72	-8.42	-8.09	-7.69	-7.11	-6.34	-5.32	-3.50	-1.16	-0.11
$\tau_u = 30\% \ \tau_{max}$	-9.06	-8.72	-8.34	-7.89	-7.27	-6.46	-5.42	-3.58	-1.21	-0.13
Zero shear transfer	-9.53	-9.12	-8.70	-8.19	-7.52	-6.68	-5.59	-3.71	-1.29	-0.16

τ_u = ultimate shear strength for the horizontal interface spring elements

τ_{max} = maximum shear stress transferred in the infinite shear transfer condition

Table (7.4.b)   Plane strain solution.   Averaged bending stresses (Ksi)
in the top of the pot bearing steel plate.
Gauss integration points 2 and 4.

Shear transfer condition	Element no. 1	2	3	4	5	6	7	8	9	10
Infinite shear transfer	-9.38	-9.33	-9.15	-8.78	-8.20	-7.40	-6.31	-4.37	-1.72	-0.24
$\tau_u = 70\%\ \tau_{max}$	-9.35	-9.30	-9.14	-8.79	-8.24	-7.47	-6.40	-4.45	-1.77	-0.25
$\tau_u = 50\%\ \tau_{max}$	-9.23	-9.24	-9.17	-8.91	-8.42	-7.65	-6.55	-4.57	-1.84	-0.28
$\tau_u = 30\%\ \tau_{max}$	-9.48	-9.47	-9.36	-9.04	-8.49	-7.68	-6.57	-4.59	-1.87	-0.29
Zero shear transfer	-10.02	-9.89	-9.63	-9.20	-8.58	-7.75	-6.62	-4.64	-1.92	-0.31

table (7.1.b) and fig. (6.7), notice that slip did not occur in the horizontal interface spring elements beneath steel elements nos. 1, 2, 3, and 4, while the horizontal spring beneath steel element no. 5 has just slipped with a slip modulus equalling 2900 Ksi. That indicates that shear stresses do in fact restrain bending of the steel plates. The percentage change of negative bending stresses in the top of the pot bearing plate steel elements is shown in fig. (7.6). Bending stresses increase nonlinearly along the pot bearing steel elements following the nonlinear slip function. When all the horizontal interface spring elements are in full slip (slip modulus equal 29 Ksi), bending stress along the pot bearing steel elements tends to change linearly because the modulus of slip becomes the same in all horizontal spring elements. Bending stress distribution curves for the different shear transfer conditions are shown in fig. (7.7.a) and fig. (7.7.b) for the axisymmetric and the plane strain solution methods, respectively. However, the effect of varying the shear transfer conditions on the negative bending stresses along the top of the pot plate is practically insignificant, due to the thickness of the plate which is assumed to behave with the masonry plate as a continuum. Figure (7.8) represents the change of the bending stresses, along a vertical section taken through the center of the pot bearing and the masonry

$\tau_u = 70\% \ \tau_{max}$ ——————
$\tau_u = 50\% \ \tau_{max}$ . . . . . .
$\tau_u = 30\% \ \tau_{max}$ — — — — — —
$\tau_u = 0$ + + + + + + +

(a)   Axisymmetric solution

(b)   Plane strain solution
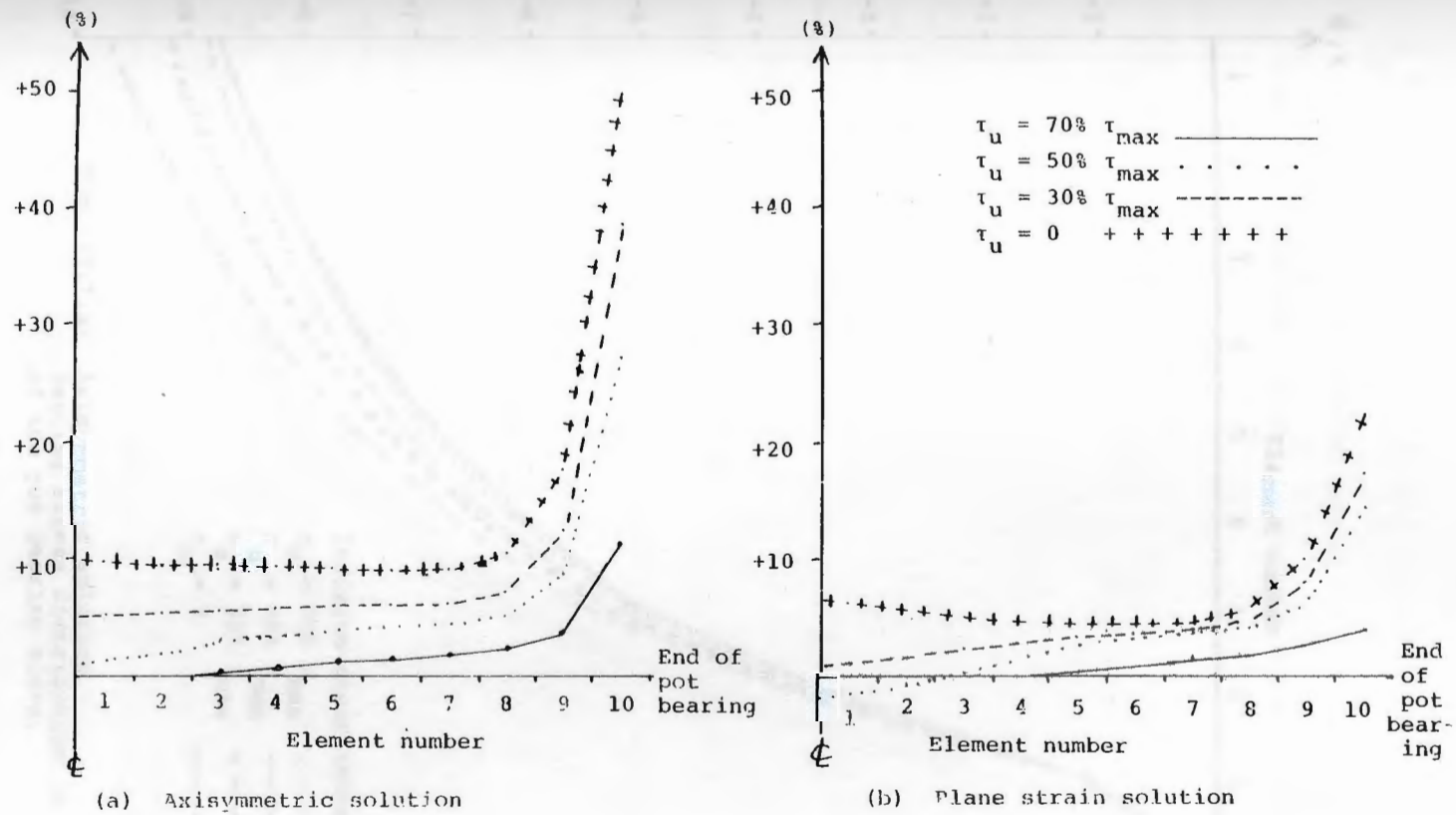
Fig. (7.6) Percentage of change in bending stresses in top of the pot bearing steel plate.
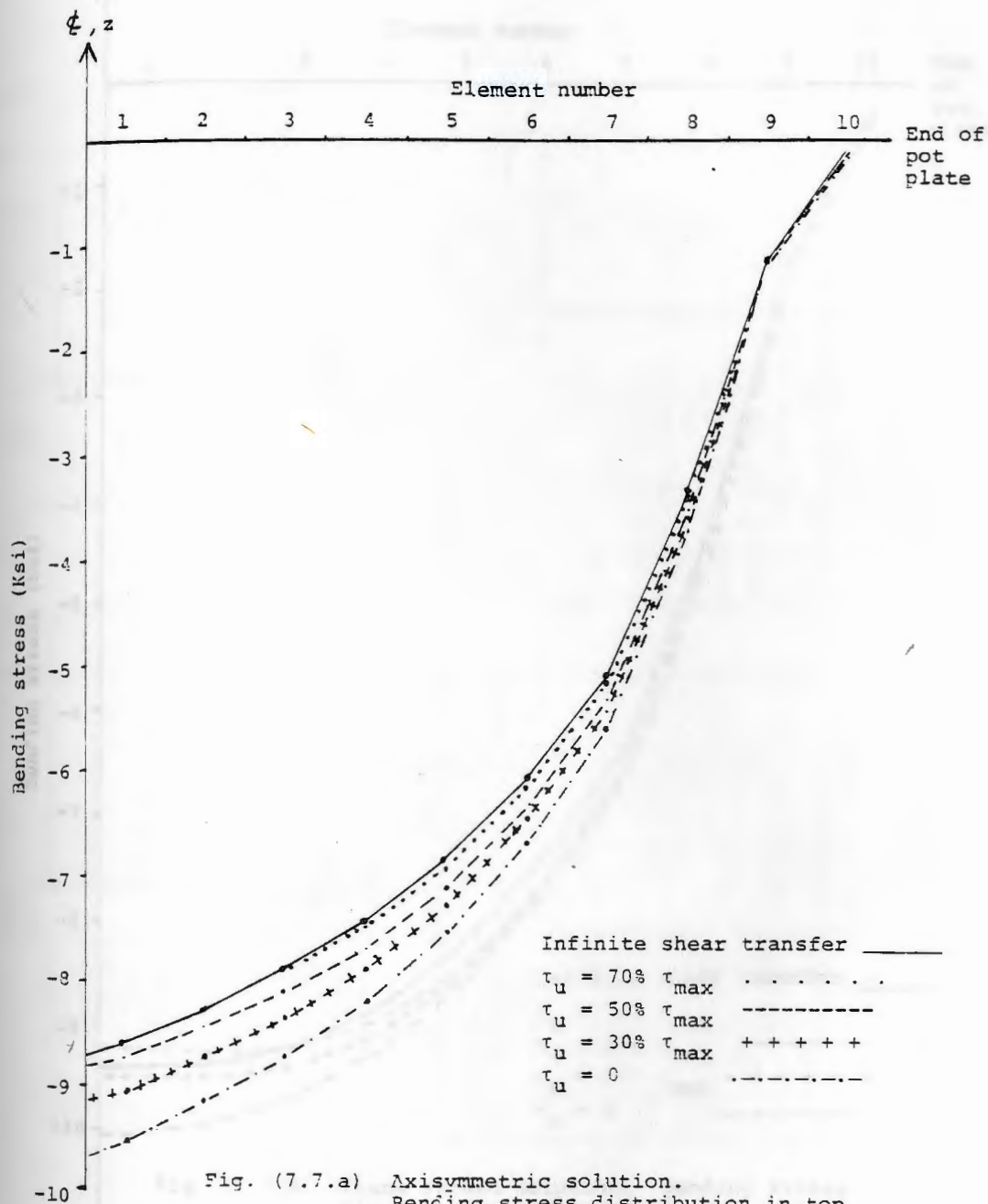
Fig. (7.7.a) Axisymmetric solution.
Bending stress distribution in top
of the pot bearing plate.

Fig. (7.7.b) Plane strain solution. Bending stress distribution in top of the pot bearing plate.
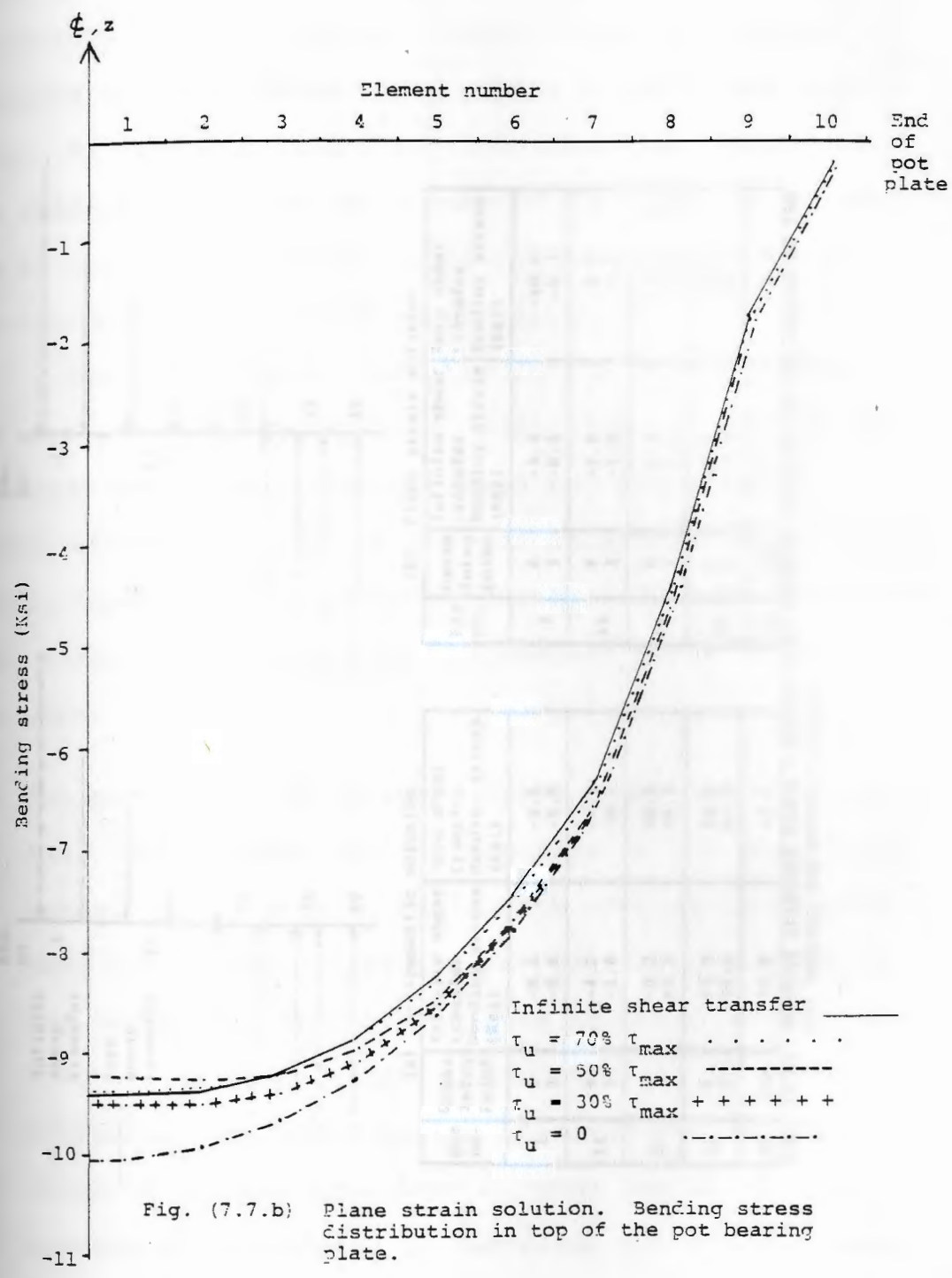
Scale: 1/4" = 1 Ksi
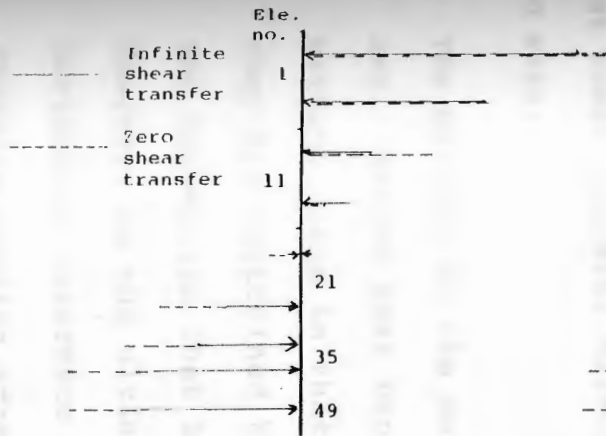
(a) Axisymmetric solution

Ele no.	Gauss integ point	Infinite shear transfer Bending stress (Ksi)	Zero shear transfer Bending stress (Ksi)
1	4	-8.6	-9.6
	3	-5.6	-5.8
11	4	-4.2	-4.1
	3	-1.6	-0.7
21	4	-0.3	+0.9
	3	+2.4	+4.4
35	4	+3.3	+5.5
	3	+4.6	+7.3
49	Avg.	+4.8	+7.2
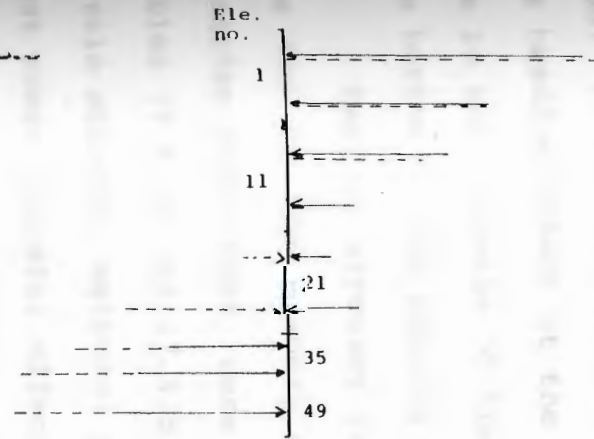
(b) Plane strain solution

Ele no.	Gauss integ point	Infinite shear transfer Bending stress (Ksi)	Zero shear transfer Bending stress (Ksi)
1	4	-9.4	-10.0
	3	-6.4	-6.3
11	4	-4.8	-4.2
	3	-1.9	-0.6
21	4	-1.3	+1.4
	3	-2.1	+5.1
35	4	+3.7	+6.6
	3	+4.7	+8.4
49	Avg.	+5.5	+8.5

Fig. (7.8) Bending stresses along a normal line through elements at the center of the pot bearing and masonry plates.

155

steel plates, for the infinite and zero shear transfer conditions. for triangular steel elements, bending stresses in Gauss integration points 3 and 4 were averaged. It appeared from fig. (7.8) that the increase in the bending moment at the center of the plate is actually due to the increase of the positive bending stress at the bottom of the masonry steel plate.

Bending stresses resulted in the steel elements at the top of the masonry steel plate from different shear transfer conditions, were averaged and listed in tables (7.5.a) and (7.5.b) for the axisymmetric and plane strain solution methods, respectively. Results indicated that shear transfer affects the masonry steel plate in two ways:

1) The portion of the masonry plate under the pot bearing. Notice that bending stresses in the top of the masonry plate in that region are very small because they are restrained by the pot bearing plate due to the assumption that both plates behave as a continuum. However, as the ultimate shear strength of the horizontal interface spring elements was redcued, negative bending stresses in that region of the masonry plate started to decrease, converging toward becoming positive bending stresses as the slip in the interface increased. Bending stress distribution curves, for both solution methods, are shown in

Table (7.5.a) Axisymmetrical solution. Averaged bending stresses (Ksi) in the top of the masonry steel plate. Gauss integration points 2 and 4.

Shear transfer condition \ Element no.	21	22	23	24	25	26	27	28	29	30	31	32	33	34
Infinite shear transfer	-0.36	-0.36	-0.36	-0.36	-0.36	-0.36	-0.46	-0.77	-1.26	-1.82	-2.56	-0.47	+0.13	+0.08
$\tau_u = 70\% \ \tau_{max}$	-0.31	-0.31	-0.30	-0.29	-0.28	-0.28	-0.38	-0.70	-1.22	-1.79	-2.50	-0.38	+0.19	+0.10
$\tau_u = 50\% \ \tau_{max}$	-0.04	-0.03	-0.02	-0.00	+0.01	-0.01	-0.15	-0.51	-1.07	-1.70	-2.46	-0.39	+0.16	+0.09
$\tau_u = 30\% \ \tau_{max}$	+0.31	+0.30	+0.30	+0.29	+0.26	+0.21	+0.04	-0.35	-0.95	-1.62	-2.40	-0.37	+0.16	+0.08
Zero shear transfer	+0.85	+0.81	+0.77	+0.71	+0.63	+0.54	+0.33	-0.11	-0.78	-1.52	-2.37	-0.36	+0.14	+0.07

τ_u = ultimate shear strength value for the horizontal interface spring elements.

τ_{max} = maximum shear stress transferred in the infinite shear transfer condition.

Table (7.5.b) Plane strain solution. Averaged bending stresses (Ksi) in the top of the masonry steel plate.
Gauss integration points 2 and 4.

Shear transfer condition \ Element no.	21	22	23	24	25	26	27	28	29	30	31	32	33	34
Infinite shear transfer	-0.34	-0.34	-0.26	-0.21	-0.18	-0.16	-0.23	-0.53	-1.10	-1.82	-2.73	-0.39	+0.29	+0.18
$\tau_u = 70\% \ \tau_{max}$	-0.30	-0.30	-0.21	-0.15	-0.11	-0.08	-0.15	-0.46	-1.04	-1.78	-2.66	-0.25	+0.39	+0.22
$\tau_u = 50\% \ \tau_{max}$	+0.02	+0.04	+0.16	+0.25	+0.31	+0.33	+0.23	-0.13	-0.78	-1.58	-2.45	-0.17	+0.41	+0.22
$\tau_u = 30\% \ \tau_{max}$	+0.56	+0.56	+0.65	+0.70	+0.70	+0.66	+0.52	+0.12	-0.56	-1.37	-2.17	-0.02	+0.47	+0.23
Zero shear transfer	+1.43	+1.41	+1.38	+1.32	+1.24	+1.15	+0.94	+0.48	-0.25	-1.09	-1.82	+0.15	+0.53	+0.24

figs. (7.9.a) and (7.9.b). Considering the plane strain solution, in the shear transfer condition where $\tau_u = 70\%\ \tau_{max}$, bending stresses in the top of the masonry plate under the pot bearing were all negative; the minimum negative bending stress appeared to be in steel element no. 26, lying exactly above the horizontal interface element where slip has started with a slip modulus equal to 290 Ksi, see table (7.1.b) and fig. (6.7). In the shear transfer condition where $\tau_u = 50\%\ \tau_{max}$, the bending stresses became positive in element no. 22 and started to increase nonlinearly until they peaked in steel element no. 26, which lies above the horizontal interface spring element where slip has started with a slip modulus equal to 290 Ksi. Nevertheless, in the case representing zero shear transfer, the positive bending stresses were uniformly distributed along that portion of the interface zone because most horizontal spring elements slipped with a uniform slip modulus. Thus as the ultimate shear strength value of the horizontal interface spring elements decreases, the pot bearing and the masonry plate modeled as a continuum, will have an increasing bending moment in the center, refer to fig. (7.8).
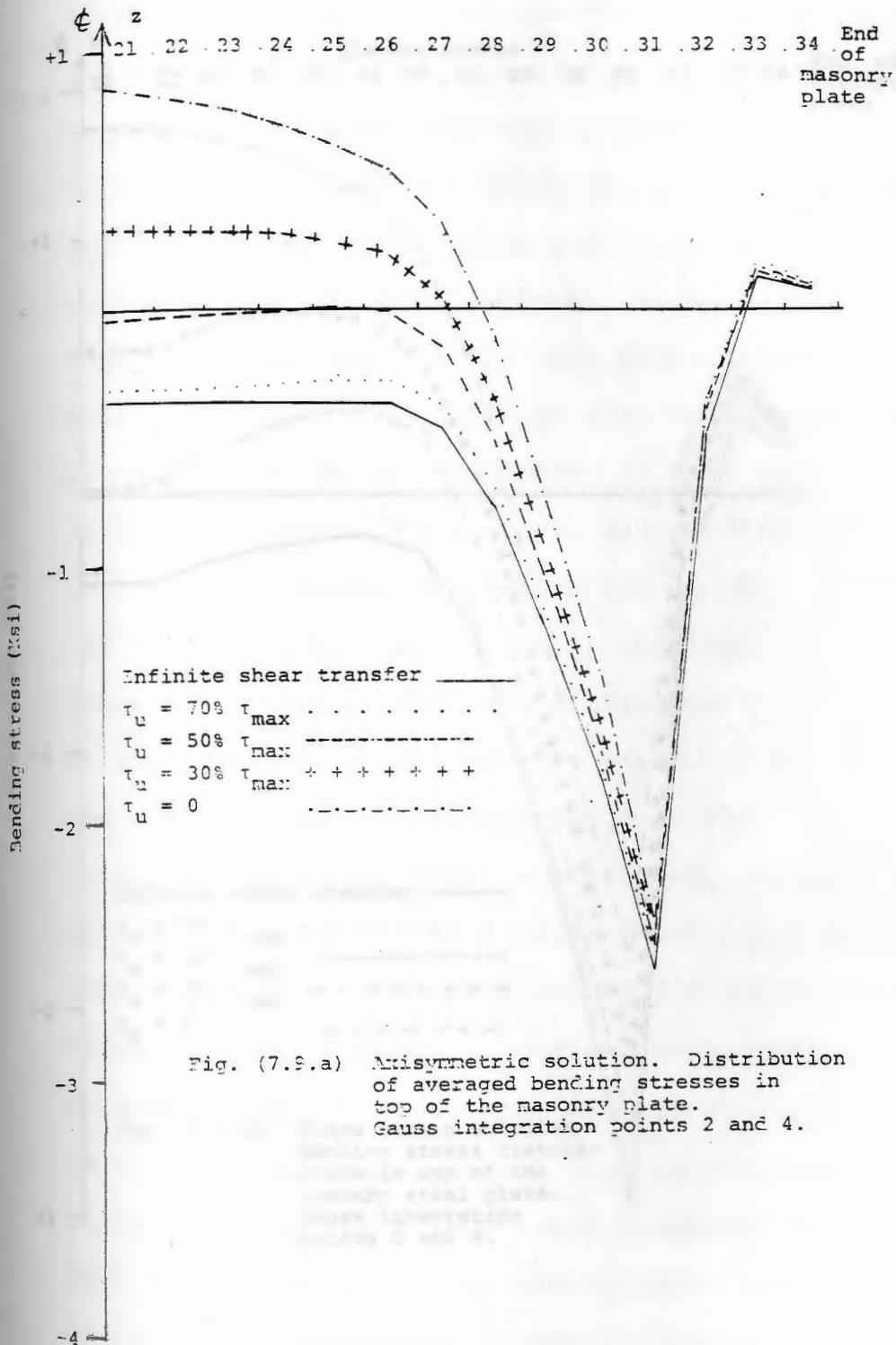
Fig. (7.9.a) Axisymmetric solution. Distribution
of averaged bending stresses in
top of the masonry plate.
Gauss integration points 2 and 4.

Element number

21 22 23 24 25 26 27 28 29 30 31 32 33 34

End of masonry plate

Bending stress (Ksi)

Infinite shear transfer ——————
$\tau_u = 70\% \ \tau_{max}$ ············
$\tau_u = 50\% \ \tau_{max}$ ----------------
$\tau_u = 30\% \ \tau_{max}$ + + + + + + + +
$\tau_u = 0$._._._._._._.

Fig. (7.9.b) Plane strain solution.
Bending stress distrib-
ution in top of the
masonry steel plate.
Gauss integration
points 2 and 4.
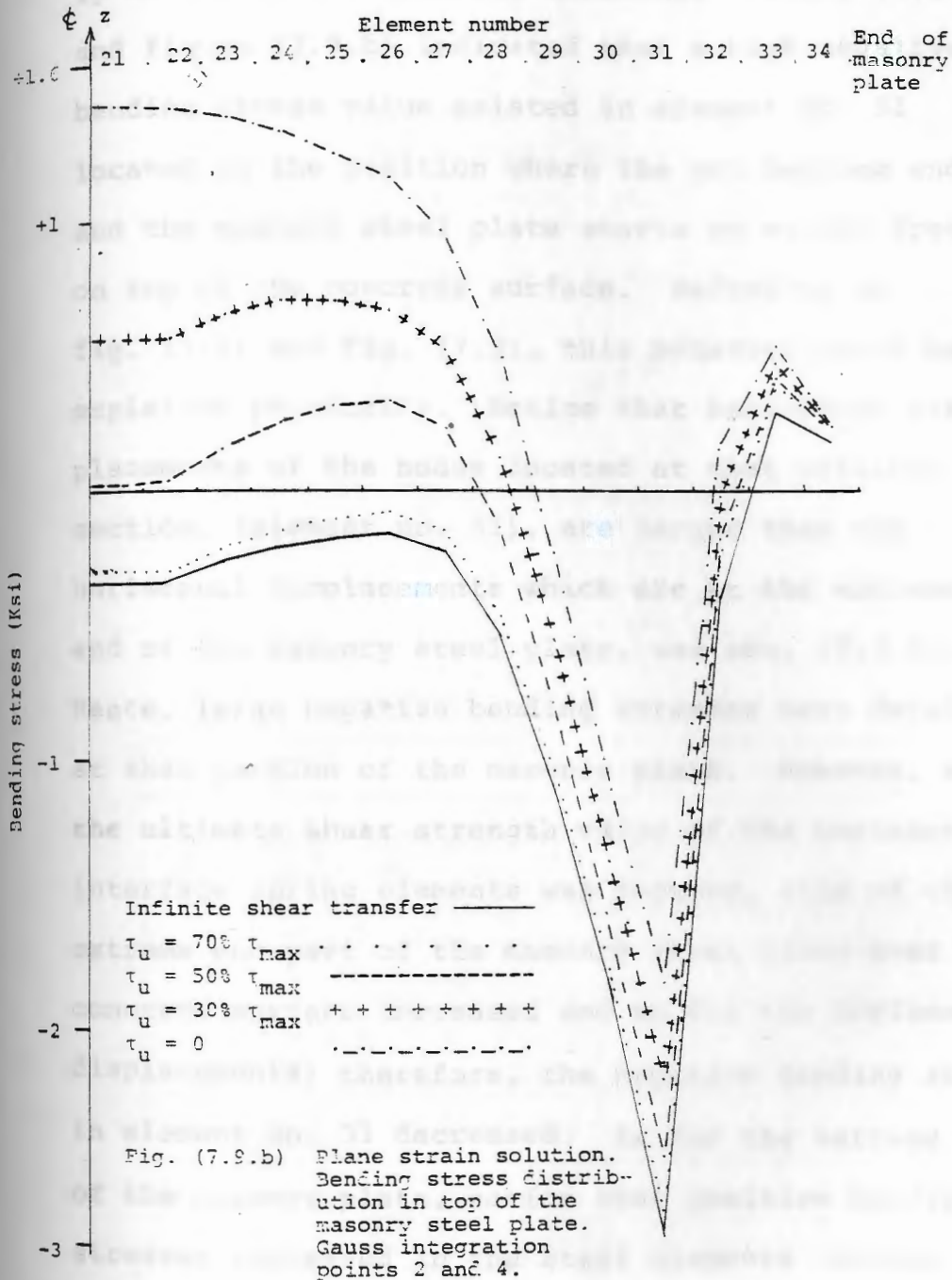
2) The portion of the masonry steel plate extending freely on top of the concrete abutment. Figure (7.9.a) and figure (7.9.b) indicated that a high negative bending stress value existed in element no. 31 located in the position where the pot bearing ends and the masonry steel plate starts to extend freely on top of the concrete surface. Referring to fig. (7.2) and fig. (7.3), this behavior could be explained physically. Notice that horizontal displacements of the nodes located at that critical section, (element no. 31), are larger than the horizontal displacements which are at the extreme end of the masonry steel plate, see sec. (7.3.1). Hence, large negative bending stresses were developed at that portion of the masonry plate. However, when the ultimate shear strength value of the horizontal interface spring elements was reduced, slip of the extreme end part of the masonry steel plate over the concrete surface increased and so did the horizontal displacements; therefore, the negative bending stress in element no. 31 decreased. As for the extreme end of the masonry plate, notice that positive bending stresses increased in the steel elements located at that end of the plate, as the ultimate shear strength value of the horizontal interface spring elements was decreased.

Bending stress (Ksi)

| +2.0 | +1.0 | 0.0 | -1.0 | -2.0 | -3.0 |

Element no.

31

45

59

Infinite shear transfer ————

$\tau_u = 70\% \ \tau_{max}$ . . . . . .

$\tau_u = 50\% \ \tau_{max}$ ----------

$\tau_u = 30\% \ \tau_{max}$ + + + + +

$\tau_u = 0$.—.—.—.—.
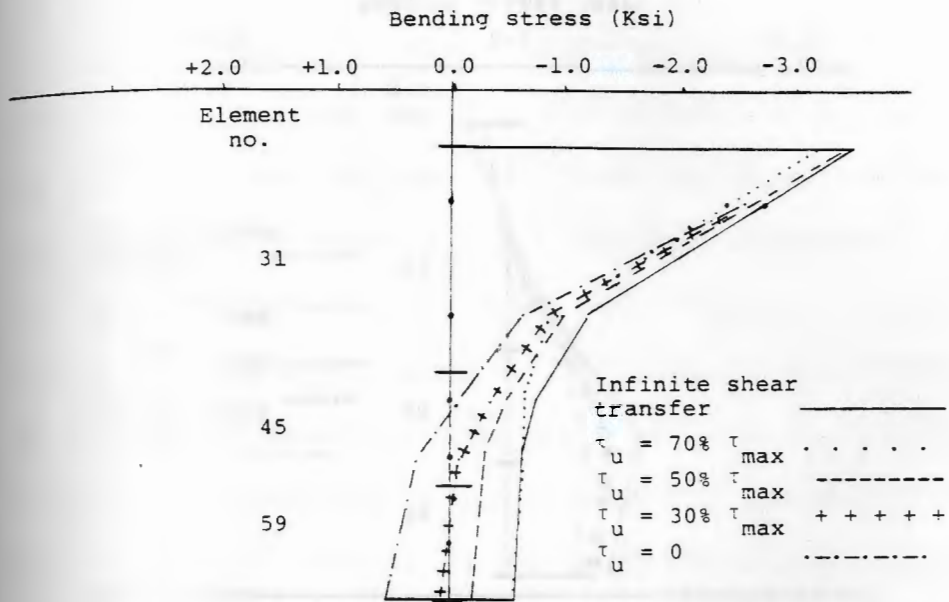
Shear transfer condition		Bending stresses (Ksi)				
Ele. no.	Gauss integ. point	Infinite shear transfer	$\tau_u = 70\% \tau_{max}$	$\tau_u = 50\% \tau_{max}$	$\tau_u = 30\% \tau_{max}$	$\tau_u = 0$
31	2	-2.69	-2.64	-2.60	-2.55	-2.52
	1	-1.18	-1.16	-0.97	-0.83	-0.61
45	2	-0.74	-0.74	-0.49	-0.32	-0.03
	1	-0.61	-0.62	-0.30	-0.07	+0.30
59	1 & 2 averaged	-0.53	-0.59	-0.23	+0.03	+0.45

Fig. (7.10.a) Axisymmetric solution. Bending stress distribution along a vertical line passing through the critical section of the masonry steel plate.

Bending stress (Ksi)

+1.0   0.0   -1.0

Ele. no.

Infinite shear transfer ———— 31

τ_u = 70% τ_{max} ......

τ_u = 50% τ_{max} ------

τ_u = 30% τ_{max} +++++ 45

τ_u = 0 ._._._._.

59
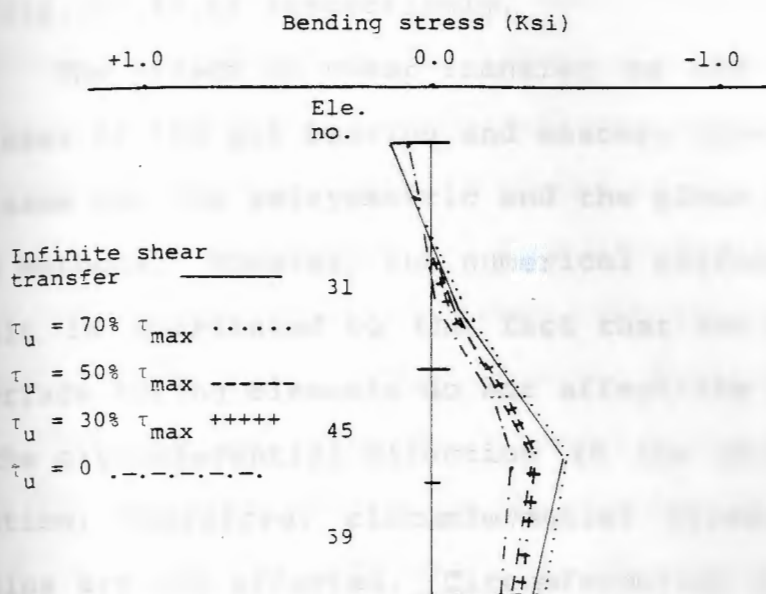
Shear transfer condition		Bending stresses (Ksi)				
Ele. no.	Gauss integ. point	Infinite shear stress	τ_u = 70% τ_{max}	τ_u = 50% τ_{max}	τ_u = 30% τ_{max}	τ_u = 0
34	2	+0.05	+0.06	+0.05	+0.05	+0.04
	1	-0.11	-0.12	-0.09	-0.07	-0.03
48	2	-0.31	-0.32	-0.24	-0.26	-0.21
	1	-0.45	-0.47	-0.35	-0.36	-0.28
62	1 & 2 averaged	-0.40	-0.42	-0.31	-0.33	-0.26

Fig. (7.10.b)   Axisymmetric solution. Bending stress distribution along a vertical line passing through the end steel elements of the masonry steel plate.

Bending stress distribution along vertical lines passing through the critical section and the end steel elements of the masonry plate is shown in fig. (7.10.a) and fig. (7.10.b) respectively.

The effect of shear transfer on the bending stresses of the pot bearing and masonry steel plates is the same for the axisymmetric and the plane strain solution methods. However, the numerical difference in the result is attributed to the fact that the horizontal interface spring elements do not affect the deformation in the circumferential direction in the axisymmetric solution; therefore, circumferential stresses and strains are not affected. Circumferential or in general out-of-plane strains are assumed to equal zero in the plane strain solution.

7.2.3 EFFECT OF SHEAR TRANSFER ON THE NORMAL AND SHEAR STRESS DISTRIBUTION IN THE CONCRETE ABUTMENT

The effect of shear transfer on the vertical and horizontal deformation as well as on the bending of the steel plates on top of the concrete abutment surface, was examined in the previous sections. Vertical displacement distribution curves along the masonry steel plate for different shear transfer conditions were shown in fig. (7.3) and fig. (7.5.b) for the axisymmetric and the plane strain solution methods, respectively. The general deformation curve representing the deformation

of the masonry steel plate under different shear transfer
assumptions for the axisymmetric solution was shown in
fig. (7.4). Generally speaking, all deformation curves
indicated that as the ultimate shear strength of the
horizontal interface spring elements was decreased,
vertical displacements of the masonry steel plate tend
to increase in the direction normal to the surface of the
concrete near the center and decrease toward the end,
with respect to results achieved from the infinite shear
transfer condition. Furthermore, it has been shown in
sec. (7.2.2), that the masonry steel plate tends to bend
over the concrete surface at the section of the plate
which is above the position where slip starts in the
interface zone. Averaged vertical stresses along the
concrete elements nos. 161 to 170, (selected about
1.25 inches below the concrete surface to avoid direct
effect from the interface spring elements and the modeling
of the interface), for the different shear transfer condi-
tions were listed in tables (7.6.a) and (7.6.b) for the
axisymmetric and plane strain solution methods. Results
generally indicate that normal (compression) stresses
increased in the center of the concrete abutment and
decreased at the end, see fig. (7.11.a) and fig. (7.11.b).
However, with a closer look at the results it was found
that maximum increase in the concrete normal stresses for
all shear transfer conditions appeared to be at the
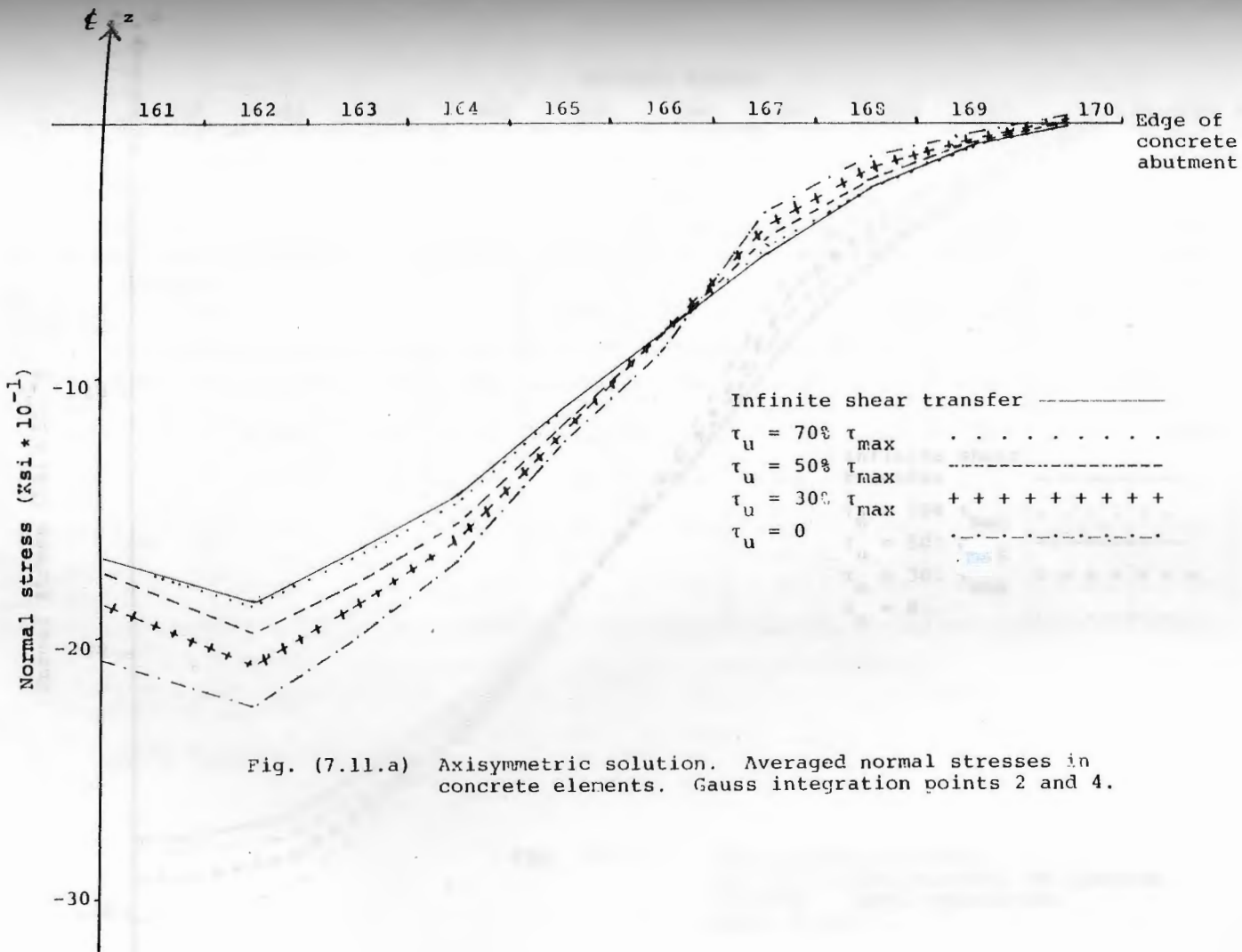
Fig. (7.11.a) Axisymmetric solution. Averaged normal stresses in concrete elements. Gauss integration points 2 and 4.
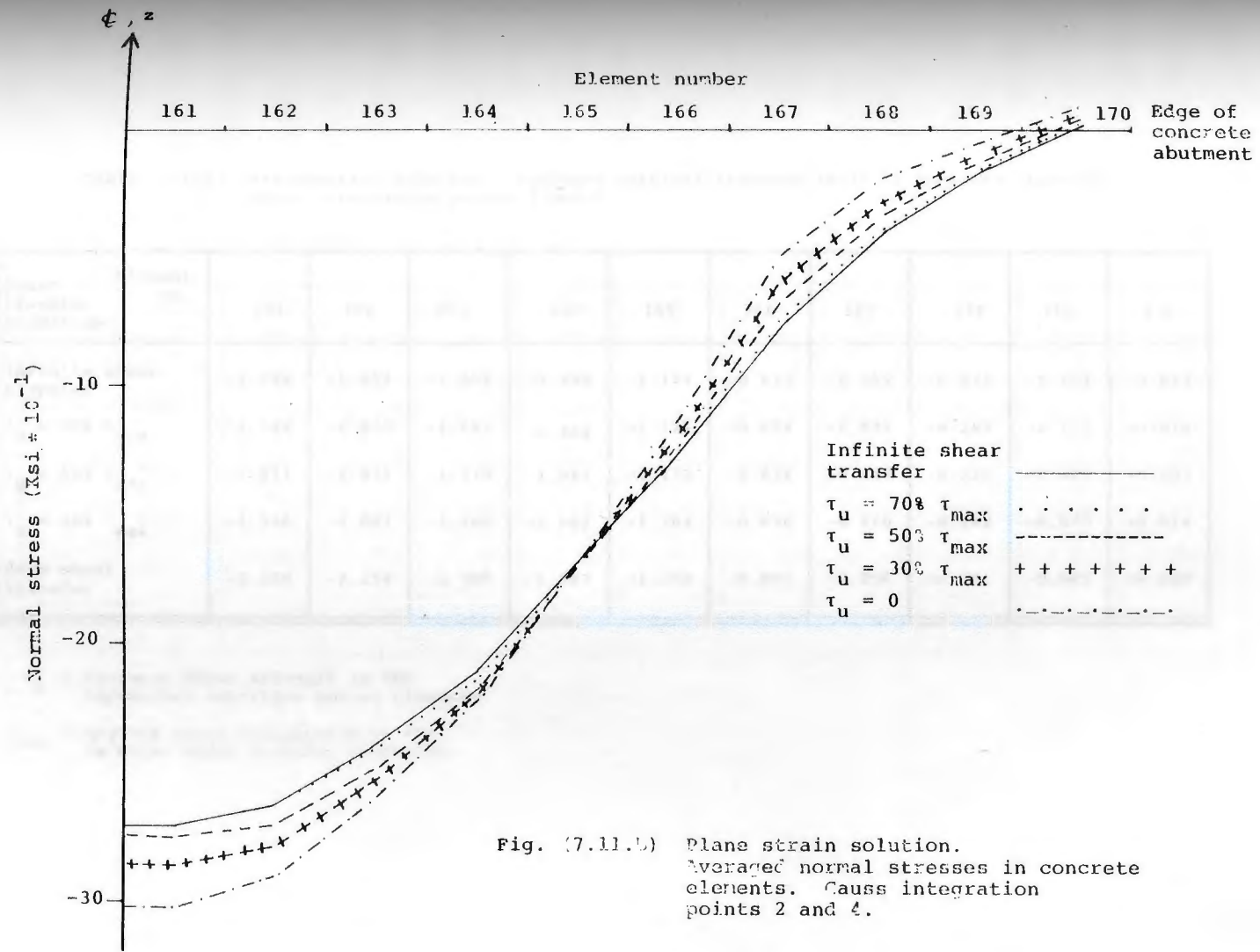
Fig. (7.11.5)   Plane strain solution.
Averaged normal stresses in concrete
elements. Gauss integration
points 2 and 4.

Table (7.6.a)   Axisymmetric solution.   Averaged vertical stresses (Ksi) in concrete elements
Gauss integration points 2 and 4.

Shear transfer condition	Element no. 161	162	163	164	165	166	167	168	169	170
Infinite shear transfer	-1.739	-1.854	-1.654	-1.440	-1.114	-0.833	-0.509	-0.272	-0.104	-0.012
$\tau_u = 70\% \ \tau_{max}$	-1.748	-1.870	-1.682	-1.468	-1.125	-0.824	-0.495	-0.265	-0.101	-0.010
$\tau_u = 50\% \ \tau_{max}$	-1.811	-1.971	-1.779	-1.541	-1.170	-0.834	-0.449	-0.226	-0.085	+0.002
$\tau_u = 30\% \ \tau_{max}$	-1.936	-2.087	-1.860	-1.602	-1.204	-0.836	-0.410	-0.192	-0.070	+0.014
Zero shear transfer	-2.129	-2.254	-1.985	-1.693	-1.254	-0.883	-0.356	-0.141	-0.045	+0.028

τ_u = ultimate shear strength in the
horizontal interface spring elements

τ_{max} = maximum shear transferred in the
infinite shear transfer condition.

Table (7.6.b) Plane strain solution. Averaged vertical stresses (Ksi) in concrete elements. Gauss integration points 2 and 4.

Shear transfer condition \ Element no.	161	162	163	164	165	166	167	168	169	170
Infinite shear transfer	-2.718	-2.634	-2.398	-2.112	-1.680	-1.271	-0.776	-0.418	-0.164	+0.013
$u = 70\%$ max	-2.721	-2.639	-2.414	-2.133	-1.684	-1.252	-0.760	-0.412	-0.162	+0.014
$u = 50\%$ max	-2.755	-2.710	-2.493	-2.183	-1.701	-1.230	-0.675	-0.342	-0.127	+0.040
$u = 30\%$ max	-2.862	-2.792	-2.536	-2.201	-1.692	-1.189	-0.599	-0.285	-0.099	+0.060
Zero shear transfer	-3.028	-2.904	-2.600	-2.229	-1.677	-1.129	-0.496	-0.201	-0.054	+0.085

concrete element under the horizontal interface spring
elements which fully slipped (slip modulus equal 29 Ksi).
The percentage changes in the concrete elements normal
compressive stress resulting from the different shear
transfer conditions, with respect to results from the
infinite shear transfer condition, were listed in
table (7.6.c) considering an axisymmetric solution. In
the shear transfer condition where τ_u = 70% τ_{max}, maxi-
mum increase in the average normal compressive stress
appeared to be in element no. 164 which is aligned
vertically with horizontal interface spring elements
nos. 99 and 100, see fig. (6.7). Referring to
table (7.1.b), notice that element no. 99 was the first
horizontal spring element in the full slip range (slip
modulus equals 29 Ksi). Similarly, in the shear transfer
condition where τ_u = 50% τ_{max}, maximum change appeared in
element no. 163 which is aligned vertically with horizon-
tal interface spring elements nos. 96 and 97. Referring
to table (7.1.c), notice that elements 96 and 97 have fully
slipped. Maximum change in this case did not appear in
concrete element no. 162, even though it is below the
horizontal spring element no. 95 which was the first in
the full slip range. However, since average stresses
were considered, it came out that for maximum change in
normal compression stresses to appear in one of those
analyzed concrete elements, both horizontal interface

Table (7.6.c) Axisymmetric solution. Percentage of change
in averaged normal concrete compressive
stresses.

Concrete element number	Shear transfer condition			
	$\tau_u = 70\% \; \tau_{max}$ %	$\tau_u = 50\% \; \tau_{max}$ %	$\tau_u = 30\% \; \tau_{max}$ %	$\tau_u = 0$ %
161	+0.52	+4.14	+11.33	+22.43
162	+0.86	+6.31	+12.57	+21.57
163	+1.69	+7.56	+12.45	+20.01
164	+1.94	+7.01	+11.25	+17.57
165	+0.99	+5.03	+8.08	+12.57
166	-1.09	+0.12	+0.36	+6.00
167	-2.83	-13.36	-24.15	-42.98
168	-2.64	-20.35	-41.67	-92.91
169	-2.97	-22.35	-48.57	-231.11
170	-16.67	-120.00	-216.67	-333.33

[Notice: Change > 100% should indicate a change from
compression to tension.]

τ_u = ultimate shear strength in the horizontal
interface spring elements.

τ_{max} = maximum shear transferred in the infinite shear
transfer condition.

spring elements aligned vertically with it must be in full slip range. Notice similsrly that when $\tau_u = 30\% \ \tau_{max}$, maximum change in concrete normal compressive stress appeared in element no. 162 near the center, and in the case of zero shear transfer the maximum change appeared in concrete element no. 161, at the center, because in this case all horizontal interface spring elements slipped by assumption. Normal stresses near the edge of the concrete abutment decreased as shown due to the increase of plate bending.

Shear stresses in concrete elements nos. 161 to 170 for all shear transfer conditions, were listed in tables (7.7.a) and (7.7.b). Results indicated that shear stresses in the concrete decreased as the ultimate shear strength value of the horizontal interface spring elements was lowered. That is because the masonry plate was allowed to slip more over the surface of the concrete while less shear stresses were transferred to the concrete abutment. The average decrease of concrete shear stresses in conjunction with average decrease of the shear stresses transferred through the interface zone for the axisymmetric and the plane strain solution methods were listed in table (7.8.a) and (7.8.b) respectively. Shear stress distribution curves for the different shear transfer conditions in the axisymmetric solution are shown in fig. (7.12). Generally speaking, the shear stress
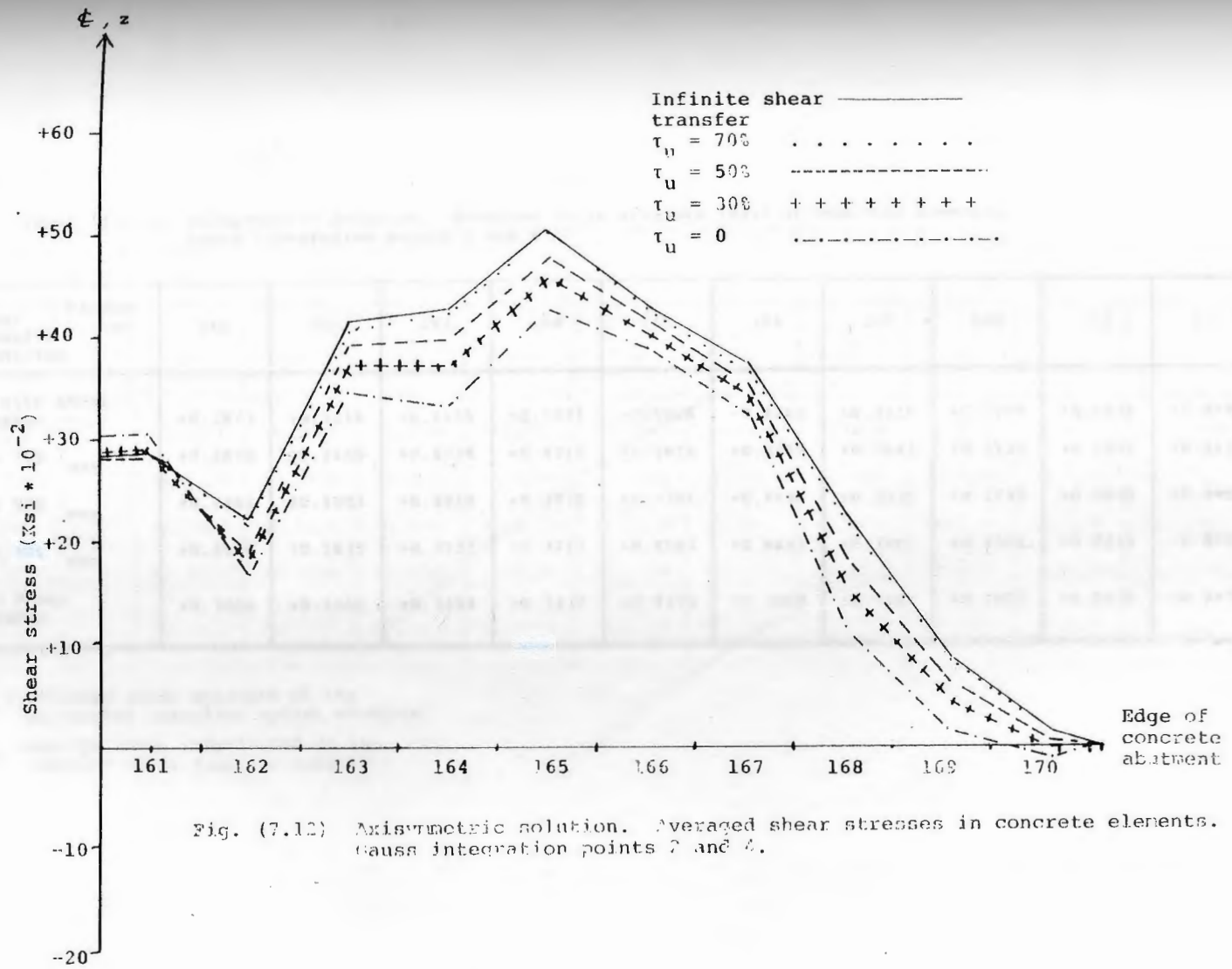
Fig. (7.12) Axisymmetric solution. Averaged shear stresses in concrete elements.
Gauss integration points ? and 4.

$\pounds$, z

Infinite shear ——————
transfer
$\tau_u = 70\%$ . . . .
$\tau_u = 50\%$ - - - - - - - - - - -
$\tau_u = 30\%$ + + + + + + + + +
$\tau_u = 0$.—.—.—.—.—.—.—.

Shear stress (Ksi * 10^{-2})

+60
+50
+40
+30
+20
+10
-10
-20

161 162 163 164 165 166 167 168 169 170

Edge of
concrete
abutment

Table (7.7.a) Axisymmetric solution. Averaged shear stresses (Ksi) in concrete elements.
Gauss integration points 2 and 4.

Shear transfer condition / Element no.	161	162	163	164	165	166	167	168	169	170
Infinite shear transfer	+0.2873	+0.2216	+0.4155	+0.4271	+0.5028	+0.4262	+0.3719	+0.2200	+0.0878	+0.0145
$\tau_u = 70\% \ \tau_{max}$	+0.2878	+0.2160	+0.4074	+0.4214	+0.5014	+0.4245	+0.3641	+0.2127	+0.0842	+0.0133
$\tau_u = 50\% \ \tau_{max}$	+0.2842	+0.1903	+0.3919	+0.3978	+0.4791	+0.4140	+0.3535	+0.1792	+0.0635	+0.0053
$\tau_u = 30\% \ \tau_{max}$	+0.2907	+0.1835	+0.3737	+0.3717	+0.4583	+0.4027	+0.3402	+0.1501	+0.0448	-0.0018
Zero shear transfer	+0.3056	+0.1668	+0.3454	+0.3337	+0.4276	+0.3864	+0.3207	+0.1075	+0.0139	-0.0116

τ_u = ultimate shear strength of the horizontal interface spring elements.

τ_{max} = maximum shear transferred in the infinite shear transfer condition.

Table (7.7.b) Plane strain solution. Averaged shear stresses (Ksi) in concrete elements.
Gauss integration points 2 and 4.

Shear transfer condition \ Element no.	161	162	163	164	165	166	167	168	169	170
Infinite shear transfer	+0.1637	+0.2549	+0.5494	+0.5724	+0.7110	+0.6179	+0.5631	+0.3224	+0.1295	+0.0139
$\tau_u = 70\% \ \tau_{max}$	+0.1638	+0.2532	+0.5424	+0.5677	+0.7108	+0.6153	+0.5506	+0.3144	+0.1258	+0.0125
$\tau_u = 50\% \ \tau_{max}$	+0.1524	+0.2227	+0.5218	+0.5373	+0.6736	+0.5883	+0.5213	+0.2577	+0.0840	-0.0040
$\tau_u = 30\% \ \tau_{max}$	+0.1428	+0.2046	+0.4367	+0.4944	+0.6338	+0.5575	+0.4854	+0.2072	+0.0499	-0.0132
Zero shear transfer	+0.1463	+0.1737	+0.4351	+0.4324	+0.5750	+0.5119	+0.4319	+0.1317	-0.0041	-0.0337

Table (7.8.a) Axisymmetric solution. Average decrease of concrete shear
stresses in conjunction with the average decrease of shear
stresses transferred through the interface zone.

Shear transfer condition	Average decrease in shear stresses transferred through the interface zone %	Average decrease in concrete shear stresses %
$\tau_u = 70\% \; \tau_{max}$	5.75	1.41
$\tau_u = 50\% \; \tau_{max}$	15.63	7.26
$\tau_u = 30\% \; \tau_{max}$	37.10	12.13
$\tau_u = 0$	88.75	19.45

τ_u = ultimate shear strength in the
horizontal interface spring elements.

τ_{max} = maximum shear transferred in the
infinite shear transfer condition.

Table (7.8.b) Plane strain solution. Average decrease of concrete shear stresses in conjunction with the average decrease of shear stresses transferred through the interface zone.

Shear transfer condition	Average decrease in shear stresses transferred through the interface zone %	Average decrease in concrete shear stresses %
$\tau_u = 70\% \; \tau_{max}$	4.07	1.07
$\tau_u = 50\% \; \tau_{max}$	11.21	8.80
$\tau_u = 30\% \; \tau_{max}$	31.81	16.75
$\tau_u = 0$	80.74	28.17

τ_u = ultimate shear strength in the horizontal interface spring elements.

τ_{max} = maximum shear transferred in the infinite shear transfer condition.

distribution curves indicate that shear stresses drop with different slopes depending on the ultimate shear strength of the horizontal interface spring elements. For lower shear strength value, the shear stresses in concrete elements 161 and 162, see fig. (7.12) dropped with a steeper slope; however, the variation of the curve along the concrete elements became more consistent for the different shear transfer conditions, where at element no. 162, concrete shear stresses started to increase as positive bending stresses increased at the bottom steel elements of the masonry plate, see fig. (7.9.a) and (7.9.b). (Plane strain and axisymmetric solution methods showed similar behavior in all conditions.) Maximum shear stress in the concrete elements for all shear transfer conditions appeared in element no. 165, which is beneath the critical section in the masonry plate. Beyond concrete element no. 167, beneath the unloaded concrete surface, shear stresses dropped very steeply.

It is worthwhile at this point to examine the effect of the variation in the concrete yield status resulting from different shear transfer conditions. The concrete has been modeled as an elastic - plastic model with strain hardening properties, see sec. (5.2), and was assumed to follow von Mises yield criterion,

sec. (5.2.1), which considers the octahedral shearing stress as the key factor of causing the yield in the concrete. The yield status for concrete elements nos. 161 to 170 is presented in tables (7.9.a) and (7.9.b), resulting in the axisymmetric and plane strain solution methods, respectively. Notice that yield is defined as the point on the concrete stress — strain diagram where normal stresses and strains are in the elastic - plastic range in a uniaxial compression test. However, that is not exactly the case for the concrete abutment being considered in this study because of an internal lateral confining pressure coming from sur-rounding elements. Therefore, yield status shown in tables (7.9.a) and (7.9.b) does not really mean that concrete has actually yielded, but as mentioned above, it means that, based on the concrete material constants taken from a uniaxial compression and tension tests, see Appendix C (sec. (C.2)), concrete would have yielded at that level of stress. Thus, results indicated that as the shear stresses transferred through the interface zone decreased, concrete elements at the edge of the abutment would stay in the elastic range. Notice that this is consistent with the results of normal and shear stress distribution in the concrete elements. Whereas the shear stresses transferred through the interface zone decreased, normal compressive and shear stresses

at the edge of the concrete abutment decreased as shown
in figs. no. (7.11.a), (7.11.b) and (7.12).

shear transfer condition		Concrete yield status				
element no.	Gauss integr. point	Infinite shear transfer	$\tau_u = 70\%$ τ_{max}	$\tau_u = 50\%$ τ_{max}	$\tau_u = 10\%$ τ_{max}	$\tau_u = 0$
161		plastic	plastic	plastic	plastic	plastic
162						
163						
164						
165						
166						
167						
168						elastic
169					elastic	elastic
170			elastic	elastic	elastic	elastic

Table (7.9.a) Axisymmetric solution. Concrete yield status in different shear transfer conditions.

Shear transfer condition		Concrete yield status				
Element no.	Gauss integ. point	Infinite shear transfer	$\tau_u = 70\%$ τ_{max}	$\tau_u = 50\%$ τ_{max}	$\tau_u = 30\%$ τ_{max}	$\tau_u = 0$
161	2	plastic	plastic	plastic	plastic	plastic
	4	"	"	"	"	"
162	2	"	"	"	"	"
	4	"	"	"	"	"
163	2	"	"	"	"	"
	4	"	"	"	"	"
164	2	"	"	"	"	"
	4	"	"	"	"	"
165	2	"	"	"	"	"
	4	"	"	"	"	"
166	2	"	"	"	"	"
	4	"	"	"	"	"
167	2	"	"	"	"	"
	4	"	"	"	"	"
168	2	"	"	"	"	"
	4	"	"	"	"	elastic
169	2	"	"	"	"	elastic
	4	"	"	"	elastic	elastic
170	2	"	"	elastic	elastic	elastic
	4	"	elastic	elastic	elastic	elastic

Table (7.9.b)   Plane strain solution.   Concrete yield status in different shear transfer conditions.

Shear transfer condition		Concrete yield status				
Element no.	Gauss integ. point	Infinite shear transfer	$\tau_u = 70\%$ τ_{max}	$\tau_u = 50\%$ τ_{max}	$\tau_u = 30\%$ τ_{max}	$\tau_u = 0$
161	2 4	plastic "	plastic "	plastic "	plastic "	plastic "
162	2 4	" "	" "	" "	" "	" "
163	2 4	" "	" "	" "	" "	" "
164	2 4	" "	" "	" "	" "	" "
165	2 4	" "	" "	" "	" "	" "
166	2 4	" "	" "	" "	" "	" "
167	2 4	" "	" "	" "	" "	" "
168	2 4	" "	" "	" elastic	" "	" elastic
169	2 4	" "	" "	elastic elastic	elastic elastic	elastic elastic
170	2 4	elastic elastic	elastic elastic	elastic elastic	elastic elastic	elastic plastic

CHAPTER 8
SUMMARY AND CONCLUSIONS

The standard procedure followed in practice for the design of the bearing system, is to assume that concrete stresses beneath the masonry plate have a uniform distribution. However, a previous finite element analysis of the bearing system has shown that there is in fact a little lateral distribution in concrete stresses beneath the masonry plate. It has also shown that bending stresses of opposite sign can result in the unloaded area of the masonry plate if tension forces can develop between the plate and the concrete, as might be the situation with anchor bolts. Therefore, the finite element analysis was carried out in this study to examine the effect of the shear transfer along the interface between the masonry plate and the concrete.

The anslysis conducted here is based on the assumption that shear stresses continue to be transferred along the interface zone until a certain ultimate shear strength is reached, then the bonds between the steel and concrete elements will break causing the masonry steel plate to slip over the surface of the concrete abutment. Vertical and horizontal interface spring elements were used to

simulate the behavior of the interface with a nonlinear description of slip. The stiffnesses of the interface spring elements selected to represent varying shear transfer conditions, were based on trying different values and comparing outcoming results against those of the known infinite and zero shear transfer conditions. The ultimate shear strength value for the horizontal interface spring elements was randomly set to equal 70%, 50%, and 30% of the maximum shear stress transferred through the horizontal spring elements in the infinite shear transfer condition. The analysis was carried out by using both axisymmetric and plane strain solution methods.

Results of the study show that:

1) The behavior of stresses and deformation of the bearing system was essentially the same in both the axisymmetric and the plane strain solution methods. However, the numerical difference in the results could be attributed to the displacement in the circumferential direction in the axisymmetric elements. Nevertheless, the axisymmetric solution represents a more realistic approximation of the actual three-dimensional solid structure and shows that compression stresses in the concrete are not as high as anticipated in the previous finite element analysis of the bearing system.

2) As the ultimate shear strength of the horizontal
interface spring elements decreases, the masonry plate
starts to slip increasingly and bend over the concrete
abutment. Bending stresses in top of the bearing
plate in the area beneath the uniformly applied load
were not significantly affected by the slip. However,
bending stresses increased greatly in the unloaded
portion. Positive bending stresses increased in the
masonry plate more significantly, however, negative
bending stresses appeared in the masonry steel ele-
ments beneath the end of the pot bearing plate.
Nevertheless, those negative bending stresses de-
creased as the masonry plate was permitted to slip.
Therefore, it could be stated that bending stresses
could change signs in the critical section of the
masonry plate, if tension forces can develop between
the plate and the concrete.

3) The increased bending in the plate resulting from the
decrease of the shear stresses transferred through the
interface, cause the compression stresses transferred
to the concrete near the center of the abutment to
increase, and to decrease in the area beyond where the
load ends. This leads to the conclusion, at least for
the geometry considered here, that the applied load
is transferred to the concrete essentially by direct
compression with little lateral distribution of load.

It also results in significant bending action occur-
ring at the end of the plate if it is permitted to
deform. Hence, shear stresses transferred through
the interface zone plate a restraining role against
the bending action of the plates.

4) Shear stresses in the concrete decrease if less shear
is transferred through the interface. However, it has
been noticed that there has been no significant change
in the concrete shear stress distribution, at least
for the nonlinear slip function used in this study.

Examining the results from a practical viewpoint,
they indicate the following:

1) In the case where the ultimate shear strength in the
horizontal interface spring elements equals 70% of the
maximum shear stress transferred in the infinite shear
transfer condition, shear stresses transferred through
the interface decreased, on the average, only about
5.75% in the axisymmetric solution, and about 4.07%
in the plane strain solution. However, slip occurred
in approximately 70% of the interface spring elements,
representing 70% slip of the interface zone, 20% being
in the full slip range in both solution methods.
Physically, that represents a lot of slip for that low
reduction in the shear stresses transferred in the
interface. Therefore it might be concluded that
interface spring elements with a shear strength value

less than 70% would not be considered practical.
Results from the case where $\tau_u = 70\% \ \tau_{max}$, did not
vary by much from the infinite shear transfer condi-
tion. Hence, when $\tau_u > 70\% \ \tau_{max}$, the change in bear-
ing stresses with respect to the infinite shear
transfer condition will be practically insignificant.

2) The maximum bending stresses in the critical section
   of the masonry plate are considerably less than those
   obtained when assuming a uniform stress distribution
   beneath the plate. When analyzed as a circular plate
   with central constraint by assuming uniform stress
   distribution [22], resulting maximum bending stress
   at the critical section was equal to 15.12 Ksi
   compared to -2.56 Ksi resulting in the axisymmetric
   solution, table (7.5.a). When the free portion of the
   masonry plate was analyzed as a cantilever beam,
   resulting maximum bending stress at the critical
   section came out to be -13.71 Ksi, compared to
   -2.73 Ksi in the plane strain solution, table (7.5.b).

Based on the above findings, it could be concluded,
at least for the interface spring elements used in this
study, that the effect of shear transfer in the interface
zone does not have practical significance on the design
of the bearing system. However, results indicated that
the normal procedure followed in the design of pot

bearings is too conservative. A circular or parabolic function representing the normal stress distribution in the concrete beneath the masonry plate could probably give a safe and more economical design than assuming uniform stress distribution. However, more research is needed to define an exact stress distribution function.

Finally, results indicated that stresses in the concrete supporting structure are actually less than the resulting stresses from plane solution methods. Hence, failure level of the concrete is higher than anticipated due to existing lateral out-of-plane and in-plane confining pressure in the three-dimensional solid structure.

REFERENCES

[1] "Standard Specifications for Highway Bridges"
AASHTO, 12th Ed., 1977.

[2] McEwen, E. E. "Behavior of Masonry Bearing Plates",
unpublished report at the University of Rhode
Island, Kingston, December 1979.

[3] Chen, W. F. "Plasticity in Reinforced Concrete"
McGraw-Hill, Inc., New York, 1st Ed., 1982.

[4] Bathe, K. J., Wilson, E. L., Iding, R. H.
"NONSAP A Structural Analysis Program for Static
and Dynamic Response of Nonlinear Systems",
University of California, Berkeley, Report
No. UC SESM 74-3, February 1974.

[5] Holand, I., Bell, K.. (Editors), "Finite Element
Methods in Stress Analysis", TAPIR, The Technical
University of Norway, Trondheim-Norway,
2nd printing, 1970.

[6] Cook, R. D. "Concepts and Applications of Finite
Element Analysis", John Wiley and Sons, Inc.,
New York, 2nd Ed., 1974.

[7] Gallagher, R. H. "Finite Element Analysis Funda-
mentals", Prentice-Hall Inc., Englewood Cliffs,
New Jersey, 1st Ed., 1975.

[8] Cheung, Y. K., Yeo, M. F. "A Practical Introduc-
tion to Finite Element Analysis", Pitman Publishing
Limited, 39 Parker St., London WC2B 5PB, 1st Ed.,
1979.

[9] Bathe, K. J., Wilson, E. L., Ozdemir, H. "Static and Dynamic Geometric and Nonlinear Analysis", University of California, Berkeley, Report No. UC SESM 74-4, February 1974.

[10] "Dixon Shortspan Bearings", (catalog) Spencer Dynamics Corporation, Promenade Street, Providence, RI, 02908, USA.

[11] "Steel Construction Manual", American Institute of Steel Construction, Inc., 8th Ed., pp. (2-47)-(2-49).

[12] Zienkiewicz, O. C. "The Finite Element Method", McGraw-Hill, Inc., New York, 3rd Ed., 1977.

[13] "Elastomeric Bearings Design, Construction and Materials", National Cooperative Highway Research Program, Report No. 248, University of Washington, Seattle, Washington, August 1982.

[14] Wang, C., Salmon, C. G. "Reinforced Concrete Design", Harper and Row, Inc., New York, 3rd Ed., 1979.

[15] Goodman, R. E., Taylor, R., Brekke, T. L. "A Model for the Mechanics of Jointed Rock", Journal of Soil Mechanics and Foundations Division, ASCE, vol. 94, No. SM3, Proc. paper 5937, May 1968, pp. 637-659.

[16] Ngo, D., Scordelis, A. C. "Finite Element Analysis of Reinforced Concrete Beams", Journal of American Concrete Institute, Title No. 64-14, March 1967, pp. 152-163.

[17] Ghaboussi, J., Wilson, E. L., Isenberg, J. "Finite Element for Rock Joints and Interfaces", Journal of Soil Mechanics and Foundations Division, ASCE, vol. 99, No. SM10, Proc. paper 10095, October 1973, pp. 833-847.

[18] Gudehus, G. (Ed.), "Finite Element in Geomechanics", John Wiley and Sons, Inc., New York, 1st Ed., 1977 Chapter 10.

[19] Schafer, H. "A Contribution to the Solution of Contact Problems with the Aid of Bond Elements", Computer Methods in Applied Mechanics and Engineering 6, North Holland Publishing Company, February 20, 1975, pp. 335-353.

[20] Buragohain, D. N., Shah, V. L.   "Curved Interface Elements for Interaction Problems", Journal of the Structural Division, ASCE, Vol. 104 No. St1, January 1978, pp. 205-209.

[21] Buragohain, D. N., Shah, V. L. "Curved Interface Elements for Interaction Problems", Proceedings, International Symposium on Soil-Structure Interaction, University of Roorkee, Roorkee, India, January 1977, pp. 197-201.

[22] Alexander, B. "Practical Stress Analysis Engineering Design", Marcel Dekker Inc., New York and Basel, 1st Ed., 1982.

APPENDIX A

A.1   FORMULATION OF THE LINKAGE ELEMENT
       BY NGO AND SCORDELIS

For the linkage element shown in Fig. (3.3), let the springs in elements local axes H and V have the stiffness K_H and K_V respectively.

The stress - strain relation is given by:

$$\begin{Bmatrix} \sigma_H \\ \sigma_V \end{Bmatrix} = \begin{bmatrix} K_H & 0 \\ 0 & K_V \end{bmatrix} \begin{Bmatrix} \epsilon_H \\ \epsilon_V \end{Bmatrix} \qquad (A.1)$$

APPENDIX

where ϵ_H and ϵ_V are the components of the relative strain in the spring connecting points I and J. σ_H and σ_V are the corresponding stress components. Note that the strain components are shown in the elements local coordinates and they are positive when the spring connecting points I and J is in tension.

Rewriting (A.1) symbolically:

$$\{\sigma^L\} = [H^L] \ \{\epsilon^L\} \qquad (A.2)$$

where σ^L and ϵ^L are the springs stress and strain components written in local coordinates, and H^L is the spring's stiffness matrix in local coordinates.

APPENDIX A

A.1 FORMULATION OF THE LINKAGE ELEMENT BY NGO AND SCORDELIS

For the linkage element shown in fig. (5.3), let the springs in elements local axes H and V have the stiffness K_H and K_V respectively.

The stress - strain relation is given by:

$$\begin{Bmatrix} \sigma_H \\ \sigma_V \end{Bmatrix} = \begin{bmatrix} K_H & 0 \\ 0 & K_V \end{bmatrix} \begin{Bmatrix} \varepsilon_H \\ \varepsilon_V \end{Bmatrix} \tag{A.1}$$

where ε_H and ε_V are the components of the relative strain in the spring connecting points I and J. σ_H and σ_V are the corresponding stress components. Note that the strain components are shown in the elements local coordinates and they are positive when the spring connecting points I and J is in tension.

Rewriting (A.1) symbolically:

$$\{\sigma^L\} = \begin{bmatrix} K^L \end{bmatrix} \{\varepsilon^L\} \tag{A.2}$$

where σ^L and ε^L are the springs stress and strain components written in local coordinates, and $[K^L]$ is the spring's stiffness matrix in local coordinates.

However, if the spring's stiffness matrix is to be added to the structure stiffness matrix, it has to be transferred into global coordinates.

Let the transformation matrix, [A], relate the strains and displacements as such,

$$\{\varepsilon^L\} = [A] \{\delta^G\} \tag{A.3}$$

where δ^G are displacements of joints I and J written in global coordinates.

Substituting (A.3) in (A.2),

$$\{\sigma^L\} = [K^L] [A] \{\delta^G\} \tag{A.4}$$

The transformation matrix [A] is an orthogonal matrix by definition, therefore its transpose equals its inverse.

Multiplying [A] transpose, by both sides of (A.4),

$$[A]^T \{\sigma^L\} = [A]^T [K^L] [A] \{\delta^G\} \tag{A.5}$$

but

$$\{\sigma^G\} = [A]^T \{\sigma^L\} \tag{A.6}$$

where σ^G are the stresses at nodes I and J written in global coordinates.

Rewriting (A.5),

$$\{\sigma^G\} = [A]^T [K^L] [A] \{\delta^G\} \tag{A.7}$$

However, the element stress - strain relation in global coordinates is

$$\{\sigma^G\} = [K^G] \{\delta^G\} \tag{A.8}$$

where $[K^G]$ is the global stress - strain relation.

By comparing matrices of equations (A.7) and (A.8), it must be concluded that the global stiffness matrix for the linkage element is defined as

$$[K^G] = [A]^T [K^L] [A] \tag{A.9}$$

or

$$[K^G] = \begin{bmatrix} -c & s \\ -s & -c \\ c & -s \\ s & c \end{bmatrix} \begin{bmatrix} K_H & 0 \\ 0 & K_V \end{bmatrix} \begin{bmatrix} -c & -s & c & s \\ s & -c & -s & c \end{bmatrix} \tag{A.10}$$

The linkage element global stiffness matrix is shown in table (A.1).

Note that in this element formulation a linear stress - strain relation was assumed to describe the relationship between bond slip and bond stress, see

Table (A.1) Linkage element's global stiffness matrix

$$
\begin{bmatrix}
K_H c^2 + K_V s^2 & K_H s c - K_V s c & -K_H c^2 - K_V s^2 & -K_H s c + K_V s c \\
 & K_H s^2 + K_V c^2 & -K_H s c + K_V s c & -K_H s^2 - K_V c^2 \\
 & & K_H c^2 + K_V s^2 & K_H s c - K_V s c \\
\text{symmetric} & & & K_H s^2 + K_V c^2
\end{bmatrix}
$$

· equations (A.2) and (A.8). It was suggested here that K_H and K_V values are not easily determined but they could be found experimentally.

A.2 FORMULATION OF THE TWO-DIMENSIONAL INTERFACE ELEMENT BY GHABOUSSI, WILSON AND ISENBERG

A.2.1 PLANE INTERFACE ELEMENT

The interface element uses relative displacements as the independent degrees of freedom. The displacement degrees of freedom adjacent to the interface have been transformed in the top continuum element into relative displacements between the two sides of the slip surface. The transformation relations are as follows:

$$u_{yi}^{T} = u_{y\ell}^{B} + \Delta_{yi}$$

$$u_{zi}^{T} = u_{z\ell}^{B} + \Delta_{zi}$$

$$u_{yj}^{T} = u_{yk}^{B} + \Delta_{yj}$$

$$u_{zj}^{T} = u_{zk}^{B} + \Delta_{zj}$$

(A.11)

where Δ's represent relative displacements, and u^{T}'s and u^{B}'s represent nodal displacements of the top and bottom continuum elements, respectively, following the notation shown in fig. (A.1).

To avoid numerical difficulties, the element stiffness was formulated in the element's local coordinates and then was transformed into global coordinates, see fig. (A.2). The element thickness, h, is small relative to the size of the continuum elements, therefore, the relative displacement is considered
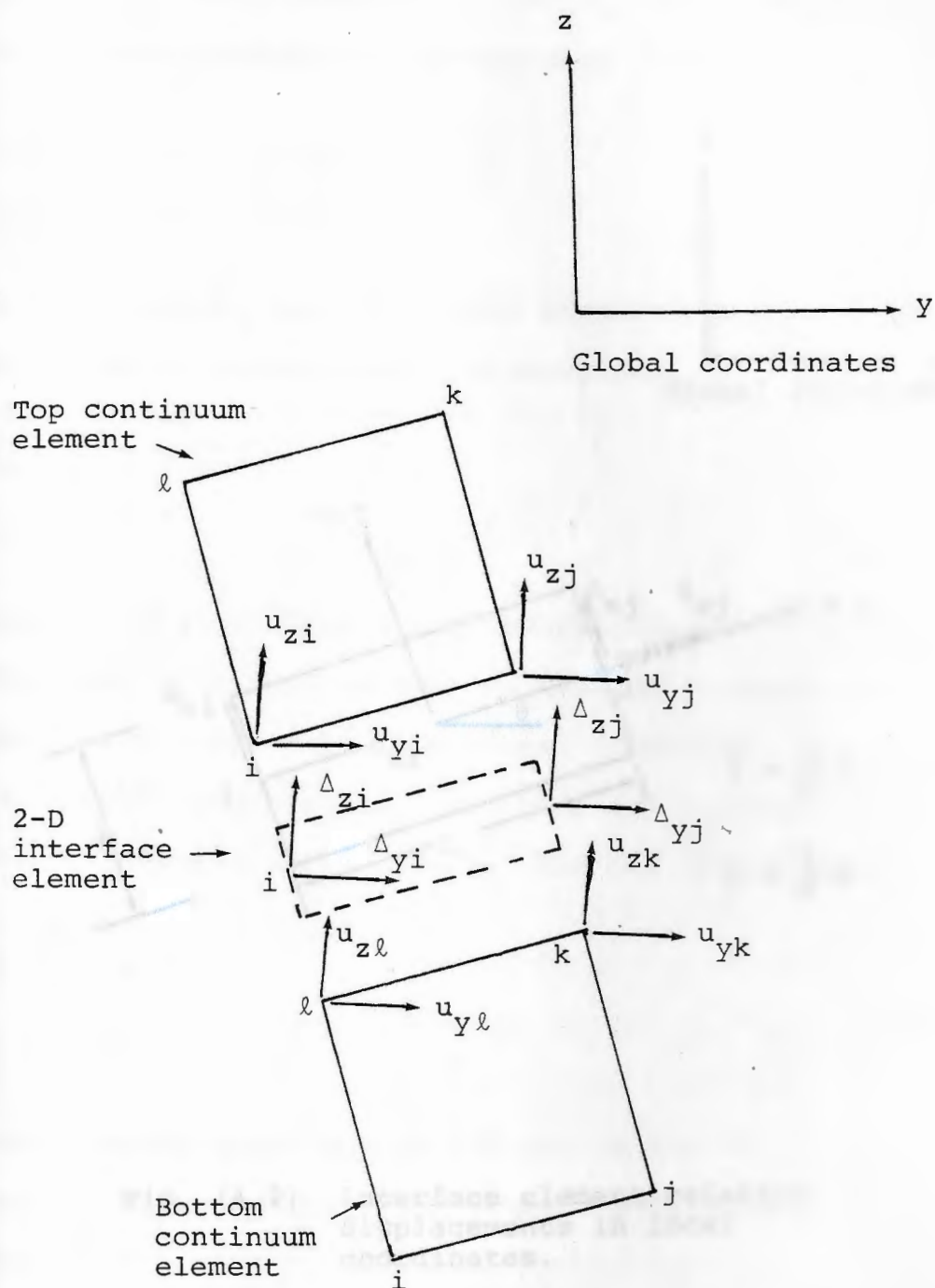
Fig. (A.1) Geometry of the 2-D interface element.

constant across the thickness. However, the normal and
tangential displacements, Δ_n and Δ_s are considered to
vary linearly along the elements as follows:

Global coordinates

where N_i and N_j are the linear shape (interpolation)
functions at nodes i and j respectively.

where ζ is a nondimensional coordinate.

$$\xi = \frac{2}{L}\,s$$

$$\zeta = \frac{2}{h}\,n$$
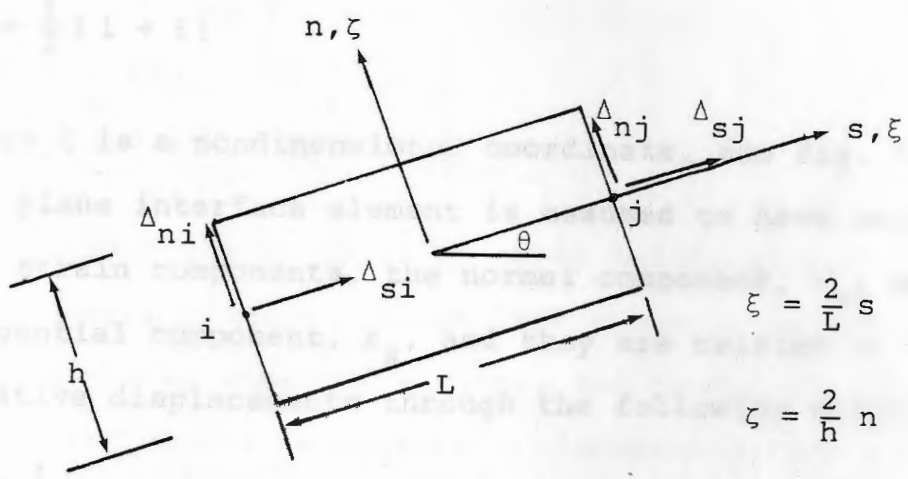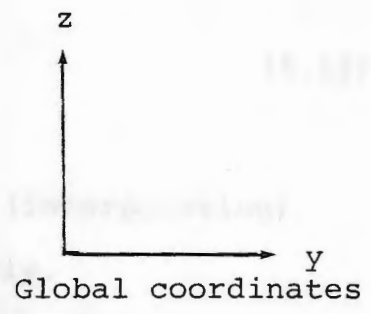
Fig. (A.2) Interface element relative
displacements in local
coordinates.

constant across the thickness. However, the normal and tangential displacements, Δ_n and Δ_s are considered to vary linearly along the elements as follows:

$$\Delta_n = N_i \, \Delta_{ni} + N_j \, \Delta_{nj}$$
$$\Delta_s = N_i \, \Delta_{si} + N_j \, \Delta_{sj}$$

(A.12)

where N_i and N_j are the linear shape (interpolation) functions at nodes i and j respectively.

$$N_i = \frac{1}{2} (1 - \xi)$$
$$N_j = \frac{1}{2} (1 + \xi)$$

(A.13)

where ξ is a nondimensional coordinate, see fig. (A.2). The plane interface element is assumed to have only two strain components, the normal component, ε_n, and the tangential component, ε_s, and they are related to the relative displacements through the following relations:

$$\varepsilon_n = \frac{1}{h} \, \Delta_n$$
$$\varepsilon_s = \frac{1}{h} \, \Delta_s$$

(A.14)

Substituting equations (A.12) and (A.13) in (A.14) results in the strain-displacement relations for the element:

$$
\begin{Bmatrix} \varepsilon_n \\ \varepsilon_s \end{Bmatrix} = \frac{1}{2h} \begin{bmatrix} (1-\xi) & 0 & (1+\xi) & 0 \\ 0 & (1-\xi) & 0 & (1+\xi) \end{bmatrix} \begin{Bmatrix} \Delta_{ni} \\ \Delta_{si} \\ \Delta_{nj} \\ \Delta_{sj} \end{Bmatrix}
\tag{A.15}
$$

written symbolically as

$$
\{\varepsilon\} = [B]\ \{\Delta\}
\tag{A.16}
$$

The stresses are related to the strains through the material property matrix [C],

$$
\begin{Bmatrix} \sigma_n \\ \sigma_s \end{Bmatrix} = \begin{bmatrix} C_{nn} & 0 \\ 0 & C_{ss} \end{bmatrix} \begin{Bmatrix} \varepsilon_n \\ \varepsilon_s \end{Bmatrix}
\tag{A.17}
$$

Notice that the material property matrix represents a nondilatant element meaning that there is no volume change due to shearing strains, and therefore, the shear and normal components of deformation are un-coupled. C_{nn} and C_{ss} are nonlinear functions. In relating stress to deformation in the direction normal to the element, three distinct stages are defined, refer to fig. (5.6.a).

1) Separation, $C_{nn} = C_{ss} = 0$ when $\varepsilon_n \geq 0$.

2) Crushing of the surface irregularities, if any, $C_{nn} = E_c (\varepsilon_n^c < \varepsilon_n < 0)$.

3) Contact, $C_{nn} = E_f (\varepsilon_n < \varepsilon_n^c)$.

The tangential stress‑strain relationship is assumed to be elastic—perfectly plastic using a Mohr-Coulomb yield criterion, [3], refer to fig. (5.6.b):

C_{ss} = G   for $\sigma_s < c + \sigma_n \tan \phi$ (elastic)

C_{ss} = 0   for $\sigma_s = c + \sigma_n \tan \phi$ (plastic, σ_s has reached the ultimate shear strength)

where G is the interface element shear stiffness, and c and ϕ are the cohesion and the angle of friction, respectively.

The element stiffness matrix in the local coordinates (s,n) is formed as follows:

$$[K^L] = \int_{vol} [B]^T [C] [B] \, d_{vol} \qquad (A.18)$$

The global element stiffness matrix is:

$$[K^G] = [T]^T [K^L] [T] \qquad (A.19)$$

where [T] is the transformation matrix containing the direction cosines.

The complete global element stiffness matrix for a nondilatant material is shown in table (A.2).

Table (A.2) Plane interface element global stiffness matrix
for nondilatant materials.

$$
\frac{L}{6h}
\begin{bmatrix}
2A_1 & 2A_3 & A_1 & A_3 \\
 & 2A_2 & A_3 & A_2 \\
 & & 2A_1 & 2A_3 \\
\text{symmetric} & & & 2A_2
\end{bmatrix}
$$

where $A_1 = C_{ss}a^2 + C_{nn}b^2$ and $a = \frac{1}{L}(y_j - y_i)$

$A_2 = C_{nn}a^2 + C_{ss}b^2$ $b = \frac{1}{L}(z_j - z_i)$

$A_3 = (C_{nn} - C_{ss})ab$

A.2.2 AXISYMMETRIC INTERFACE ELEMENT

A similar joint element has been developed for axisymmetric problems, where the integration in equation (A.18) is carried out over the volume of the axisymmetric element, which includes the circumferential direction also.

The geometry and the independent degrees of freedom for the axisymmetric element are exactly as shown in fig. (A.1) and fig. (A.2), except that the global y-axis is substituted by the global radial r-axis. However, the strain displacement relation now involves three equations:

$$\varepsilon_n = \frac{1}{h} \Delta_n$$

$$\varepsilon_s = \frac{1}{h} \Delta_s \tag{A.20}$$

$$\varepsilon_\theta = \frac{1}{r} (u_r^B + \frac{\Delta_r}{2})$$

where ε_θ is the circumferential strain component and u_r^B is the radial displacement of the surface of the bottom elements as shown in fig. (A.1).

The axisymmetric displacement functions are defined as:

$$\Delta_r = N_1 \Delta_{ri} + N_2 \Delta_{rj}$$

$$\Delta_z = N_1 \Delta_{zi} + N_2 \Delta_{zj}$$

$$u_r^B = N_1 u_{ri}^B + N_2 u_{rj}^B \tag{A.21}$$

The strain-displacement may be expressed as:

$$\begin{Bmatrix} \varepsilon_n \\ \varepsilon_s \\ \varepsilon_\theta \end{Bmatrix} = [B] \begin{Bmatrix} \Delta_{ri} \\ \Delta_{zi} \\ \Delta_{rj} \\ \Delta_{zj} \\ u^B_{ri} \\ u^B_{rj} \end{Bmatrix} \tag{A.22}$$

where [B] is shown in table (A.3).

The stress-strain relation is defined as:

$$\begin{Bmatrix} \sigma_n \\ \sigma_s \\ \sigma_\theta \end{Bmatrix} = \begin{bmatrix} C_{nn} & 0 & 0 \\ 0 & C_{ss} & 0 \\ 0 & 0 & C_{\theta\theta} \end{bmatrix} \begin{Bmatrix} \varepsilon_n \\ \varepsilon_s \\ \varepsilon_\theta \end{Bmatrix} \tag{A.23}$$

where C_{nn} and C_{ss} are defined as in equation (A.17), and $C_{\theta\theta}$ is added to account for the stress and strain components in the θ direction, but its physical meaning is not clear and is assumed to equal zero.

The global stiffness matrix for the axisymmetric element is shown in table (A.4). For more details see the source [17,18].

Table (A.3)   [B] matrix in the axisymmetric element strain - displacement relation.

$$\frac{1}{2}\begin{bmatrix} -\dfrac{s}{h}(1-\xi) & \dfrac{c}{h}(1-\xi) & -\dfrac{s}{h}(1+\xi) & \dfrac{c}{t}(1+\xi) & 0 & 0 \\[2em] \dfrac{c}{h}(1-\xi) & \dfrac{s}{h}(1-\xi) & \dfrac{c}{h}(1+\xi) & \dfrac{s}{t}(1+\xi) & 0 & 0 \\[2em] \dfrac{1-\xi}{2r_i} & 0 & \dfrac{1+\xi}{2r_j} & 0 & \dfrac{1-\xi}{r_i} & \dfrac{1+\xi}{r_j} \end{bmatrix}$$

where $s = \sin\theta$ and $c = \cos\theta$.

Table (A.4) Axisymmetric interface element global stiffness matrix for nondilatant material.

$$
\begin{bmatrix}
A^2(s^2C_{nn}+c^2C_{ss})+c^2C & A^2sc(C_{ss}-C_{nn}) & AB(s^2C_{nn}+c^2C_{ss})+CDC_{\theta\theta} & ABsc(C_{ss}+C_{nn}) & 2c^2C_{\theta\theta} & 2CDC_{\theta\theta} \\
 & A^2(c^2C_{nn}+s^2C_{ss}) & ABsc(C_{ss}-C_{nn}) & AB(c^2C_{nn}+s^2C_{ss}) & 0 & 0 \\
 & & B^2(s^2C_{nn}+c^2C_{ss})+D^2C_{\theta\theta} & B^2sc(C_{ss}-C_{nn}) & 2CDC_{\theta\theta} & 2D^2C_{\theta\theta} \\
 & & & B^2(c^2C_{nn}+s^2C_{ss}) & 4C^2C_{\theta\theta} & 4CDC_{\theta\theta} \\
 & \text{symmetric} & & & & 2D^2C_{\theta\theta}
\end{bmatrix}
$$

where $A^2 = \dfrac{L}{3h^2}(r_j - 3r_i)$ and $C^2 = \dfrac{L}{2(r_j - r_i)^2}(r_i - 3r_j) + \dfrac{2r_j^2}{r_j - r_i}\log\left(\dfrac{r_j}{r_i}\right)$

$B^2 = \dfrac{L}{3h^2}(3r_j - r_i)$ $\qquad\qquad$ $D^2 = \dfrac{L}{2(r_j - r_i)^2}(r_j - 3r_i) + \dfrac{2r_i^2}{r_j - r_i}\log\left(\dfrac{r_j}{r_i}\right)$

$AB = \dfrac{L}{3h^2}(r_i + r_j)$ $\qquad\qquad$ $CD = \dfrac{L}{2(r_j - r_i)^2}r_j + r_i - \dfrac{r_j r_i}{r_j - r_i}\log\left(\dfrac{r_j}{r_i}\right)$

APPENDIX B

B.1 HORIZONTAL INTERFACE SPRING ELEMENT STRESS – STRAIN DIAGRAMS FOR THE DIFFERENT SLIP CONDITIONS

The stress – strain diagram, shown in fig. (B.1), describes the proposed nonlinear slip relation presented in sec. (6.5). The ultimate shear strength, τ_u, equals X% of the maximum shear values, τ_{max}, transferred through the horizontal spring elements in the model representing infinite shear transfer condition (no slip condition).

Data for the stress – strain relation assuming τ_u 70%, 50%, and 30% of τ_{max} are shown in tables (B.1), (B.2), and (B.3), respectively, for both axisymmetric and plane strain solution methods, where

$$\tau_8 = \tau_u + 0.10 \ \tau_u$$
$$\tau_9 = \tau_u + 0.20 \ \tau_u$$
$$\tau_{10} = \tau_u + 0.30 \ \tau_u$$
$$\tau_{11} = 29000 \ Ksi.$$

E_1 = 29000 Ksi (no slip modulus, E_{SH})

E_2 = 2900 Ksi

E_3 = 290 Ksi

E_4 = 29 Ksi (full slip modulus, E_p)

$\tau_u = \tau_7$

$\tau_1 = -\tau_{11}$

$\tau_2 = -\tau_{10}$

$\tau_3 = -\tau_9$

$\tau_4 = -\tau_8$

$\tau_5 = -\tau_7$ (ultimate shear strength, τ_u)

$\tau_6 = 0.0$
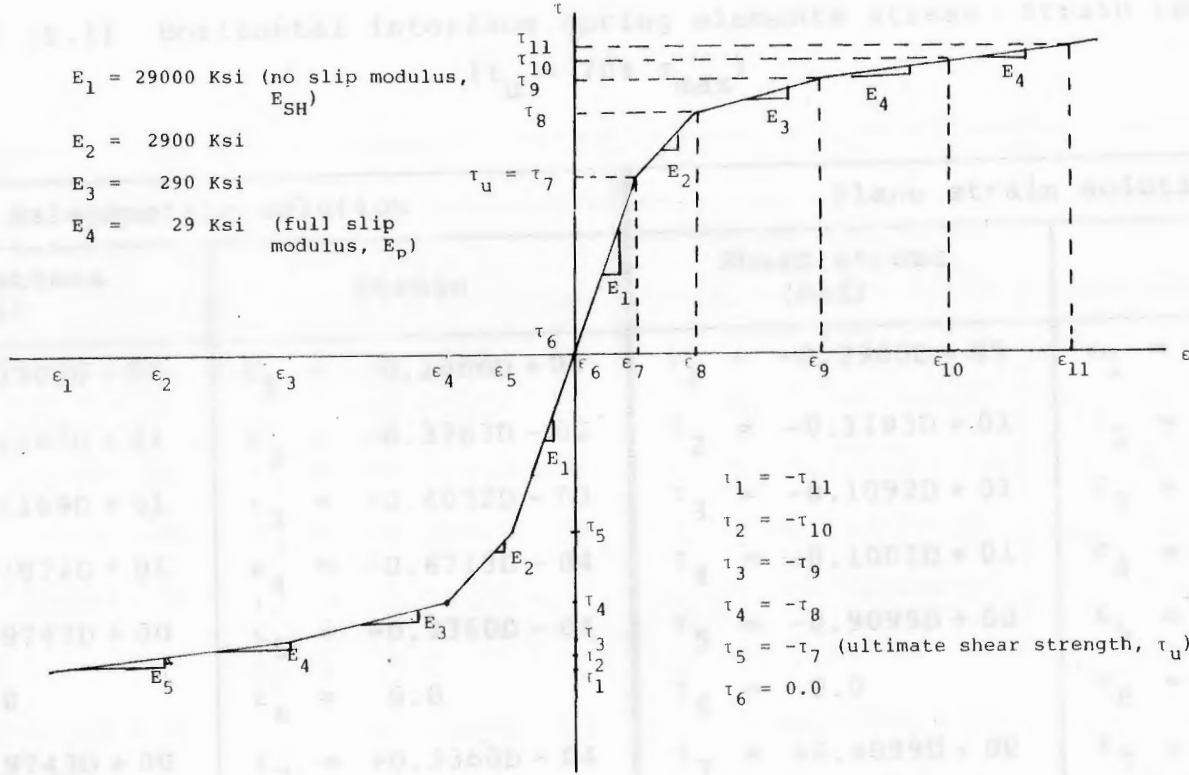
Fig. (B.1) Horizontal interface spring elements stress – strain diagram (not to scale).

Table (B.1) Horizontal interface spring elements stress - strain relation

$$(\tau_u = 70\% \ \tau_{max})$$

Axisymmetric solution		Plane strain solution	
Shear stress (Ksi)	Strain	Shear stress (Ksi)	Strain
τ_1 = -0.2900D + 05	ε_1 = -0.1000D + 04	τ_1 = -0.2900D + 05	ε_1 = -0.1000D + 04
τ_2 = -0.1267D + 01	ε_2 = -0.3763D - 02	τ_2 = -0.1183D + 01	ε_2 = -0.3514D - 02
τ_3 = -0.1169D + 01	ε_3 = -0.4032D - 03	τ_3 = -0.1092D + 01	ε_3 = -0.3765D - 03
τ_4 = -0.1072D + 01	ε_4 = -0.6719D - 04	τ_4 = -0.1001D + 01	ε_4 = -0.6275D - 04
τ_5 = -0.9743D + 00	ε_5 = -0.3360D - 04	τ_5 = -0.9099D + 00	ε_5 = -0.3138D - 04
τ_6 = 0.0	ε_6 = 0.0	τ_6 = 0.0	ε_6 = 0.0
τ_7 = +0.9743D + 00	ε_7 = +0.3360D - 04	τ_7 = +0.9099D + 00	ε_7 = +0.3138D - 04
τ_8 = +0.1072D + 01	ε_8 = +0.6719D - 04	τ_8 = -0.1001D + 01	ε_8 = +0.6275D - 04
τ_9 = +0.1169D + 01	ε_9 = +0.4032D - 03	τ_9 = +0.1092D + 01	ε_9 = +0.3765D - 03
τ_{10} = +0.1267D + 01	ε_{10} = +0.3763D - 02	τ_{10} = +0.1183D + 01	ε_{10} = +0.3514D - 02
τ_{11} = +0.2900D + 05	ε_{11} = +0.1000D + 04	τ_{11} = +0.2900D + 05	ε_{11} = +0.1000D + 04

Table (B.2)   Horizontal interface spring elements stress - strain relation
$$(\tau_u = 50\% \ \tau_{max})$$

Axisymmetric solution		Plane strain solution	
Shear stress (Ksi)	Strain	Shear stress (Ksi)	Strain
τ_1 = -0.2900D + 05	ε_1 = -0.1000D + 04	τ_1 = -0.2900D + 05	ε_1 = -0.1000D + 00
τ_2 = -0.9047D + 00	ε_2 = -0.2688D - 02	τ_2 = -0.8449D + 00	ε_2 = -0.2510D - 02
τ_3 = -0.8351D + 00	ε_3 = -0.2880D - 03	τ_3 = -0.7799D + 00	ε_3 = -0.2686D - 03
τ_4 = -0.7655D + 00	ε_4 = -0.4800D - 04	τ_4 = -0.7149D + 00	ε_4 = -0.4453D - 04
τ_5 = -0.6959D + 00	ε_5 = -0.2400D - 04	τ_5 = -0.6499D + 00	ε_5 = -0.2241D - 04
τ_6 = 0.0	ε_6 = 0.0	τ_6 = 0.0	ε_6 = 0.0
τ_7 = +0.6959D + 00	ε_7 = +0.2400D - 04	τ_7 = +0.6499D + 00	ε_7 = +0.2241D - 04
τ_8 = +0.7655D + 00	ε_8 = +0.4800D - 04	τ_8 = +0.7149D + 00	ε_8 = +0.4453D - 04
τ_9 = +0.8351D + 00	ε_9 = +0.2880D - 03	τ_9 = +0.7799D + 00	ε_9 = +0.2686D - 03
τ_{10} = +0.9047D + 00	ε_{10} = +0.2688D - 02	τ_{10} = +0.8449D + 00	ε_{10} = +0.2510D - 02
τ_{11} = +0.2900D + 05	ε_{11} = +0.1000D + 04	τ_{11} = +0.2900D + 05	ε_{11} = +0.1000D + 04

Table (B.3)   Horizontal interface spring elements stress - strain relation

$$(\tau_u = 30\% \; \tau_{max})$$

Axisymmetric solution		Plane strain solution	
Shear stress (Ksi)	Strain	Shear stress (Ksi)	Strain
$\tau_1 = -0.2900D+05$	$\varepsilon_1 = -0.1000D+04$	$\tau_1 = -0.2900D+05$	$\varepsilon_1 = -0.1000D+04$
$\tau_2 = -0.5428D+00$	$\varepsilon_2 = -0.1613D-02$	$\tau_2 = -0.5069D+00$	$\varepsilon_2 = -0.1506D-02$
$\tau_3 = -0.5011D+00$	$\varepsilon_3 = -0.1728D-03$	$\tau_3 = -0.4680D+00$	$\varepsilon_3 = -0.1614D-03$
$\tau_4 = -0.4593D+00$	$\varepsilon_4 = -0.2880D-04$	$\tau_4 = -0.4290D+00$	$\varepsilon_4 = -0.2689D-04$
$\tau_5 = -0.4176D+00$	$\varepsilon_5 = -0.1440D-04$	$\tau_5 = -0.3900D+00$	$\varepsilon_5 = -0.1345D-04$
$\tau_6 = 0.0$	$\varepsilon_6 = 0.0$	$\tau_6 = 0.0$	$\varepsilon_6 = 0.0$
$\tau_7 = +0.4176D+00$	$\varepsilon_7 = +0.1440D-04$	$\tau_7 = +0.3900D+00$	$\varepsilon_7 = +0.1345D-04$
$\tau_8 = +0.4593D+00$	$\varepsilon_8 = +0.2880D-04$	$\tau_8 = +0.4290D+00$	$\varepsilon_8 = +0.2689D-04$
$\tau_9 = +0.5011D+00$	$\varepsilon_9 = +0.1728D-03$	$\tau_9 = +0.4680D+00$	$\varepsilon_9 = +0.1614D-03$
$\tau_{10} = +0.5428D+00$	$\varepsilon_{10} = +0.1613D-02$	$\tau_{10} = +0.5069D+00$	$\varepsilon_{10} = +0.1506D-02$
$\tau_{11} = +0.2900D+05$	$\varepsilon_{11} = +0.1000D+04$	$\tau_{11} = +0.2900D+05$	$\varepsilon_{11} = +0.1000D+04$

B.2 NORMAL STRESSES TRANSFERRED THROUGH THE VERTICAL SPRINGS

[Zero shear transfer condition, interface spring elements not included, see model in fig. (4.6)].

Table (B.4)

Element number	Axisymmetric solution normal stress (Ksi)	Plane strain solution normal stress (Ksi)
49	-1.167	-6.162
50	-2.529	-6.133
51	-2.293	-6.006
52	-2.259	-5.869
53	-2.174	-5.626
54	-2.051	-5.314
55	-1.880	-4.900
56	-1.702	-4.474
57	-1.516	-3.993
58	-1.344	-3.518
59	-1.142	-2.963
60	-0.894	-2.300
61	-0.603	-1.479
62	-0.237	-0.345

B.3 NORMAL STRESSES TRANSFERRED THROUGH THE INTERFACE
      SPRING ELEMENTS FOR DIFFERENT SHEAR TRANSFER
      CONDITIONS

[Model including vertical and horizontal interface spring
 elements, see fig. (4.7)]

Table (B.5.a) Axisymmetrical solution

Ele-ment No.	Shear transfer condition				
	Infinite shear transfer normal stress (Ksi	τ_u=70% τ_{max} normal stress (Ksi)	τ_u=50% τ_{max} normal stress (Ksi)	τ_u=30% τ_{max} normal stress (Ksi)	τ_u = 0 normal stress (Ksi)
63	-0.915	-0.933	-1.042	-1.248	-1.761
64	-5.361	-5.791	-6.845	-5.568	-4.708
65	-1.788	-1.785	-2.105	-3.300	-2.599
66	-4.679	-4.025	+3.784	-1.817	-4.262
67	-1.723	-1.905	-22.187	-0.574	-2.438
68	-4.832	-1.697	+31.958	-1.491	-5.065
69	-1.722	-2.273	-59.087	+1.034	-2.496
70	-4.550	+3.542	+70.720	-41.590	-5.829
71	-1.610	-7.381	+19.958	+2.908	-2.727
72	-4.427	+15.750	+50.946	+1.403	-6.962
73	-1.527	-34.895	+24.029	+4.351	-3.654
74	-4.032	+38.064	+46.323	+2.393	-8.129
75	-1.332	-51.762	+15.642	+5.100	-4.944
76	-3.686	+58.717	+40.820	+3.145	-9.457
77	-1.195	-12.325	+22.031	+5.202	-7.152
78	-3.243	+62.942	+35.728	+3.248	-10.579
79	-1.000	-6.096	+22.433	+4.662	-9.0239
80	-2.881	+70.695	+30.962	+3.315	-11.407
81	-0.892	-5.617	+19.140	+3.924	-10.460
82	-2.507	+7.694	+26.124	+3.010	-11.690
83	-0.727	-2.671	+16.311	+3.152	-11.180
84	-2.064	+85.153	+22.071	+2.984	-11.308
85	-0.547	-5.530	+3.736	+1.683	-12.223
86	-1.572	+8.570	+15.316	+2.115	-10.129
87	-0.367	-35.947	+1.405	-15.321	-11.986
88	-1.147	+86.424	+11.073	+3.269	-8.762
89	-0.319	-30.019	-0.883	-16.605	-10.738
90	-0.313	+92.199	+8.748	+6.275	-6.226
91	-2.382	+87.26	+6.027	+13.576	-21.039

τ_u = horizontal spring element ultimate shear strength

τ_{max} = maximum shear stress transferred in the infinite
              shear transfer condition.

Table (B.5.b)   Plane strain solution

Element No.	Shear transfer condition				
	Infinite shear transfer normal stress (Ksi)	$\tau_u=70\%\ \tau_{max}$ normal stress (Ksi)	$\tau_u=50\%\ \tau_{max}$ normal stress (Ksi)	$\tau_u=30\%\ \tau_{max}$ normal stress (Ksi)	$\tau_u = 0$ normal stress (Ksi)
63	-1.364	-1.369	-1.416	-1.550	-1.999
64	-4.55	-5.082	-6.070	-6.937	-4.474
65	-1.722	-1.726	-1.733	-17.891	-2.576
66	-4.359	-4.676	-1.428	+27.431	-6.426
67	-1.580	-1.875	-6.758	+ 0.858	-3.925
68	-4.229	-3.761	+16.420	+22.889	-10.498
69	-1.552	-2.265	-109.058	+ 9.432	- 6.821
70	-4.131	-1.741	+69.742	+30.534	-16.512
71	-1.390	-2.868	+ 6.321	+21.470	-10.958
72	-3.940	+4.643	+80.078	+37.442	-24.079
73	-1.267	-15.20	-25.887	+36.933	-17.494
74	-3.704	+19.59	+77.945	+42.887	-33.007
75	-1.040	-120.666	+34.326	+42.105	-25.794
76	-3.408	+55.226	+93.568	+46.181	-42.719
77	-0.887	-74.80	+31.201	+43.595	-37.095
78	-3.098	+82.65	+89.954	+45.965	-52.161
79	-0.675	-100.511	+33.788	+42.128	-48.063
80	-2.753	+115.649	+88.112	+44.344	-60.351
81	-0.536	-119.365	+60.118	+38.942	-58.056
82	-2.430	+138.208	+91.130	+40.828	-66.099
83	-0.330	-131.684	+61.653	+34.480	-65.075
84	-2.011	+150.684	+90.387	+37.016	-68.180
85	-0.182	-116.761	+59.572	+28.520	-71.055
86	-0.154	+121.849	+85.393	+32.725	-66.223
87	-0.042	-164.974	+39.417	+23.483	-71.458
88	-1.097	+ 92.090	+75.788	+29.516	-62.174
89	+0.003	-135.337	+29.616	+20.582	-67.508
90	-0.376	+104.763	+71.362	+28.235	-54.250
91	-1.120	+107.798	+66.791	+27.476	-43.894

APPENDIX C

BEARING SYSTEM MATERIAL PROPERTY CONSTANTS

C.1 POT BEARING AND MASONRY STEEL PLATES

Steel plates have been represented by isotropic linear elastic elements with the following material property constants:

1) Steel modulus of elasticity, E = 29000 Ksi

2) Poisson's ratio, ν = 0.25

C.2 CONCRETE ABUTMENT

Concrete elements have been modeled as an elastic - plastic material model following the von Mises yield criterion. Material property constants were taken from approximating the concrete stress - strain diagram resulting from a uniaxial compression test, see fig. (C.1), where:

1) Concrete modulus of elasticity (elastic range), E_c = 3605 Ksi.

2) Poisson's ratio, ν = 0.180

3) Yield stress in simple tension, f_t = 0.1548 Ksi.

4) Strain hardening modulus, E_t = 2454.5 Ksi.
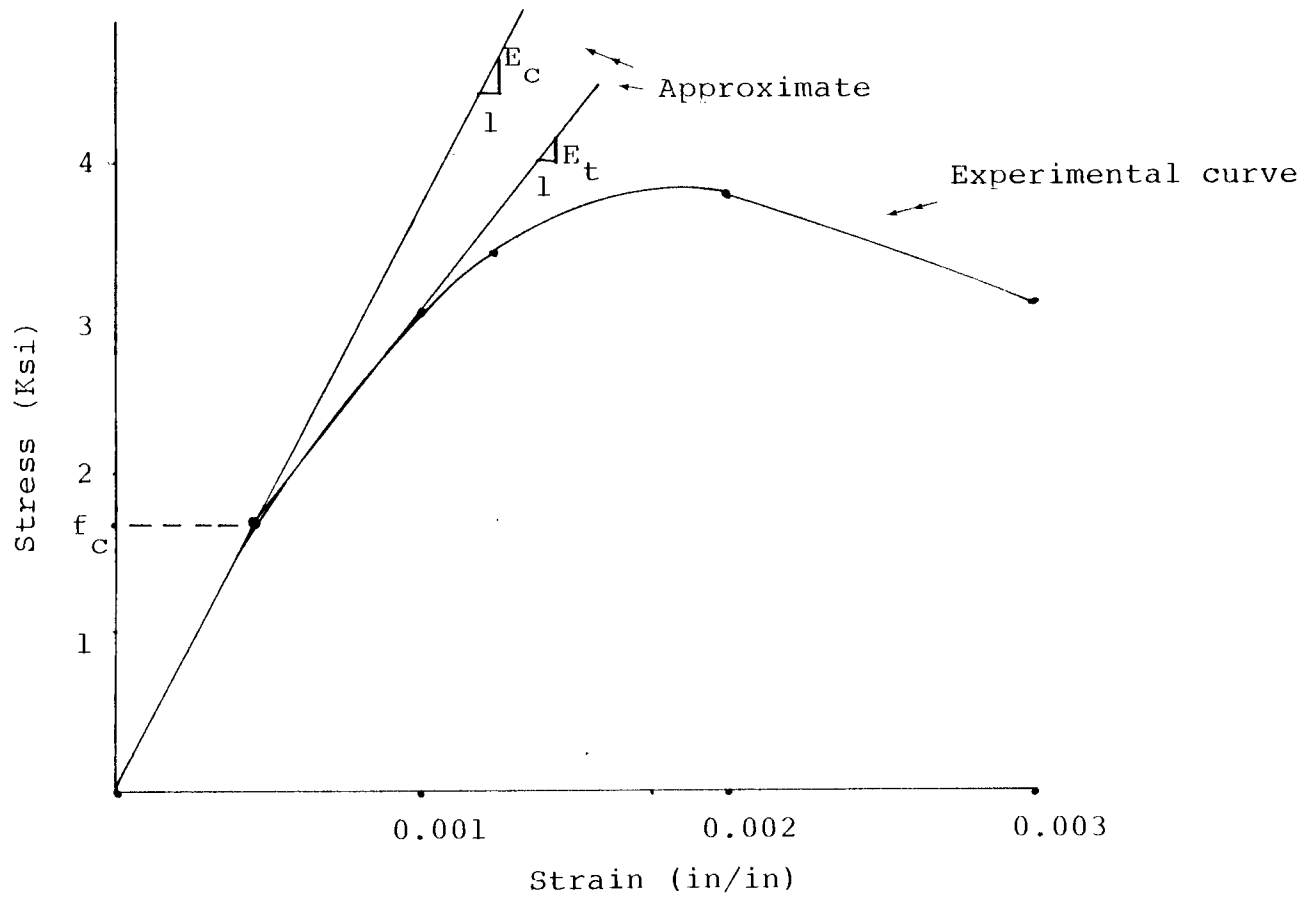   (Approximated as tangent modulus at f_c.)

Fig. (C.1) Concrete stress - strain diagram.

For this investigation, the compressive strength of the concrete, f_c', is taken as 4 Ksi, and the tensile strength, f_t' as 0.09 f_c'. Initial yield is taken to be 43% of the maximum strength such that

$$f_t = 0.43 \ f_t'$$

and

$$f_c = 0.43 \ f_c'.$$

BIBLIOGRAPHY

ALEXANDER, B. "Practical Stress Analysis Engineering Design", Marcel Dekker Inc., New York and Basel, 1st Ed., 1982.

BATHE, K. J. "Finite Element Procedures in Engineering Analysis", Prentice-Hall Inc., New Jersey, 1st Ed., 1982.

BATHE, K. J., WILSON, E. L., IDING, R. H. "NONSAP A Structural Analysis Program for Static and Dynamic Response of Nonlinear Systems", University of California, Berkeley, Report No. UC SESM 74-3, February 1974.

BATHE, K. J., WILSON, E. L., OZDEMIR, H. "Static and Dynamic Geometric and Nonlinear Analysis", University of California, Berkeley, Report No. UC SESM 74-4, February 1974.

BURAGOHAIN, D. N., SHAH, V. L. "Curved Interface Elements for Interaction Problems", Journal of the Structural Division, ASCE, Vol. 104 No. St1, January 1978, pp. 205-209.

BURAGOHAIN, D. N., SHAH, V. L. "Curved Interface Elements for Interaction Problems", Proceedings, International Symposium on Soil-Structure Interaction, University of Roorkee, Roorkee, India, January 1977, pp. 197-201.

CHEN, W. F. "plasticity in Reinforced Concrete"
McGraw-Hill, Inc., New York, 1st Ed., 1982.

CHEUNG, Y. K., YEO, M. F. "A Practical Introduction to
Finite Element Analysis", Pitman Publishing Limited,
39 Parker St., London WC2B 5PB, 1st Ed., 1979.

COOK, R. D. "Concepts and Applications of Finite Element
Analysis", John Wiley and Sons Inc., New York, 2nd Ed.,
1974.

"Dixon Shortspan Bearings", (catalog), Spencer Dynamics
Corporation, Promenade Street, Providence, RI, 02908, USA.

"Elastomeric Bearings Design, Construction and Materials",
National Cooperative Highway Research Program,
Report No. 248, University of Washington, Seattle,
Washington, August 1982.

GALLAGHER, R. H. "Finite Element Analysis Fundamentals",
Prentice-Hall Inc., Englewood Cliffs, New Jersey, 1st Ed.,
1975.

GHABOUSSI, J., WILSON, E. L., ISENBERG, J. "Finite
Element for Rock Joints and Interfaces", Journal of Soil
Mechanics and Foundations Division, ASCE, vol. 99,
No. SM10, Proc. paper 10095, October 1973, pp. 833-847.

GOODMAN, R. E., TAYLOR, R., BREEKE, T. L. "A Model for
the Mechanics of Jointed Rock", Journal of Soil Mechanics
and Foundations Division, ASCE, vol. 94, No. SM3, Proc.

paper 5937, May 1968, pp. 637-659.

GUDEHUS, G. (Ed.), "Finite Element in Geomechanics", John Wiley and Sons, Inc., New York, 1st Ed., 1977, Chapter 10.

HOLAND, I., BELL, K., (Editors), "Finite Element Methods in Stress Analysis", TAPIR, The Technical University of Norway, Trondheim-Norway, 2nd printing, 1970.

MARGUERRE, K., WOERNLE, H. T. "Elastic Plates", Blaisdell Publishing Company, Waltham, Massachusetts, 1st Ed., 1969.

McEWEN, E. E. "Behavior of Masonry Bearing Plates", unpublished report, University of Rhode Island, Kingston, RI December 1979.

NGO, D., SCORDELIS, A. C. "Finite Element Analysis of Reinforced Concrete Beams", Journal of American Concrete Institute, Title No. 64-14, March 1967, pp. 152-163.

SCHAFER, H. "A Contribution to the Solution of Contact Problems with the Aid of Bond Elements", Computer Methods in Applied Mechanics and Engineering 6, North Holland Publishing Company, February 20, 1975, pp. 335-353.

"Standard Specifications for Highway Bridges", AASHTO, 12th Ed., 1977.

"Steel Construction Manual", American Institute of Steel Construction, Inc., 8th Ed., pp. (2-47)-(2-49).

SZILARD, R.   "Theory and Analysis of Plates, Classical
and Numerical Methods", Prentice-Hall Inc.,
1st Ed., 1974.

TUMA, J. J.   "Engineering Mathematics Handbook",
McGraw-Hill Inc., New York, 2nd Ed., 1979.

WANG, C., SALMON, C. G.   "Reinforced Concrete Design",
Harper and Row Inc., New York, 3rd Ed., 1979.

WILBY, C. B.   "Concrete for Structural Engineers",
Newnes-Butterwurths, London, Boston, 1st Ed., 1977.

WINTER, G., NILSON, A. H.   "Design of Concrete Structures"
McGraw-Hill Inc., New York, 7th Ed., 1964.

ZIENKIEWICZ, O. C.   "The Finite Element Method",
McGraw-Hill Inc., New York, 3rd Ed., 1977.